

AD-A045 473

JOHNS HOPKINS UNIV LAUREL MD APPLIED PHYSICS LAB
DEVELOPMENTS IN SCIENCE AND TECHNOLOGY.(U)
1975

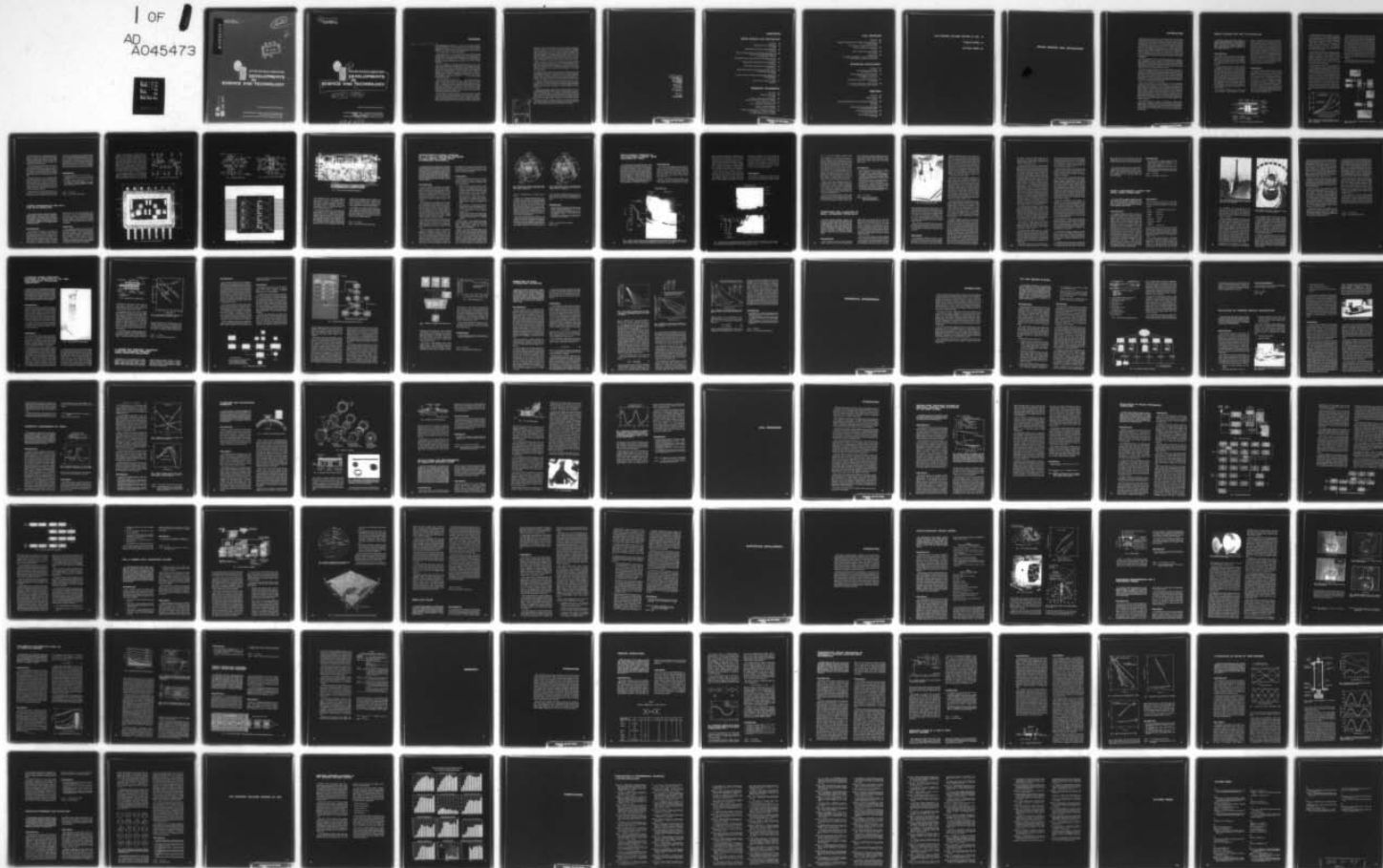
F/6 22/2

UNCLASSIFIED

APL/JHU/DST-3

N00017-72-C-4401
NL

1 OF 1
AD
A045473

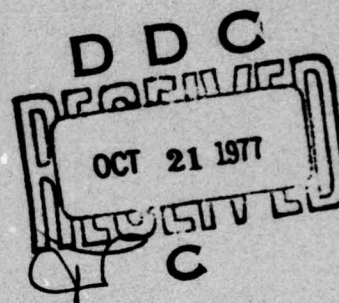


AD A 045473

APL/JHU DST-3
FISCAL YEAR 1975

12

J



APPLIED PHYSICS LABORATORY
**DEVELOPMENTS
IN
SCIENCE AND TECHNOLOGY**

AD No. _____
DDC FILE COPY

Approved for public release; distribution unlimited.

THE JOHNS HOPKINS UNIVERSITY • APPLIED PHYSICS LABORATORY
Johns Hopkins Road, Laurel, Maryland 20810
Operating under Contract N00017-72-C-4401 with the Department of the Navy

14

APL/JHU/DST-3
FISCAL YEAR 1975



6

APPLIED PHYSICS LABORATORY

**DEVELOPMENTS
IN
SCIENCE AND TECHNOLOGY.**

11 1975

12 96p.

Approved for public release; distribution unlimited.

THE JOHNS HOPKINS UNIVERSITY • APPLIED PHYSICS LABORATORY

Johns Hopkins Road, Laurel, Maryland 20810

Operating under Contract N00017-72-C-4401 with the Department of the Navy

031 650

LB

FOREWORD

↳ The principal mission of

The Applied Physics Laboratory is a division of The Johns Hopkins University, dedicated to serving the nation by performing research and development in important areas of national defense and welfare. APL is located on a 350-acre site in Howard County, Maryland. About one-half of its 2500-member staff are scientists and engineers.

The principal mission of APL is to further national defense through the application of science and technology, primarily for the Department of the Navy. With the encouragement of the Department of Defense, APL also undertakes on a noninterfering basis to apply its technical capabilities to nationally important nondefense areas to which it can make a unique contribution.

APL was established by The Johns Hopkins University in 1942 at the urgent request of the Office of Scientific Research and Development, to implement the concept that science and technology would more effectively further national defense by addressing broad tactical situations and requirements rather than by limiting efforts to specific technical objectives. APL was challenged by the assignment of applying new technology to the defense of the Fleet against air attack. The radio proximity fuse, which was developed and produced in one year, made a major contribution to American victories in Europe and the Pacific.

After World War II, the University, at the request of the Navy, agreed to continue its sponsorship of APL as a unique national resource with a broad mission to enhance the security of the Fleet through application of new science and technology. This relationship has proved fruitful in successful development and deployment of guided missile systems, Fleet defense combat systems, sea-based strategic deterrent systems, aircraft defense, a precise worldwide positioning and navigation system, and other areas in which APL has made important technical contributions.

From the beginning, technical advances in defense systems led to spinoffs in the civil area, for example, high-speed aircraft and electronics. However, it became increasingly apparent that these new techniques and capabilities could be advantageously applied more directly to important civilian areas. APL conceived, developed, and initially operated the Navy Navigation Satel-

lite System (Transit), which supplies precise worldwide position and navigation data by means of a network of earth-orbiting satellites. A simplified version of this system is now widely used by commercial shipping. The Transit System has produced precise worldwide geodetic measurements and basic new knowledge of the shape, gravitational field, and motion of the earth. Under NASA sponsorship, APL has built and flown numerous scientific satellites and space experiments that have helped to revolutionize our knowledge and understanding of the earth, the solar system, and the stellar universe.

Other civil areas in which APL is advantageously applying technology developed in defense programs include civil air safety and traffic control, harbor and inland waterway traffic management, automated urban transit systems, the environmental impact of electric power plants and other energy facilities, fire prevention and control, and the development of new energy sources and systems.

A highly successful collaborative program between APL and the Johns Hopkins Medical Institutions is conducted in the field of biomedical engineering. Technology developed in space, electronics, and computer application programs is being successfully applied to medical research, techniques, and instruments for diagnosis, therapy, and improved health care delivery systems.

To gain the insights required for future technical advances and as a part of its function as a University laboratory, APL conducts a vigorous research program in the basic sciences underlying its evolving technology. The quality of this work is attested by its recognition in scientific publications, honors, and awards.

A Center of the Evening College of the University located at APL serves the Washington-Baltimore area by offering accredited graduate courses in science and technology. Most of the faculty are drawn from the APL Senior Staff. Other areas of scholarly cooperation between APL and other divisions of the University include predoctoral and postdoctoral fellowships, visiting professorships, joint appointments, joint seminars, and collaborative research.

This volume presents a representative sample of the civilian-oriented and basic research programs that currently comprise about 20% of the total APL effort. All results of these programs are fully available to the public.

ADDRESS ONLY	
WIS	Write Section <input checked="" type="checkbox"/>
DOC	Brief Section <input type="checkbox"/>
MANAGEMENT	<input type="checkbox"/>
J.S. LOCATION	
BY	
DISTRIBUTION/AVAILABILITY CODES	
SPECIAL	
A	

Technical Coordinators

**R. J. Thompson, Jr.
M. H. Friedman
R. C. LaFever
R. A. Makofski
H. B. Riblet**

Managing Editor

M. B. Gilbert

Associate Editor

A. L. Machurek

Staff Artists

**J. L. Lew
J. Mothershead**

CONTENTS

SPACE SCIENCE AND TECHNOLOGY

Introduction	13
DISCOS System for the TIP-II Satellite <i>A. C. Sadilek</i>	14
Hybrid Microcircuits for TIP-II and TIP-III Satellites <i>G. D. Wagner</i>	16
Characteristic Energy Spectra of 1 to 500 eV Electrons Observed in the Auroral Zones from Atmosphere Explorer-C <i>T. A. Potemra and C. O. Bostrom</i>	20
Field-Aligned Currents in the Southern Auroral Zone Measured by Triad <i>T. A. Potemra</i>	22
Completion and Launching of Small Astronomy Satellite-C <i>H. B. Riblet</i>	24
GEOS-C Spacecraft Launch and Early Orbit Operations <i>L. D. Eckard, Jr.</i>	27
Hydrogen Maser Frequency Standard in Operation at APL Time and Frequency Standards Laboratory <i>L. J. Rueger</i>	30
A "Store and Forward" Telemetry Computer Program Designed Using Computer Simulation <i>N. K. Brown</i>	31
Prediction of Rain Attenuation Statistics <i>J. Goldhirsh</i>	35

BIOMEDICAL ENGINEERING

Introduction	41
JHH Mini Record System <i>B. I. Blum</i>	42
Evaluation of Powered Medical Manipulator <i>W. Seamone (APL) and G. Schmeisser, Jr. (JHMI)</i>	44
Elemental Phenomenon of Vision <i>J. F. Bird, R. W. Flower, and G. H. Mowbray</i>	46
A Monitor for Intracranial Pressure <i>L. J. Viernstein and J. G. Chubbuck</i>	48
Calculations and Measurements of Simulated Arterial Flows <i>C. B. Bergeron, O. J. Deters, L. W. Ehrlich, F. F. Mark, V. O'Brien, and M. H. Friedman</i>	50

CIVIL PROGRAMS

Introduction	55
Moving Wire Technique Studies of Ablation, Ignition, and Extinction of Polymer Flames	56
<i>R. M. Fristrom, C. Grunfelder, and L. W. Hunter</i>	
Evaluation of Radar Processing Subsystem	58
<i>P. J. Voss</i>	
DAT—A Mobile Data Acquisition System	62
<i>E. L. Brickner</i>	
Small-Car Study	64
<i>L. L. Perini, R. A. Makofski, J. F. George, R. M. Hanes, and F. F. Mark (APL); A. Levy and K. Lyall (CMPR)</i>	

SUPPORTING DEVELOPMENT

Introduction	71
Nap-of-the-Earth Radar (NOTER)	72
<i>F. W. Schenkel and A. Finkel</i>	
Electronic Beamsteering for a Parametric Sonar	74
<i>M. L. Dwarkin, J. W. Follin, Jr., R. E. Miller, and D. W. Stowe</i>	
The Earth's Electrostatic Field as an Obstacle Sensor	77
<i>C. S. Leffel, Jr.</i>	
Error Correction Encoder/Error Correction Decoder	79
<i>P. J. Luke, J. L. Machamer, and W. A. Becraft</i>	

RESEARCH

Introduction	83
Organic Conductors	84
<i>T. O. Poebler</i>	
Photoexcited Triplet Mechanism of Chemically Induced Electron Spin Polarization	86
<i>F. J. Adrian</i>	
Reaction Rates of H and O with Methyl Halides	87
<i>A. A. Westenberg and N. deHaas</i>	
Attenuation of Sound by Rigid Spheres	90
<i>S. N. Foner and B. H. Nall</i>	
Molecular Energies and Structure	92
<i>D. M. Silver</i>	

JHU EVENING COLLEGE CENTER AT APL 96

PUBLICATIONS 100

AUTHOR INDEX 106

SPACE SCIENCE AND TECHNOLOGY

INTRODUCTION

The APL program in space science and technology began in the immediate post World War II period when a group then led by Dr. James Van Allen started to study cosmic radiation and the upper atmosphere using instrumented sounding rockets. The discovery in 1957 by APL scientists that the position of the Russian Sputnik satellite could be tracked by observing the doppler shift of its radio signal led to the conception of a satellite navigation system based on the doppler tracking principle. The Navy Navigation Satellite System (Transit) developed by APL has provided precise, worldwide, all-weather navigational data to the Navy since 1964 and to commercial users since 1967. It includes a constellation of satellites; tracking, receiving, and computing stations; equipment and software; and user receiving and computing equipment.

The Transit program has been continually upgraded since its inception. Recent improvements include a single-axis active disturbance compensation system (DISCOS) to provide improved orbit prediction and improved hybrid microelectronic circuitry packaging. These are described in this section. Other improvements, not discussed in detail, yield increased satellite and ground equipment reliability and greater navigational accuracy.

The Transit program required more accurate knowledge of the shape of the earth for navigational accuracy and provided the measurement tool for acquiring this knowledge. The comprehensive geodesy program conducted by APL with the Transit System improved the accuracy of the geoid model by about two orders of magnitude and led to APL participation in other space science programs. Articles in this section describing recent experiments on the interactions of charged particles with the earth's magnetic field are representative of APL's continuing space physics research.

APL's special capabilities in attitude stabilization and control, ultrastable oscillators, precision tracking and other technologies, and component and system design and development are used in numerous space programs for NASA and DoD as well as the Navy. Particularly notable at this time are the latest members of a series of small astronomy satellites (SAS) and geodetic research satellites (GEOS) that APL has designed, built, and launched for NASA. The third members of each series, SAS-C and GEOS-C, were completed and launched this year. Both have been highly successful and are adding significant new knowledge in their areas of research. Key design features, launch, and early postlaunch operation of these scientific satellites are described in this section.

Rain attenuation may be a problem in high-frequency satellite-to-earth communication. Techniques to predict rain attenuation statistics are described. Current programs to improve time and frequency standards and the automated receipt, storage, and handling of high-speed data are also representative of the many APL activities contributing to increased capabilities in space science and technology.

DISCOS SYSTEM FOR THE TIP-II SATELLITE

A Disturbance Compensation System (DISCOS) to correct for drag effects has been incorporated in the Transit Improvement Program (TIP-II) Navy Navigation Satellite. The system will force the spacecraft to follow a predictable orbit, allowing the generation of more accurate ephemeris data for navigation fixes over a longer period of time.

BACKGROUND

The present Transit satellites require ephemeris updating at 12-hour intervals because of the disturbing effects of solar radiation pressure and atmospheric drag. To produce a longer period of accurate ephemeris, DISCOS has been incorporated in the TIP spacecraft.

The first DISCOS, installed in Triad (TIP-I), compensated for disturbances in all three axes (Ref. 1). A spherical "proof mass" in an enclosed chamber followed a nearly pure gravitational orbit. Its position was sensed, and cold-gas thrusters positioned the satellite about the proof mass, forcing the satellite to follow a "drag-free" trajectory. Although the three-axis DISCOS produced an exceptionally accurate orbit (Ref. 2), Triad was a difficult spacecraft to fabricate. The gravitational force between the proof mass and all components in Triad was disturbing enough so that bookkeeping of the mass and of the position of each component was necessary to compensate for mass attraction (Ref. 3).

The single-axis DISCOS used on TIP-II was devised to achieve a drag-free satellite in a simpler

fashion. A cylindrical proof mass was electromagnetically suspended on an axis oriented in the direction of the spacecraft velocity vector. While free to move without friction along the axis, the proof mass was constrained in radial motion by the suspension force. In this way, disturbance forces affecting the spacecraft velocity could be compensated for by firing a set of thrusters while the internal mass attraction force was nearly normal to the axis, a direction opposed by the suspension mechanism. An incrementally commandable biasing system provided trimming of any residual force components. This reduced the motion of the proof mass to a gravitational trajectory without the need for mass attraction bookkeeping, thereby simplifying fabrication of the spacecraft.

DISCUSSION

The Navy Navigation Satellite Program required the capability of maintaining the projected orbital ephemeris with an accuracy of ± 85 m for a seven-day period. This required that long-term acceleration in the along-track direction be compensated to within 1.58×10^{-11} g (1 g = acceleration of gravity = 980 cm/s^2). To provide this capability, the single-axis DISCOS was designed and fabricated at APL. The system consists of a sensor positioned at the spacecraft center of mass and connected via cabling to an electronics package located in the spacecraft main body. A set of Teflon solid propellant thrusters developed at Fairchild Industries provides the thrust necessary to counteract disturbance forces.

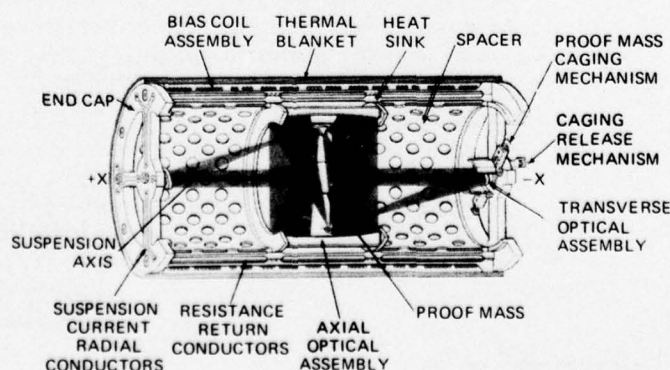


Fig. 1 Cutaway view of single-axis DISCOS sensor.

To meet a design criterion of along-track force compensation to within 10^{-11} g, the sensor was configured as a cylindrically symmetric enclosure, shielding the proof mass from external forces while producing little mass attraction along the axis (Fig. 1). A thermal control system stabilizes the sensor temperature to within $\pm 0.5^\circ$ of its nominal $70^\circ \pm 4^\circ\text{F}$ set point. Thermal gradients of less than $\pm 2^\circ\text{F}$ within the sensor neutralize radiometric pressure differentials on the ends of the proof mass.

The proof mass, formed into a cylindrical shell, is the sensed element that follows a purely gravitational trajectory. It is made of pure aluminum with low magnetic susceptibility, and its surface is vacuum deposited with 2000 nm of gold to distribute electrostatic potential evenly. A caging system protects the proof mass during launch and releases it during gravity-gradient boom deployment.

The frictionless levitation force is provided by a 2.08-kHz square-wave current passing through the axis, generating eddy current repulsion forces in the proof mass (Ref. 4). Commandable to four levels, the suspension current produces forces on the order of 10^{-7} g to balance cross-track disturbances. As shown in Fig. 2 for a sine-wave current, the suspension force constant is a function of current frequency and radial offset of the proof mass on its axis. By using a square wave, the force is increased by a factor of 2.19. A proof mass weight of 12.3 g produces an acceleration constant of 6.72×10^{-6} g/A². The suspension current is returned through evenly spaced radial conductors in the end caps and resistive wires parallel to the axis, preventing imaging effects from biasing the proof mass.

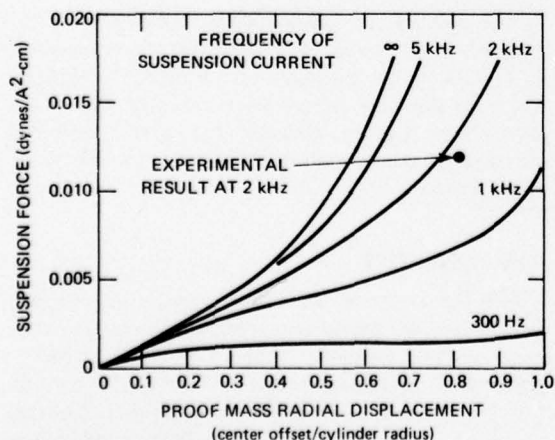


Fig. 2 Theoretical eddy current suspension force for sine-wave excitation of aluminum proof mass (1.04-cm ID by 1.70-cm OD).

Two optical systems are used to detect proof-mass position. An axial system determines along-track position, and a transverse system detects radial offset about the axis. The axial optical system uses parabolic mirrors to collimate light from a 100 000-hour-life tungsten bulb, pass the light across the ends of the proof mass, and refocus it on a set of photocells. The difference in current produced between the two photocells is a linear measure of proof-mass position along the axis. Both coarse-range (± 10 mm) and fine-range (± 2 mm) proof-mass positions are telemetered to ground receivers, providing position resolution of 0.08 and 0.015 mm, respectively. The data are used in aeronomy studies and to provide in-orbit thruster calibration.

The transverse system uses the light from the axial system bulbs. Spherical mirrors at the axis ends col-

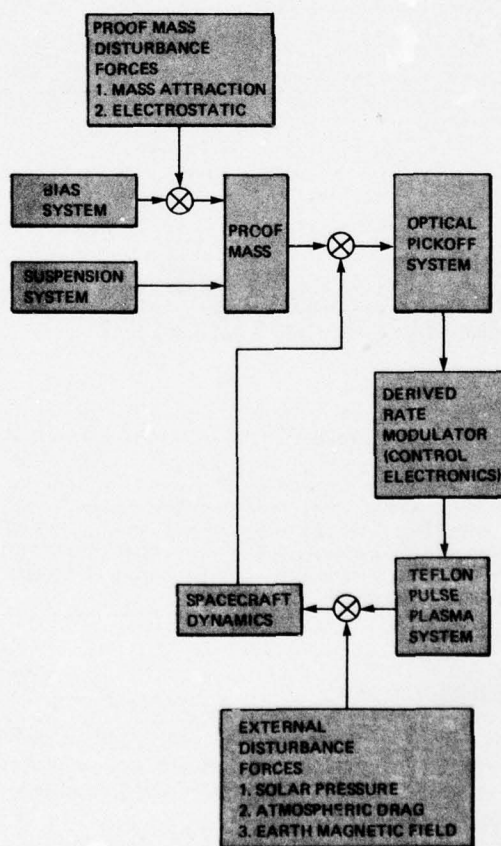


Fig. 3 Block diagram showing TIP-II single-axis DISCOS function.

limate the bulb light, pass it through the proof-mass center, and refocus it on a photocell. This signal, a measure of radial position of the proof mass, is differentiated to determine radial velocity. The result is used to modulate the suspension current, providing active damping of proof-mass dynamics.

The axial position signal is the input to the derived rate modulator (DRM) control electronics, which is the plant controller of the system. Relative motion of the proof mass is analyzed by the DRM and, allowing for hysteresis to provide damping for system stability, signals are generated to fire the thrusters at the proper time.

The thrusters consist of a pair of opposing Teflon pulse plasma engines, each of which produces an impulse of 44 dyn-s. Upon command of the DRM, a high-voltage discharge is initiated across the end surface of a Teflon stick, ionizing particles that are then accelerated by an electromagnetic field to produce the impulse. This thrust reacts against the spacecraft to counteract disturbances (Fig. 3).

A biasing system is required to balance any axial components of proof-mass disturbance forces. The system consists of two opposing coils, each configured

to provide a constant force over a proof-mass range of ± 10 mm. Over the normal operating range of ± 2.25 mm, a variation of less than 0.05% exists in the biasing force. Again, a 1.04-kHz sine-wave current passing through the selected coil produces eddy current repulsion of the proof mass. Coil current is commandable to a maximum of 10^{-8} g, in 10^{-11} -g increments, providing in-orbit tailoring of the proof-mass velocity.

REFERENCES

1. J. Dassoulas, "The Triad Spacecraft," *APL Technical Digest*, 12, No. 2, April-June 1973.
2. R. E. Jenkins, "Performance in Orbit of the Triad Disturbance Compensation System," *APL Technical Digest*, 12, No. 2, April-June 1973.
3. D. B. Debra, "Disturbance Compensation System Design," *APL Technical Digest*, 12, No. 2, April-June 1973.
4. F. F. Mobley, G. H. Fountain, A. C. Sadilek, P. W. Worden, and R. Van Patten, "Electromagnetic Suspension for the TIP-II Satellite," *IEEE Trans. on Magnetics*, MAG-11, No. 6 November 1975, pp. 1712-1716.

Author: A. C. Sadilek

Support: Strategic Systems Project Office

HYBRID MICROCIRCUITS FOR TIP-II AND TIP-III SATELLITES

The Transit Improvement Program Navy Navigation Satellite designs (TIP-II and TIP-III) required advanced electronic packaging techniques in order to meet the goals of size, weight, power consumption, and reliability. Through the effective use of hybrid microelectronic packaging, APL has assisted the TIP system, circuit, mechanical, and packaging designers in meeting their goals.

BACKGROUND

An APL hybrid microcircuit for spacecraft use typically consists of a miniature ceramic substrate that supports deposited aluminum conductors, deposited chromium resistors, and deposited silicon monoxide insulators. Such active elements as transistors, diodes, and integrated circuits or such special passive elements as capacitors, inductors, and high-value resistors are attached using eutectic soldering,

special epoxies, or solder reflow techniques. These elements are "wired in" using thermocompression wire bonding or ultrasonic wire bonding techniques. Then the assembly is sealed hermetically in an inert atmosphere. Rigorous electrical testing and reliability screening ensure a high-quality device for the space environment.

DISCUSSION

APL has designed, assembled, tested, and screened more than 1000 hybrid microcircuits used in the command system, telemetry system, computer/memory, and attitude stabilization system of the TIP-II and TIP-III satellites. In addition, assemblies for the command receiver, 5-MHz oscillator, 400-MHz transmitter, 150-MHz transmitter, and frequency multiplier/phase modulator system and approximately 100 miniature circuit substrates were assembled.

Figures 1 and 2 illustrate a relatively simple application of the technique. The high-current core-memory driver circuit shown schematically in Fig. 1 was converted to microcircuit form. If the circuits were built using miniature discrete components on printed circuit boards, the X-Y memory driver shown might occupy more than 1 sq. in. of board area and require 0.30 in. of board height. The hybrid shown in Fig. 2 occupies less than 0.20 sq. in. of board area and less than 0.080 in. of board height. The significant features of the technique are identified in Fig. 2.

A more complex example of the technology, the digit driver/differential comparator used in the TIP memory, is depicted in Figs. 3, 4, and 5. The schematics of four digit drivers (Fig. 4) and four differ-

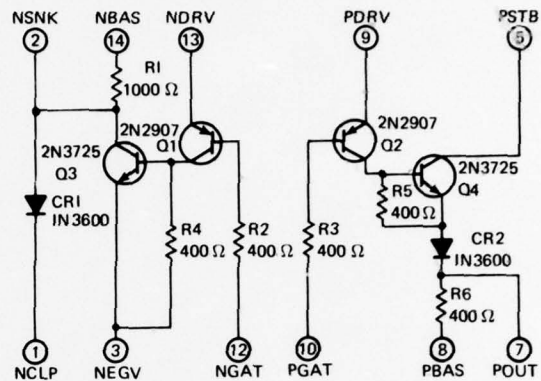


Fig. 1 Schematic of X-Y memory driver.

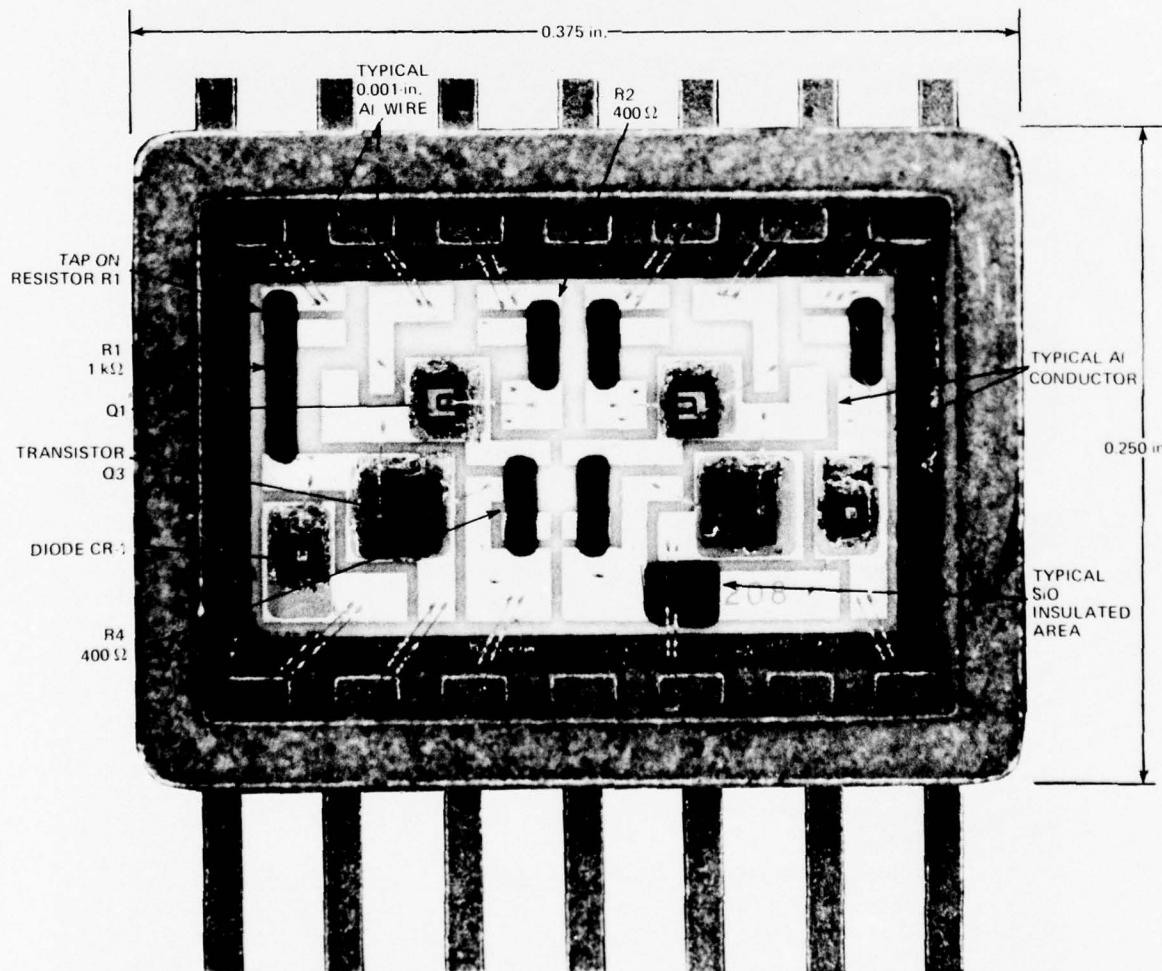
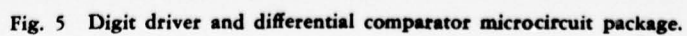
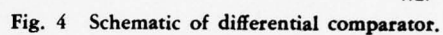


Fig. 2 X-Y memory driver hybrid microcircuit.



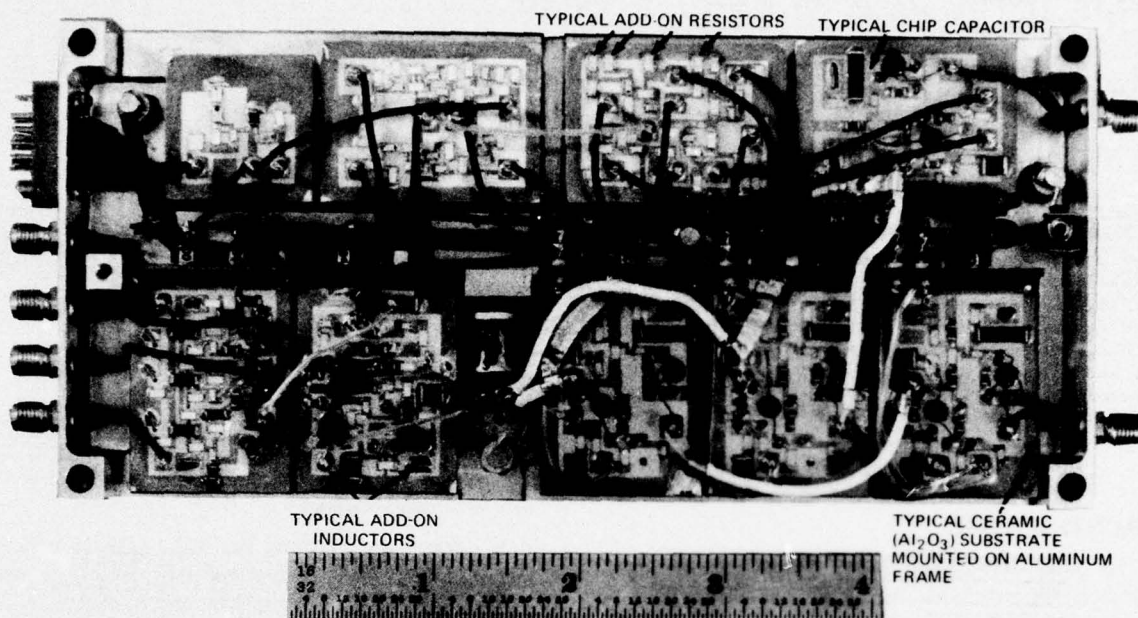


Fig. 6 TIP frequency multiplier/phase modulator.

ential comparators (Fig. 4) have been incorporated into a single 1.25 by 1.25 in. flat package (Fig. 5) comprising 16 transistors, 20 diodes, 68 resistors, eight capacitors, and four monolithic integrated circuits. More conventional technology would require approximately 10 sq. in. compared with about 2.0 sq. in. to perform this function.

Other custom miniature circuits and assemblies have been developed for TIP using hybrid technology. Typically these circuits are slightly larger than the hermetic hybrids and are built on ceramic substrates. Conductor patterns are defined by etching chromium/gold conductors; miniature uncased components are added separately using solder reflow techniques. Figure 6 illustrates the TIP frequency multiplier/phase modulator that has been assembled using these

techniques. The technology usually is applied to RF circuitry where components such as inductors, transformers, capacitors, and strip-line or microstrip elements are required. Circuits with capabilities up to several gigahertz have been fabricated successfully.

The complex and sophisticated TIP satellite electronics design and rigorous reliability requirements were successfully accommodated within the available volume and weight constraints. This could not have been done without the use of the hybrid microcircuit fabrication and packaging techniques.

Author: G. D. Wagner

Support: Strategic Systems Project Office, SP-20

CHARACTERISTIC ENERGY SPECTRA OF 1 TO 500 eV ELECTRONS OBSERVED IN THE AURORAL ZONES FROM ATMOSPHERE EXPLORER-C

Data obtained from the photoelectron experiment on board the Atmosphere Explorer-C (AE-C) satellite have been used in what is believed to be the first general classification of low-energy (1 to 500 eV) electron fluxes in the high-latitude ionospheric regions with high-resolution energy spectra measurements. In addition to the energy spectra already associated with the normal day airglow (Ref. 1), four major classes of low-energy electrons have been identified. Three of these are relatively stable while the fourth has large temporal variations.

BACKGROUND

The joint APL/JHU Department of Chemistry photoelectron experiment on AE-C was designed primarily to measure the energy distribution of photoelectrons in the daytime ionosphere (Ref. 2). The instrument was designed to detect electrons with extremely low energies (down to 1 eV) and to have very-high-energy resolution ($\Delta E/E = 2.5\%$), with on-board tape recorders providing continuous data collection.

The experiment and its mounting on the spacecraft have previously been described (Ref. 3). Briefly, two electrostatic analyzer heads are mounted on opposite sides of one end of the cylindrical spacecraft. The spacecraft operates in either a despun or a 4-rpm spinning mode. In the despun mode, one sensor head looks up away from the earth while the other looks down toward the earth. There is a large variety of possible modes of operation, including variable sweep rate and energy scan range.

The results presented here were determined from analysis of the data obtained in the 0 to 500 eV high-sweep-rate mode. In this mode, one 16-point spectrum is produced every 250 ms. The 16 energy bins are distributed linearly along the 0 to 500 eV sweep range.

The 68° inclination of the AE-C orbit takes the spacecraft to geomagnetic latitudes as high as 80°, depending on longitude. Although the AE-C orbit was not chosen primarily for high-latitude research, it has been particularly effective since the spacecraft remains in the auroral region for long periods of time. These passes have been extremely useful for the observation of relatively stable electron precipitation events. Most of the data analyzed were taken with

the spacecraft in a circular, 250-km orbit. The constant altitude near the peak of the *F* region of the ionosphere has also been extremely helpful in sorting electron precipitation phenomena.

DISCUSSION

Although the high-latitude fluxes of 1 to 500 eV electrons observed from AE-C are highly variable, it has been possible to organize the observed events into four major classes:

1. Fluxes of electrons having a peak in energy below 100 eV, approximately isotropic over the upper 2π hemisphere, and located at high invariant latitudes on the dayside, that are apparently gaining access to the ionosphere through the dayside magnetospheric cusps;
2. Structured fluxes of electrons showing one or more discrete but variable peaks in energy, reminiscent of "inverted-V" phenomena at higher energies, observed at all magnetic local times;
3. Fluxes that show a monotonically decreasing differential flux versus energy dependence proportional to $E^{-\alpha}$, where $E > 30$ eV and $1 < \alpha < 2$, characteristic of auroral secondary electrons; and
4. Intense fluxes of electrons with rapidly changing and random energy spectra, characteristic of passage through auroral arcs or breakup regions.

Fluxes of types 3 and 4 depend on precipitation of high-energy auroral primary particles while those of types 1 and 2 appear to be a consequence of fundamental processes that couple the magnetosphere and ionosphere.

Figures 1 and 2 show the spatial locations in the north polar region where the electron fluxes denoted as class 1 and 2, respectively, have been observed by AE-C. The regions are indicated along each orbit where class 1 and 2 fluxes have been observed, corresponding to geomagnetic conditions characterized by $Kp < 3$ (quiet to moderately disturbed) and $Kp \geq 3$ (disturbed). Because of its inclination, AE-C could not reach geomagnetic latitudes higher than

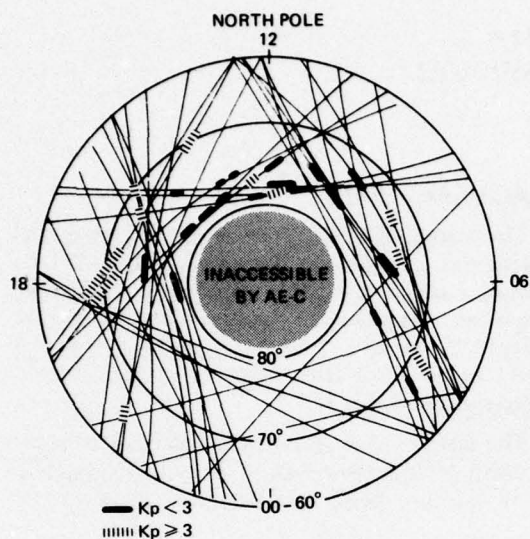


Fig. 1 Orbital tracks of AE-C over the northern high-latitude region with the location of cusp (class 1) electrons for $Kp < 3$ and $Kp \geq 3$.

81°; the "inaccessible region" is shaded in Figs. 1 and 2.

Figures 1 and 2 demonstrate that the class 1 electron fluxes occur most often in the dayside high-latitude region associated with cusp phenomena, whereas the class 2 electrons are found at nearly all local times and during almost every AE-C orbit shown. The distributions support the view that the class 1 electrons have gained direct access through the magnetospheric cusp from the magnetosheath/solar wind plasma and that the class 2 electrons have been accelerated and redistributed in the region between the source and the auroral ionosphere.

The AE-C measurements are an extension to low energies, lower altitudes, and higher-energy resolution compared with previous experiments in the high-latitude region. These more detailed data will help identify the important magnetospheric/ionospheric regions and coupling mechanisms and will help resolve cur-

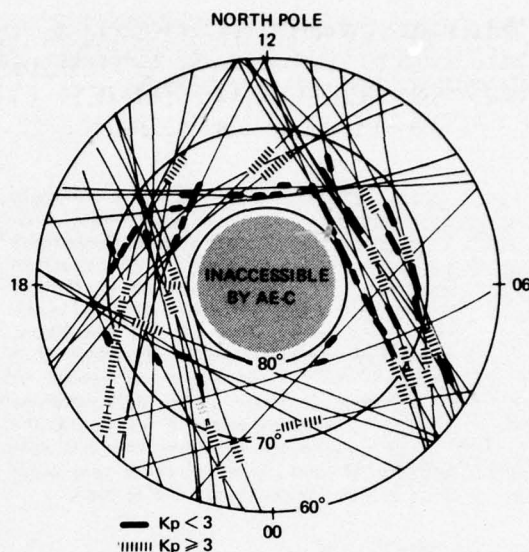


Fig. 2 Orbital tracks of AE-C over the northern high-latitude region with the location of structured (class 2) electrons for $Kp < 3$ and $Kp \geq 3$.

rent uncertainties concerning the location of the cusp region, the nature of daytime auroral phenomena, and the source and charge carriers of field-aligned currents.

REFERENCES

1. J. P. Doering, T. A. Potemra, W. K. Peterson, and C. O. Bostrom, "Characteristic Energy Spectra of 1 - 500 eV Electrons Observed in the High Latitude Ionosphere from Atmosphere Explorer-C" (submitted to *J. Geophys. Res.*).
2. J. P. Doering, W. K. Peterson, C. O. Bostrom, and J. C. Armstrong, "First Results from the Atmosphere Explorer-C Photoelectron Spectrometer Experiment," *J. Geophys. Res.*, **80**, 1975, pp. 3934-3944.
3. J. P. Doering, C. O. Bostrom, and J. C. Armstrong, "The Photoelectron Spectrometer Experiment on Atmosphere Explorer," *Radioscience*, **8**, 1973, pp. 387-392.

Authors: T. A. Potemra and C. O. Bostrom

Support: NASA

FIELD-ALIGNED CURRENTS IN THE SOUTHERN AURORAL ZONE MEASURED BY TRIAD

Auroral phenomena have been studied in the north polar regions since the last century by means of their dramatic optical emissions. Similar auroral phenomena have long been expected to occur in the southern polar regions, but because of the remote location of appropriate Antarctic land areas with respect to populated areas, and the very severe weather conditions, very few measurements have been made there. With the establishment of a satellite ground station at McMurdo, Antarctica, in March 1974, data obtained from the magnetometer experiment on board the Navy/APL Triad satellite are providing the first continuous mapping of field-aligned currents and associated phenomena in the southern auroral zone.

BACKGROUND

The concept of field-aligned currents in the auroral region was introduced by Birkeland in 1908 but remained a subject of controversy until 1966 when the single-axis magnetometer measurements from the Navy/APL satellite 1963-38C provided the first direct evidence for their existence in the northern polar regions (Ref. 1).

The first *vector* magnetic field observations in the northern polar regions were made by the Navy/APL Triad satellite, which was launched into a circular

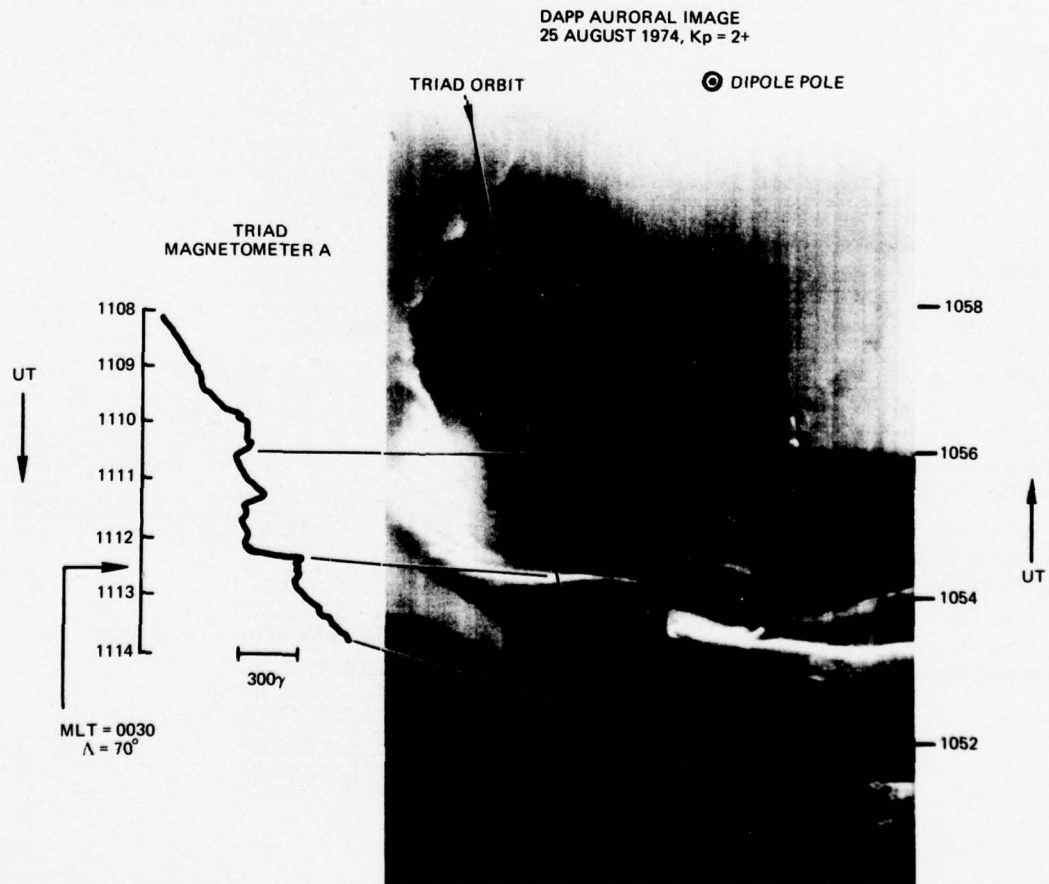


Fig. 1 Image of visual auroral arcs in the southern auroral zone obtained by the DAPP satellite, with the orbit of the Triad satellite superimposed. The magnetic field recorded by one of the magnetometers on board Triad is plotted on the left. The south magnetic (dipole) pole is shown at the top of the figure.

polar orbit at 800-km altitude on 2 September 1972. The observations were obtained with an on-board three-axis flux-gate magnetometer at a rate of 2.25 samples per axis per second with a resolution of 12γ (where the total geomagnetic field intensity is approximately 0.5 gauss, or 50 000 γ). The data, obtained from a satellite ground station in College, Alaska, have been used in several studies of auroral phenomena in the northern polar region (Refs. 2 through 6).

Data recording was begun at McMurdo, Antarctica, in March 1974 and continues to the present time. These data have been used for the first time to study the amplitudes, directions, and spatial distribution of field-aligned currents in the southern auroral zone (Ref. 7). The information accumulated by the Triad

magnetometer experiment in the north and south auroral zones is expected to play a very important role in future studies of the major complex mechanisms that couple energy from the sun, through the magnetosphere, to the atmosphere and ionosphere. The importance of the field-aligned currents can be appreciated by the fact that their total intensity varies between 1 million and 10 million amperes.

DISCUSSION

The intensity and direction of currents, J , in the auroral region are determined from the Triad magnetic field measurements, B , with the Maxwell equa-

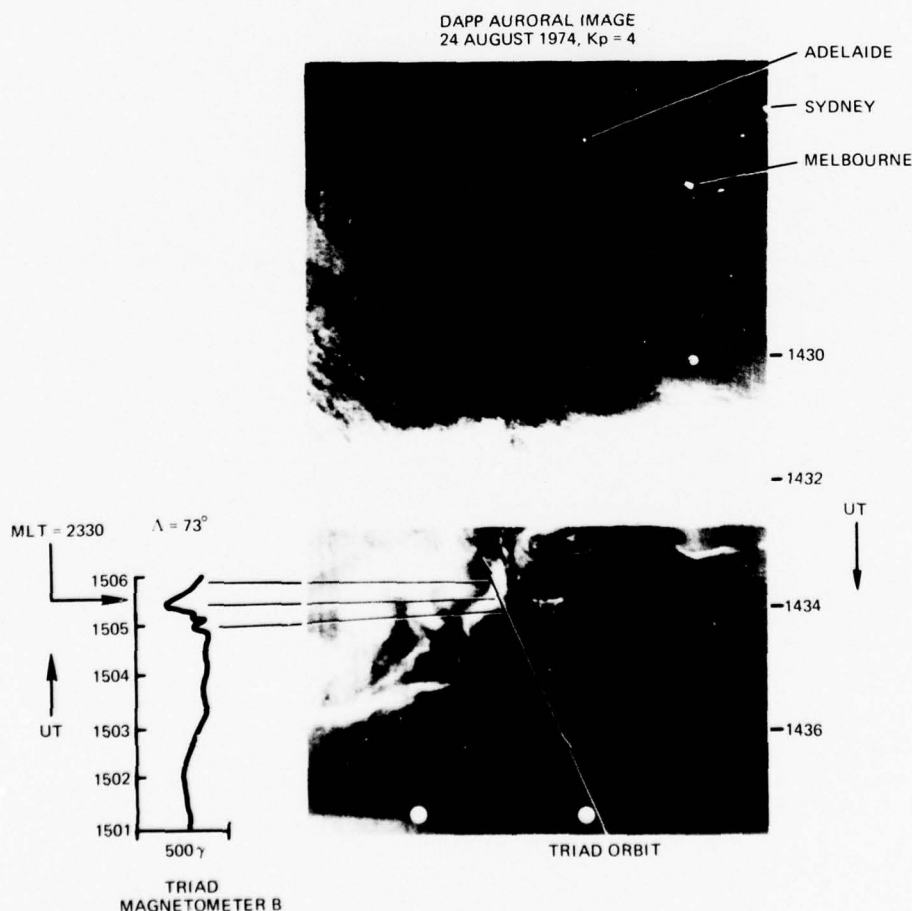


Fig. 2 Image of visual auroral features and Australian city lights obtained by the DAPP satellite, with the orbit of the Triad satellite superimposed. The magnetic field recorded by one of the Triad magnetometers is plotted on the left. The south polar region is located at the bottom of this figure.

tion $\mathbf{J} = \frac{1}{\mu_0} \nabla \times \mathbf{B}$. Therefore magnetic disturbances observed by Triad indicate the presence of electric currents that, in some cases, may be due to streams of energetic particles bombarding the auroral atmosphere and producing optical auroral forms. Figure 1 shows an example in which a pronounced magnetic disturbance was observed by Triad over a south polar region where a visual auroral arc was concurrently observed with the optical imaging system on board the U.S. Air Force DAPP satellite. In this example, a field-aligned current equal to $2 \mu\text{A}/\text{m}^2$ was observed by Triad near magnetic local midnight (at 0030 Magnetic Local Time (MLT)) in the same region where the DAPP satellite had observed a strong auroral arc approximately 18 minutes earlier.

Figure 2 shows a similar example of aurora, with the lights of major cities in Australia also appearing. In this case, the magnetic disturbance detected by Triad indicates that a pair of upward and downward current sheets with intensities of approximately $3 \mu\text{A}/\text{m}^2$ occurred in a region where a large auroral form was photographed by the DAPP satellite approximately 30 minutes earlier.

Not all current systems detected with the Triad satellite can be associated with visual auroral features, principally because of the threshold energy of the current particles required to produce optical emis-

sions. Consequently, besides providing the only continuous vector magnetic field measurements in both hemispheres, the Triad satellite is the most sensitive means of detecting the energy input to the earth's auroral zones.

REFERENCES

1. A. J. Zmuda, J. H. Martin, and F. T. Heuring, "Transverse Magnetic Disturbances at 1100 Kilometers in the Auroral Region," *J. Geophys. Res.*, 71, 1966, pp. 5033-5045.
2. J. C. Armstrong and A. J. Zmuda, "Triaxial Measurement of Field Aligned Currents at 800 Kilometers in the Auroral Region: Initial Results," *J. Geophys. Res.*, 78, 1973, pp. 6802-6807.
3. A. J. Zmuda, T. A. Potemra, and J. C. Armstrong, "Transient Parallel Electric Fields from Electromagnetic Induction Associated with Motions of Field-Aligned Currents," *J. Geophys. Res.*, 79, 1974, pp. 4222-4226.
4. T. Iijima and T. A. Potemra, "The Amplitude Distribution of Field-Aligned Currents at Northern High Latitudes Observed by Triad," *J. Geophys. Res.*, 81, 1976, pp. 2165-2174.
5. M. Sugiura and T. A. Potemra, "Net Field-Aligned Currents Observed by Triad," *J. Geophys. Res.*, 81, 1976, pp. 2155-2164.
6. R. T. Tsunoda, R. I. Presnell, and T. A. Potemra, "The Spatial Relationship between the Evening Radar Aurora and Field-Aligned Currents," *J. Geophys. Res.* (in press), 1976.
7. T. A. Potemra, T. Iijima, and S. Favin, "Field-Aligned Currents in the North and South Auroral Regions Measured with Triad," *Trans. Am. Geophys. Union*, 56, 1975, pp. 617-618.

Author: T. A. Potemra

Support: National Science Foundation,
Office of Naval Research,
and Defense Mapping Agency

COMPLETION AND LAUNCHING OF SMALL ASTRONOMY SATELLITE-C

The Small Astronomy Satellite-C (SAS-C) was launched by a Scout rocket on 7 May 1975 from the San Marco Equatorial Range, Kenya, East Africa, and is performing well in orbit. The third astronomy satellite developed by APL for NASA, SAS-C carries an X-ray experiment designed by The Massachusetts Institute of Technology. The design, fabrication, and testing of SAS-C (Fig. 1) extended over a 3½-year period and culminated in a successful astronomy mission to explore the X-ray sources of the celestial sphere.

BACKGROUND

SAS-C completes the series of three astronomy satellites built by APL for NASA Goddard Space

Flight Center and launched from the San Marco Range. After achieving the desired orbit, SAS-C was designated SAS-3 by NASA. SAS-A, also called Uhuru, was launched on 12 December 1970. It carried an X-ray detector experiment made by American Science and Engineering Company. SAS-B, launched on 16 November 1972, carried a gamma-ray telescope developed by Goddard. Much important new information about the celestial sphere was obtained from these satellite experiments.

The areas of X-ray astronomy being investigated by SAS-C include the location of X-ray sources to 15 arc seconds, the existence and identification of very weak extragalactic sources, the properties of transient X-ray phenomena associated with novae and super-

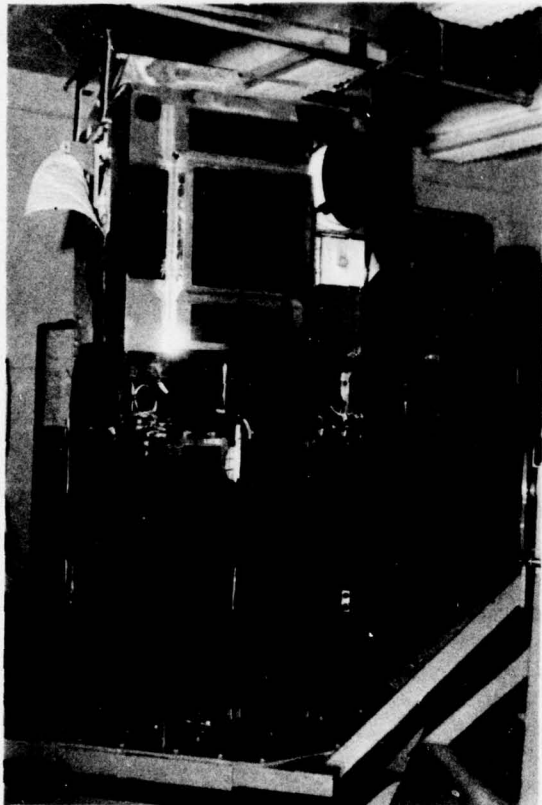


Fig. 1 SAS-C being tested by APL.

novas, the absorption of the low-energy diffuse X-ray background by interstellar matter, the long- and short-term variations of Scorpius X-1, the detailed energy spectrum of X-ray sources and the background from 0.1 to 50 keV, and the periodic time variations of X-ray sources (e.g., X-ray pulsars) with periods from 10^{-13} to 10^3 s. The instrumentation for the experiment was designed and fabricated by the Center for Space Research of MIT.

The spacecraft control section, which was designed, fabricated, and tested by APL, includes all the support instrumentation required to provide attitude control, data storage and transmission, command control, and power.

DISCUSSION

The specifications developed by NASA and MIT for the scientific missions required a complete redesign from those used in the SAS-A and SAS-B satellites. The structure was required to support up to 400 lb of

experiment instrumentation, and the larger power system involved a new solar array panel configuration and a new deployment method. Three-segment solar array panels with triple-hinge assemblies enabled the panels to be folded inside the heat shield during launch and deployment. New design techniques ensured that the array deployed symmetrically, without colliding with any part of the spacecraft. Computer simulation of the hinge-spring constants and panel mass provided good insight to its deployment characteristics. An actual deployment test with an engineering model verified the computer simulation and proved the adequacy of the design.

ATTITUDE SYSTEM. The attitude control system of SAS-C (Refs. 1 and 2) provides considerably more precise performance than did those of SAS-A and SAS-B. The heart of the SAS-C attitude system is an active closed-loop control of spin rate with redundant integrating rate gyro sensors and ground command call-ups for a specific spin rate. The desired spin rate is transmitted to the satellite as a digital word that is converted into an analog voltage to be compared with the analog output of the rate gyro. The error voltage is then used to control the speed of the reaction momentum wheel, thus adjusting the spin rate of the outer satellite body to the required value. Many other features are described in Refs. 1 and 2.

TELEMETRY SYSTEM. The telemetry system is basically a standard pulse coded modulation (PCM) digital readout phase modulating a VHF transmitter. The telemetry system has two modes of operation: a fixed format established and programmed into a PROM memory before launch, and a variable format using core storage. The variable format can be changed from the ground by loading specific programs into the core storage. In addition, bit rates can be changed from 125 bits per second in doubling steps to 16 000 bits per second.

By ground command, operation can be switched from fixed to variable format. There are two redundant sections in the fixed format and two in the variable. The variable format was operated during launch. In this way a launch format was available in one section and an experiment data format in the other. After launch, a single ground command was used to switch from the first section to the second, enabling a change from launch housekeeping data to experiment data. An ultrastable crystal-controlled oscillator is used to generate the clock for the telemetry system as well as other frequency-dependent systems. This oscillator has a basic stability of 10^{-10} per hour within the normal operating satellite temperature. Thus all the timing and control functions of the satellite have a stable frequency source. Other important features of the telem-

etry system are three 64-channel analog commutators and two 16-channel digital commutators, an analog-to-digital converter, error coding, and tape recorders for the storage of data.

COMMAND SYSTEM. The SAS-C command system uses the standard NASA 64-bit FSK word, AM modulated 50% by a sine-wave bit-synchronizing signal. The system consists of redundant antennas, receivers, bit detectors, decoder logics, power switching relay coil matrices, and delayed command systems connected so that either redundant system can be chosen by proper coding of the command word rather than by switching system connections. It provides 56 relay commands on and off and any number of data commands utilizing 24 bits of the command word for coding. A total of 15 commands of any combination can be stored in each redundant delayed command system, giving a total of 30 delayed commands if desired. Delays of from 3 s to 2.4 h can be achieved with about 2-s minimum separation. The resolution time of execution of the first command can be on the order of 0.5 ms if all parameters affecting transmission time, etc. are considered. A program of delayed commands can be stored for continual recycling since the commands are not destroyed when used but are recycled into storage. It is not necessary to use all 15 commands in either of the two storage systems since zero bits can be inserted to fill the complete storage, thus recycling all bits to their original positions.

The delayed command system is of special importance to the operation of the SAS-C attitude control system. It allows changes in altitude such as $+z$ -axis precession, spin rate changes, etc. to be done at any time in the orbit rather than only when the spacecraft is directly over the control station. Other commands can also be executed by the delayed command system, e.g., turning on heaters and other housekeeping systems at the beginning or end of a sunlit period.

POWER SYSTEM. The SAS-C power system includes a solar cell array, a nickel-cadmium battery, and a charge control system. The solar cell array provides a minimum of 65 W (orbit average), and the battery has a nominal capacity of 9 Ah.

The charge control system consists of a digital coulometer including a voltage limiter. The coulometer meters the ampere minutes charge and discharge. The coulometer is adjusted so that when 101, 105, 110, or 125% (as chosen by ground control) of the discharge power has been returned during the charge cycle, the unwanted current is shunted by the coulometer and voltage limiter.

The charge control circuits are redundant and can be chosen by command switching. A low-voltage

sensing switch removes the battery and all loads except the command system from the bus when the battery reaches a predetermined value of 13.2 V. The battery is still connected to a small portion of the solar cell array, allowing it to charge at a trickle charge rate. The nominal battery voltage is 16.1 V.

The solar cell array blades can be rotated by ground command to collect the sun's energy efficiently as the spacecraft attitude changes with respect to the sun. In this way, a relatively constant array power can be made available at all attitudes.

THERMAL CONTROL. An active thermal control system is used in SAS-C together with some passive thermal insulation. Thermal louvers were installed between the heat dissipating elements such as the battery and electronics books and the thermal radiator. The louvers, similar to venetian blinds, open and close, depending on the temperature of the thermal sensors. When the louvers are open, heat is released through a low radiation path to the radiator. When the louvers are closed, the radiation path resistance is increased and heat is conserved by restriction to the radiator panels. Thus a relatively constant internal temperature is maintained with changing heat loads, either internal or external.

POSTLAUNCH OPERATIONS. The spacecraft was shipped to the San Marco Equatorial Range on 5 April 1975 and was launched as scheduled on 7 May 1975. The first few days of orbit operation indicated that all systems were functioning as designed. Scientific observations began about four or five days after launch. It was then discovered that the passive nutation damper had stuck to one side and no longer was able to oscillate with nutation motion. After a week or so, the nutation damper became free and has been operating satisfactorily since.

The active spin rate control has been performing beyond expectations. A dither mode has been used wherein the spin rate is made to vary in an oscillatory fashion to permit scanning of a specific X-ray source until it is obscured by the earth. The dither mode can be repeated as needed by allowing the delayed command program to be recycled.

A zero spin rate command is initiated at a specific time by means of the delayed command feature to provide a constant space stabilized azimuth angle for a period of time. This gives a longer integration time for the data from a simple source than does the scanning mode.

A variable spin rate using a faster or slower spin rate during the dark side with respect to the sunlit side can be programmed during one orbit so that the inte-

grated spin rate is one revolution per orbit. This enables the X-ray sensors to scan the same portion of the sky during each orbit for a long integration time.

The orientation of the spin axis is controlled or maneuvered by programming the strength of the z magnetic dipole reacting against the earth's magnetic field. A desired declination and right ascension can be accomplished to 1 or 2°. The z-axis drift is less than 0.5° per day.

GEOS-C SPACECRAFT LAUNCH AND EARLY ORBIT OPERATIONS

On 9 April 1975, the GEOS-C spacecraft, built by APL, was successfully launched by a NASA Delta Class 1410 rocket from SAMTEC, Vandenberg Air Force Base, CA. The satellite is demonstrating the feasibility of radar altimetry from satellites as well as the feasibility of satellite-to-satellite tracking.

BACKGROUND

APL began developing the GEOS-C spacecraft for NASA Wallops Flight Center in July 1972. GEOS-C represents a transition from the National Geodetic Satellite Program, which included the ANNA and GEOS-1 and -2 spacecraft developed by APL, to the emerging Earth and Ocean Dynamics Applications Program. In addition to the radar altimeter, this spacecraft carries an S-band transponder, two C-band transponders, a laser retroreflector, and a dual-frequency doppler beacon. It is being tracked by ground-based S- and C-band radars, by laser trackers from both fixed and mobile sites, by the U.S. Defense Mapping Agency's network of satellite tracking stations (TRANET) including Station 111 at APL, and by geocivers. This multiple tracking capability serves to calibrate the radar altimeter accurately and is providing further calibrations of NASA and other ground-based C-band systems as well as data for continued geodetic studies. The laser retroreflector also supports long-term (20-year) geodetic studies as well as the San Andreas Fault Experiment.

REFERENCES

1. G. A. Fountain and F. F. Mobley, "SAS-C Attitude Control System," *Applied Physics Laboratory Developments in Science and Technology, Fiscal Year 1974*, APL/JHU DST-2.
2. American Institute of Aeronautics and Astronautics (AIAA), Paper No. 74-901, August 1974.
3. "A Programmable Sampling Format Telemetry System," *Proceedings of 1973 International Telemetry Conference*, October 1973, pp. 350-361.
4. M. R. Peterson, "A Programmable Sampling Format Telemetry System for the Small Astronomy Satellite-C," *Applied Physics Laboratory Developments in Science and Technology, Fiscal Year 1973*, APL/JHU DST-1.

Author: H. B. Riblet

Support: NASA Office of Space Science

DISCUSSION

Following liftoff at 2358 UT on 9 April 1975 (Fig. 1), near-nominal performance of the Delta 1410 launch vehicle placed GEOS-C into the following orbit:

Epoch	75Y10M07D, 00 h 00.00 min UT
Apogee	853.05 km
Perigee	829.56 km
Period	101.74 min
Inclination	114.989°
Eccentricity	0.001627
Semimajor axis	7219.47 km

These parameters are all well within the tolerances specified before launch and will facilitate carrying out the scientific objectives of the mission. The orbiting satellite has been identified by NASA as GEOS-3 (international designation 1975 027A, Spadat Catalog No. 7734).

Prior to launch, GEOS-C was given a comprehensive series of electrical performance and environmental tests at APL and at NASA Goddard Space Flight Center. These tests extended from late in the spring of 1974 through February 1975. The flight radar altimeter was received from General Electric

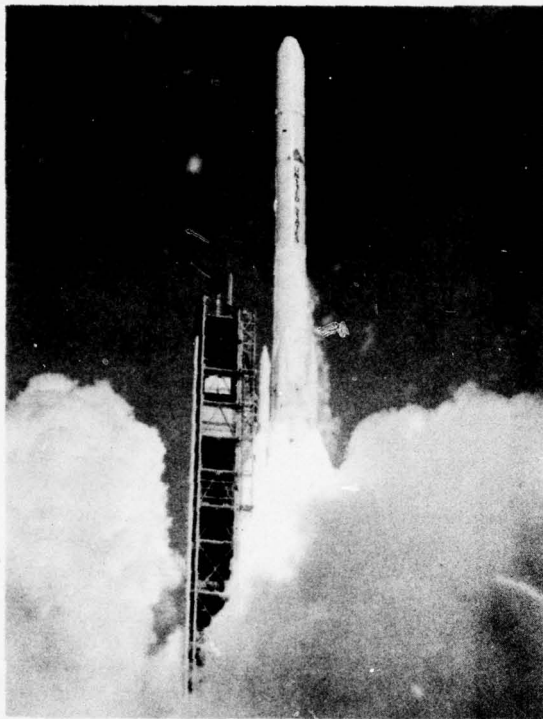


Fig. 1 Liftoff of Delta rocket, Serial No. 109, on 9 April 1975, which successfully launched the GEOS-C spacecraft into the desired orbit.

Co. in September 1974 and integrated with the spacecraft. The test series verified the ability of the spacecraft and its experiments to meet all performance requirements and showed that performance would not be adversely affected by the launch and orbital environments.

Only two significant anomalies occurred during the test program. Thermal balance tests determined that the internal spacecraft temperatures were too low. Localized changes in thermal coatings and adjustments to thermal insulation corrected the problem. During the cold-temperature excursion portion of the thermal-vacuum performance test, the telemetry transmitter modulation index decreased. The transmitter was removed from the spacecraft and subjected to a series of special tests, which indicated that the anomaly was probably a tuning problem within the transmitter induced by low temperatures within a narrow range. Comparison with the acceptance test results for the transmitter indicated that the condition may have existed at that time and was probably stable.

Based upon these conclusions and calculations showing that some link margin exists in the presence

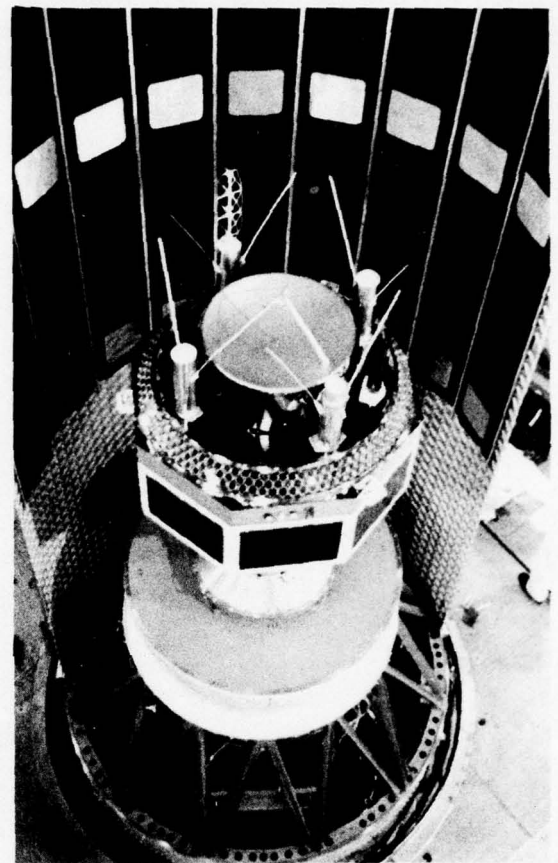


Fig. 2 GEOS-C mounted on Delta launch vehicle, showing half of the nose fairing installed.

of the anomalous behavior, and the fact that even if the transmitter were to fail altogether the Project Approval Document objectives could be achieved by using the S-band link, it was decided to fly the transmitter unchanged. APL then completed the spacecraft acceptance tests and, following a NASA Consent to Ship Review on 13 and 14 February 1975, shipped the spacecraft to Vandenberg Air Force Base. On 1 April, the spacecraft was mounted on the launch vehicle (Fig. 2), and final tests were conducted during the countdown.

On the first pass after injection into orbit telemetry telltales revealed that all systems were still in the launch state and the solar array was producing electrical power. A test load was injected into the delayed command system from the NASA Winkfield, England, station during this first orbit, and actuation of the commands was observed at the NASA Ororal, Australia, station.

During the second orbit, the gravity gradient boom was deployed approximately 0.76 m (2.5 ft), and the planned gravity capture scheme was initiated. On 11 April, the boom was extended to about 1.2 m (4 ft) to excite some yaw motion. By 12 April, the gravity capture sequence was completed, with the boom fully extended and then trimmed to about 6.5 m (21 ft 2.45 in.). On 14 April, the pitch angles were less than 3.7° , and roll and yaw angles were less than 1° . Specified attitude control (less than 1° for all axes) was achieved during the week of 20 April.

During the gravity capture phase, the C-band transducers were activated and the doppler beacons were turned on and successfully tracked by TRANET. Nominal operation of all spacecraft systems was verified, and satellite temperatures were found to be within the expected range.

Successful operation of the radar altimeter in global mode was achieved during orbits 66, 69, and 75 (14 and 15 April). The S-band antenna switching system checked out correctly on 15 April. During orbit 89 (16 April), the S-band satellite-to-satellite link was verified. For this demonstration the satellite was in an all-up condition, with the altimeter functioning and its data being relayed via the Applications Technology Satellite 6 (ATS-6) to the NASA Rosman, NC, station. Altimeter data were also telemetered via the VHF link directly to NASA stations at Quito, Ecuador, and Merritt Island, FL.

Engineering evaluation of the satellite was complete on 20 April; experiment calibration commenced the following day and continued until 20 May. During this period, Wallops conducted underflights with C-54 aircraft to provide ground truth.

The satellite continued to perform satisfactorily until an evening pass on 12 May 1975, when the command system started throwing spurious relays whenever OFF relay commands were sent through logic 1 matrix 1. The ON relay commands through matrix 1 and ON or OFF commands through matrix 2 are operating properly. Analysis of the problem indicated the most probable cause to be a wire shorted across a diode. Recommendations on how to reduce the operational consequences of the failure to a negligible level were given to NASA and have been implemented.

Since 20 May 1975, the satellite has been used for global activities (Phase C of the mission operations plan) wherein the ATS-6 satellite is used to obtain four arcs of Satellite-to-Satellite Experiment (SSE) data per day. During each of the SSE arcs, radar altimeter data will be scheduled for most portions of the arcs that are over ocean areas. Also, C-band, S-band, laser, and doppler data are being obtained to support orbit determination for the SSE and radar altimeter data arcs.

During Fiscal Year 1976, the GEOS-3 satellite will enter Phase D of the mission operations plan, which consists of unique experiments and localized grid activities. In addition to these major activities, intermittent calibration and evaluation activities will be conducted at the nominal rate of once per month.

Author: L. D. Eckard, Jr.

Support: NASA Wallops Flight Center

HYDROGEN MASER FREQUENCY STANDARD IN OPERATION AT APL TIME AND FREQUENCY STANDARDS LABORATORY

The APL Time and Frequency Standards Laboratory has placed in operation a NASA Model NP hydrogen maser frequency standard. The unit, the primary reference standard for a NASA hydrogen maser development program at APL, permits the Laboratory to make more accurate stability measurements than were previously possible. The hydrogen maser is also being used in the evaluation of precision time and frequency instrumentation developed for other APL programs.

BACKGROUND

Precision time and frequency measurements depend strongly on the quality and stability of the reference standards available. When the reference standards are of a quality comparable to the devices being measured, tedious statistical means must be used to separate the errors associated with the device from those of the reference. However, when the reference standard is highly superior, the measurements can be made directly and less data-processing time is needed.

The atomic hydrogen maser is the most stable type of frequency source known. Its short-term stability, or spectral purity, is outstanding, making it a superior reference standard.

DISCUSSION

APL received the NASA hydrogen maser Model NP-1 (Fig. 1) from Goddard Space Flight Center in early 1975 for retention as a reference working model. APL, with Goddard assistance, has restored the maser to working condition. The APL Time and Frequency Standards Laboratory has gained experience in its operation and monitors it continuously.

The hydrogen maser is an active oscillator powered by energy from electron-proton magnetic interaction of excited hydrogen atoms. The working components of the hydrogen maser are shown in Fig. 2. Molecular hydrogen gas is introduced into a dissociation bulb. There, RF excitation converts the molecular hydrogen, to excited atomic hydrogen, which passes through a collimator (a number of small parallel tubes) into a state selection magnet. Atoms of the desired atomic energy are focused into a beam that passes through a hole in the vacuum enclosure and into a Teflon-lined quartz storage bulb that is centered

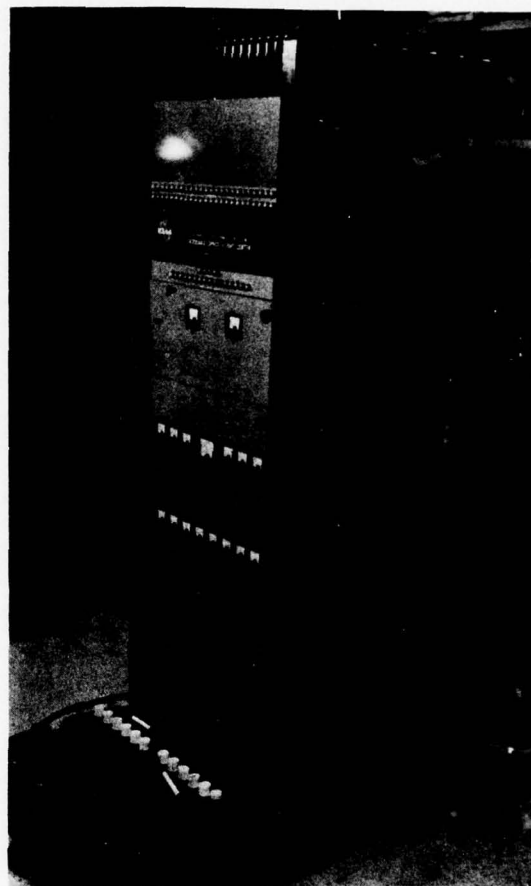


Fig. 1 NASA Model NP-1 hydrogen maser.

in a resonant microwave cavity. The atoms moving with thermal kinetic energy collide with the wall of the storage bulb and are reflected back and forth until they finally leave by the hole they entered and are absorbed by the VACION vacuum pump. While the excited atoms are in the storage bulb (about one second), they give up their excited state energy to increase the energy in the RF field of the resonant microwave cavity. In accordance with the uncertainty principle, this unusually long energy decay time (about one second) provides the characteristic for a very

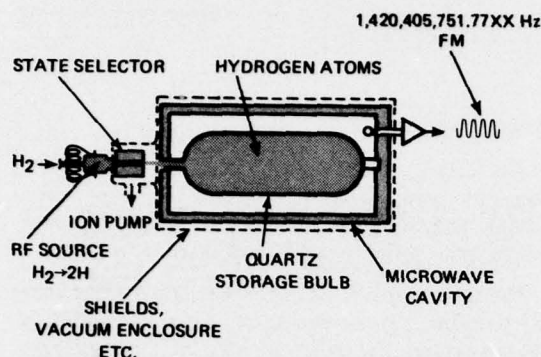


Fig. 2 Components of the hydrogen maser.

monochromatic radiation field to exist in the cavity. This energy at 1 420 405 751 Hz is coupled out loosely and used to phase lock standards at more convenient working frequencies such as 5 MHz.

The hydrogen maser has been used to evaluate the performance of another unit of the same design, NP-1/NP-4, and to measure the performance of the cesium frequency standard of the APL Time and Frequency Standards Laboratory. It has also been used to measure the characteristics of two crystal oscillators designed for spacecraft applications. The results are presented as Allan variances in Fig. 3. The Allan variance is a statistical determination of the uncertainty of a frequency measurement made over a specified interval of time using the device under test as a time standard.

As a part of the maser development program, APL is training staff members to make major repairs on the NP type masers to sustain service from these designs in experimental field operations. The NP-4

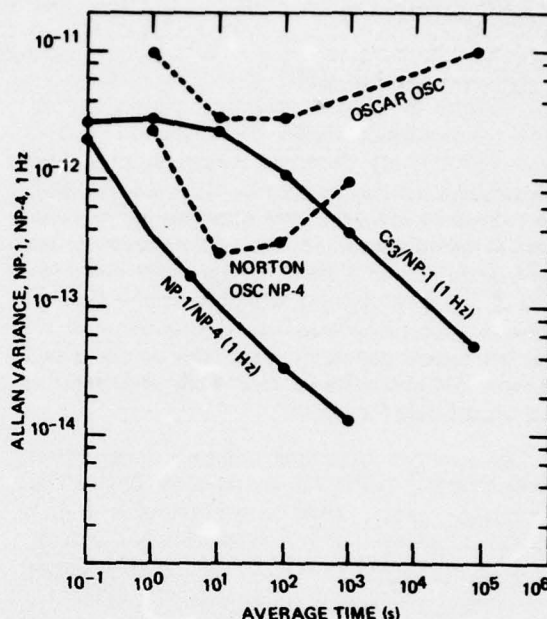


Fig. 3 Allan variance measurements of precision frequency standards relative to a hydrogen maser.

maser, the second unit to be worked on, was disassembled, repaired, revised, and reassembled. After a training and education period of five months, APL feels qualified to build for NASA additional hydrogen masers of an improved design for field service.

Author: L. J. Rueger

Support: NASA Goddard Space Flight Center

A "STORE AND FORWARD" TELEMETRY COMPUTER PROGRAM DESIGNED USING COMPUTER SIMULATION

The design of a set of interrupt-driven software algorithms has been accomplished by APL for NASA Goddard Space Flight Center (GSFC). The key algorithm, Digital Storage System (DSS), automates collection, storage, and forwarding of high-rate digital

telemetry information using a network of minicomputers. Extensive simulation testing by computer permitted assessment of the impact on system throughput of various hardware/software tradeoffs before system implementation.

APL was asked by GSFC in 1972 to investigate a configuration of computer equipment proposed to augment the worldwide Satellite Tracking and Data Network (STADAN). Increased remote-site capabilities are required because the number of transmitting satellites and their individual data rates have increased far beyond the information capacity of the present system. Such disparities as a predicted aggregate data input rate of 1 000 000 bits per second to remote sites now provided with a maximum data relaying rate of 28 500 bits per second require a considerable on-site storage capacity for non-real-time data, while real-time data are immediately forwarded.

APL was requested to propose a new computer interface for the existing rotating magnetic drum and to define software strategies for the file processor that

DISCUSSION

The specific objectives of the simulation effort were (a) to prove the correctness of software algorithms, (b) to explore the effect on subsystem performance of various equipment alternatives, and (c) to determine performance parameters of the optimized system. IBM's Computer System Simulation Language (Ref. 1) was chosen as the simulation vehicle since it had sufficient generality to permit detailed modeling of the projected minicomputer control program, but was of a high enough level to require only the parameterized specification of standard digital computer peripherals.

The design philosophy applied to the DSS control program was one of interrupt-responsiveness, motivated by the relentless arrival of telemetry information in real time from sources external to the subsystem. The identification of key subsystem functions permitted a fixed priority ranking among software components and suggested an optimum priority place-



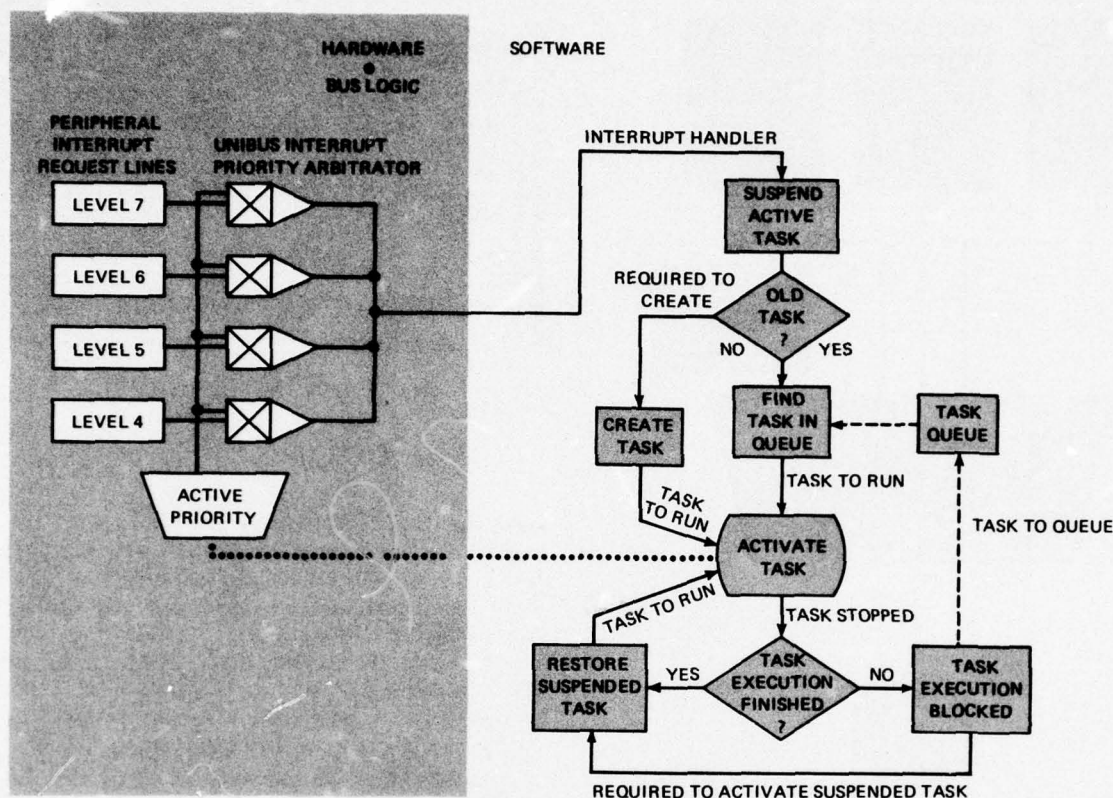


Fig. 2 Digital Storage System hardware/software scheduler.

ment of computer peripherals on the file processor UNIBUS. This placement, combined with both the fixed priority ranking of software functions and the PDP-11/20 computer's interrupt architecture, permitted responsive, highly adaptive software interruptibility.

The general input/output scheduling strategies chosen for DSS involve immediate initiation of an operation to an idle peripheral, placing a command into a list threaded by priority if the peripheral is still engaged in a previous operation, and always choosing the top element of the preordered list upon receipt of an operation-complete interrupt (Fig. 2). A significant exception is applied to the file processor drum since, if its rotation is unaccounted for, immediate initiation of an operation to a random data sector will cause unacceptably long waiting times for a correct sector to arrive under the read/write heads. The strategy developed involves building many threaded lists, three for each drum sector, representing the storage functions, telemetry data storage, network data forwarding, and on-line temporary tape storage.

The drum interface schedules the drum operation-initiation software via a position interrupt, which acknowledges the arrival of sector S , to which the software responds by initiating a previously selected operation for sector $S + 1$ and then preselects an operation for sector $S + 2$ from among the three possible functions for that sector. Furthermore, the choice of preselected operations is determined by the amount of core-resident telemetry data waiting to be stored on the drum.

The temporary clearing of telemetry data from the drum to the tape drives is necessary because, at the predicted aggregate data input rates and the limited forwarding rates, the drum capacity is sufficient to store only two minutes of telemetry information without overflowing. The drum space-clearing function, initiated shortly before overflow, applies a set of criteria including forwarding status, message length, and intermessage priority to select the optimum message to be transferred for drum space recovery (Fig. 3). If the message selected has been completely forwarded, space may be regained quickly by merely

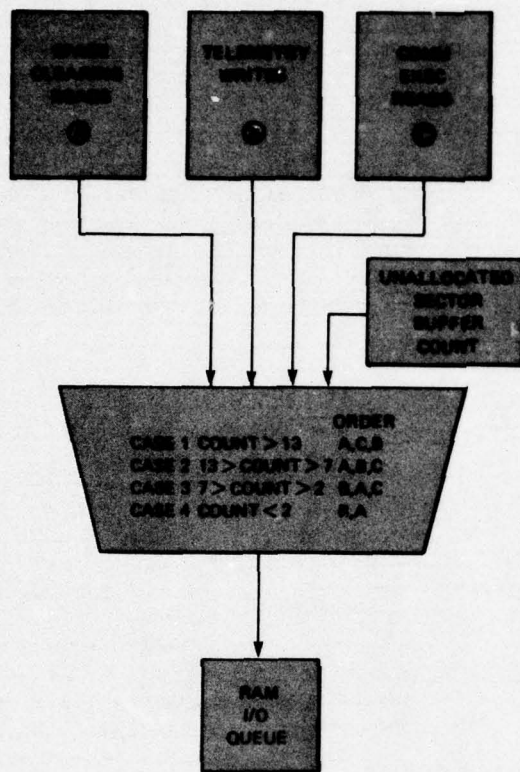


Fig. 3 Algorithm for adaptive drum operation selection.

detecting drum data index entries. For still-resident data, clearing is accomplished at almost maximum tape-writing speeds by overlapped read command generation utilizing two tape buffers. Finally, since the computer operator must assist in replacing full tapes, two tape drives are devoted to space clearing to lessen operator fatigue.

The results of many simulation runs are summarized in Fig. 4. They demonstrate that the DSS software design is capable of meeting a maximum steady-state input rate of 925 000 bits per second. Comparison of these results with earlier runs indi-

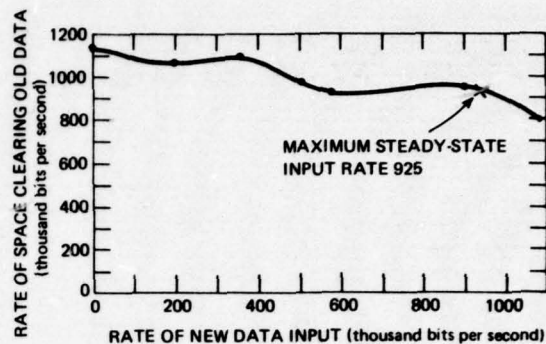


Fig. 4 DDPS performance curve.

cated that only a 5% increase in space-clearing rate was achieved by a 25% increase in tape speed, and led to the incorporation of a multisector read capability in the drum hardware interface design to reduce the number of clearing-related interrupts that were revealed to be the limiting factor. Inspection of the file processor software utilization suggests that UNIBUS loading may limit subsystem performance even if a faster processor is used.

GSFC has requested that APL implement a prototype file processor subsystem to validate the simulation results and to provide a test site for the APL drum interface design.

REFERENCES

1. *Computer System Simulator II (CSS-II), Program Description and Operations Manual*, International Business Machines Corporation GH20-4163-0, December 1970.

Author: N. K. Brown

Support: NASA Goddard Space Flight Center

PREDICTION OF RAIN ATTENUATION STATISTICS

Attenuation by reflection and scattering of electromagnetic signals by rain increases as the frequency increases. Because of the present emphasis on the use of frequencies above 10 GHz for satellite-earth communication systems, knowledge of the statistics of attenuation caused by rain becomes increasingly important. Techniques to predict attenuation statistics using radar reflection data have been developed for frequencies up to 100 GHz and for arbitrary path elevation angles.

BACKGROUND

Rain may seriously attenuate satellite-earth communication signals. Useful rain attenuation statistics should not only provide an estimate of the amount of time per year that the attenuation along an earth-satellite path exceeds a given level but should also establish the optimum spacing between earth terminals so that a satellite communicating with one earth station with high path attenuation could automatically be switched to a second station having significantly less path attenuation (space diversity). Such statistics can be arrived at directly by means of experimental satellites communicating with earth terminals separated by known distances or indirectly by means of radiometry or radar measurements. At present, space diversity and attenuation statistics are still meager, and those giving the dependence on path elevation angle, frequency, and climatology are practically nonexistent.

Radar can measure rain reflectivity profiles over a large coverage area. By means of stored radar data in three dimensions, attenuation statistics may be obtained over various path elevation angles and frequencies.

During the summer of 1973, radar reflectivity profiles of rain regimes were recorded on digital tape at the Radar Atmospheric Research Facility at Wallops Island, VA, by the Radar Atmospheric Physics Group of APL. These data were obtained for various rain types out to 139 km from the radar facility (SPANDAR) and were stored on digital tape in bins for which the radar reflectivity is defined as a function of azimuth and range. By injection of this data base into modeling procedures, attenuation and space diversity statistics have been obtained for selected frequencies in the 13- to 100-GHz interval and at path elevation angles from 20 to 90° (Refs. 1 and 2).

Subsequent analysis has also demonstrated the ability to predict (a) attenuation statistics at other path elevation angles when given the statistics at a particular path angle, and (b) attenuation statistics at a third frequency when given the statistics at two frequencies.

DISCUSSION

A useful descriptor in characterizing rain observed by radar is the reflectivity factor Z (in mm^6/m^3), a quantity dependent upon the raindrop size distribution. The radar rain reflectivity, which represents a measure of the received power scattered from the rain at a particular wavelength, may be shown to be proportional to Z . A computer program was developed that can find profiles of the measured rain reflectivity factors $Z(l)$ along constructed representative earth-satellite paths passing through rain regions, where l represents the distance (in kilometers) along a path referenced to the ground terminal. The corresponding profiles for the attenuation coefficient $k(l)$ (in decibels per kilometer) were modeled from the relation

$$k(l) = a[Z(l)]^b \quad (1)$$

where the values of a and b at the individual frequencies were calculated using the raindrop distribution measured by Joss et al. in Locarno, Switzerland, for thunderstorm activity (Ref. 3).

The total attenuation, A , expressed in decibels (also referred to as the "fade depth") associated with propagation along a representative path is given by

$$A = \int_0^{l_m} k \, dl \quad (2)$$

where dl is the differential length along the path and l_m is the length along the path beyond which the measured reflectivity is negligible.

Probability estimates have been obtained by sampling the calculated attenuations along 15 080 constructed paths contained in 232 azimuths (great circle planes) covering a period of 14 rain days. Only those azimuths were selected for which an attenuation of 2 dB or greater at $f = 30$ GHz and $\theta = 45^\circ$ (equivalent to approximately 8 dB at 100 GHz) existed along at least one path per azimuth. Therefore the probability estimates obtained are "conditional" in the sense

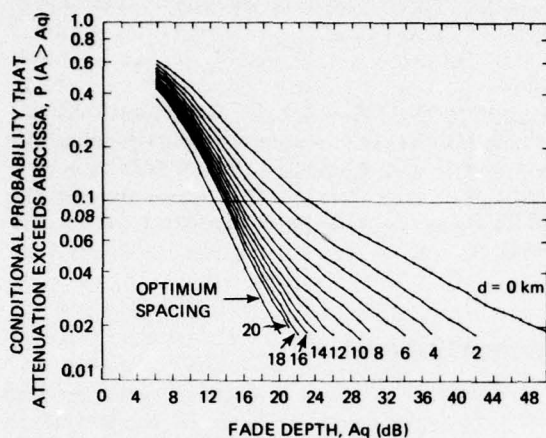


Fig. 1 Joint conditional probability that the attenuation at two terminals separated by a distance d exceeds the abscissa at a path elevation angle θ of 45° and at f of 100 GHz.

that an "attenuation event" has occurred. Figure 1 shows, as an example, probability estimates at $f = 100$ GHz and $\theta = 45^\circ$. The curve labeled $d = 0$ km represents the probability (single terminal) that the attenuation along an earth-satellite path exceeds the abscissa. The curves labeled $d = 2, 4, \dots, 20$ km represent the joint probabilities that two stations separated a distance, d , experience simultaneous fades that jointly exceed the abscissa. The curve labeled optimum spacing represents the joint probability for the case that two stations in "independent" rain environments experience fades that jointly exceed the abscissa. This joint probability is given by the square of the probability levels of the single terminal. The indicated points in the curves of Fig. 1 represent the probability levels calculated using the experimentally acquired rain reflectivity data base. All the curves are relatively smooth and approach the optimum spacing curve as the separation increases. Similar probability curves have been obtained at 13, 18, 25, and 30 GHz at path angles of 30° , 45° , and 60° .

Given the fade depth $A_q(\theta_0)$ for a path angle θ_0 , the predicted fade depth at another angle θ is given by

$$A_q(\theta) = A_q(\theta_0) \frac{\csc \theta}{\csc \theta_0} \quad (3)$$

where we associate with both fades equal probabilities of being exceeded. In Fig. 2 we examine the validity of Eq. (3) over a path angle interval ranging from 20° to 90° at $f = 100$ GHz. The solid curves repre-

θ	rms ERROR (dB)	rms ERROR (%)
20°	1.6	9.7
30°	0.8	5.2
60°	1.1	3.4
90°	0.9	7.2

— CALCULATED FROM REFLECTIVITY DATA
 ○ PREDICTED USING CSC θ VARIATION
 NORMALIZED TO $\theta = 45^\circ$ CURVE

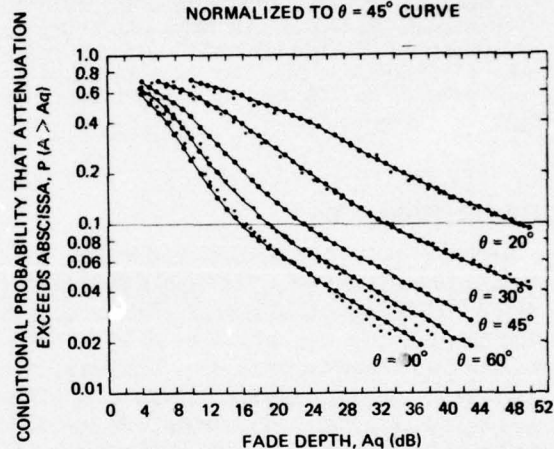


Fig. 2 Comparison of fade statistics calculated at a series of path elevation angles using the $\csc \theta$ variation at $f = 100$ GHz.

sent the single-terminal probabilities for the various path angles calculated independently using Eq. (2). The circled points represent the predicted probabilities using Eq. (3) given only the values at $\theta_0 = 45^\circ$. From the table in Fig. 2, the rms errors over the probability range considered for all the cases are less than 10%. Comparable accuracies have been demonstrated for 13 to 30 GHz over a similar probability interval.

Close agreement between the fade statistics determined using Eq. (3) and those independently determined using Eq. (2) implies that, over the range of probabilities considered, the environment may be assumed to possess an equivalent uniform reflectivity with an associated probability of being exceeded. Under such conditions of uniformity, the fade depth is proportional to path length, which in turn is proportional to $\csc \theta$ as given by Eq. (3).

The techniques used to predict statistics at a third frequency when given similar statistics at two frequencies are as follows. We use the previous conclusion that an equivalent uniform reflectivity may be defined in a region with an associated probability of being exceeded. We assign to the level of the

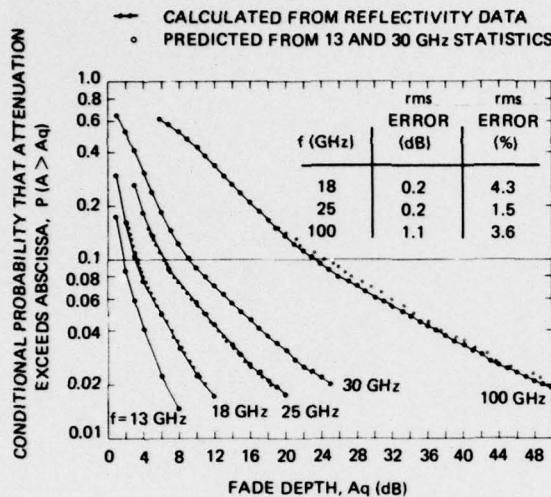


Fig. 3 Comparison of fade statistics calculated at other frequencies using 13 and 30 GHz fade statistics ($\theta = 45^\circ$).

reflectivity factor $Z = Z_0$ the probability P_0 of exceeding this level (i.e., $P_0 = P(Z > Z_0)$). Using Eqs. (1) and (2), the attenuations at frequencies f_1 and f_2 are

$$A_1 = a_1 Z_0^{b_1} l_0 \quad (4)$$

$$A_2 = a_2 Z_0^{b_2} l_0 \quad (5)$$

where l_0 is the path length through rain. We may state equivalently that the attenuations at f_1 and f_2 are A_1

and A_2 and each has associated with it the same probability P_0 that these respective attenuations are exceeded. Given the fade statistics at frequencies f_1 and f_2 , Eqs. (4) and (5) represent two equations whose unknowns are Z_0 and l_0 at each P_0 level. Hence, solving for these parameters as a function of P_0 , the fade statistics at any third frequency f_3 may be obtained using a formulation similar to Eqs. (4) or (5). Examples in Fig. 3 demonstrate the validity of the technique. The curves represent the single-terminal fade statistics calculated individually using Eq. (2) at the indicated frequencies. The circled points associated with the 18, 25, and 100 GHz curves represent the predicted levels, assuming only a knowledge of the 13 and 30 GHz statistics. Note that the predicted levels have rms errors of less than 5%.

REFERENCES

1. J. Goldhirsh and F. L. Robison, "Attenuation and Space Diversity Statistics Calculated from Radar Reflectivity Data of Rain," *IEEE Trans. Antennas and Propagation*, AP-23, No. 2, March 1975, pp. 221-227.
2. J. Goldhirsh, "Prediction Methods for Rain Attenuation Statistics at Variable Path Angles and Carrier Frequencies Between 13 and 100 GHz," *IEEE Trans. Antennas and Propagation*, November 1975.
3. J. Joss, J. C. Thams, and A. Waldvogel, "The Variation of Raindrop Size Distribution at Locarno," *Proceedings of the International Conference on Cloud Physics*, Toronto, Canada, 26-30 August 1968.

Author: J. Goldhirsh

Support: NASA Goddard Space Flight Center

BIOMEDICAL ENGINEERING

INTRODUCTION

The Johns Hopkins University School of Medicine, the School of Hygiene and Public Health, and the Applied Physics Laboratory have collaborated in a program of biomedical research and development since 1965. An important objective of the program is to apply the "know-how" of physical sciences and engineering and the systems engineering approach acquired by APL in its defense and space research to the practical solution of problems in medical research and health care delivery. The success of this program has fully justified the confidence of its founders that fruitful collaboration of engineering and medical specialists would be attained through working side by side in solving real and important problems.

The program has grown to include nearly all the clinical departments and several of the basic science departments of the medical divisions. More recently, the Johns Hopkins Hospital has joined the collaboration. Active program areas include Nuclear Medicine, Ophthalmology, Neurosensory Instrumentation, Radiography, Cardiovascular Systems, Prosthetic Systems, Biomedical Engineering, and Clinical Engineering. The application of state-of-the-art technology has contributed to basic biomedical research, clinical diagnosis, and patient therapy through improved knowledge, instruments, and techniques.

The results of biomedical engineering research and development are disseminated by about 10 to 20 publications per year in the medical and biological literature, by presentations at scientific and medical meetings, and through the teaching activities of the Johns Hopkins Medical Institutions. Representative of the latter is the Masters program in Clinical Engineering developed in collaboration with the Department of Biomedical Engineering of the Medical School, which is completing its second year.

The accomplishments reported here are representative of the wide scope of activities in the program, from basic research to improved health care delivery systems.

JHH MINI RECORD SYSTEM

The Mini Record Demonstration was developed by APL in conjunction with the Johns Hopkins Hospital staff as a pilot effort. The primary objective of the Mini Record Demonstration is to implement and evaluate the use of a low-cost, medical-summary/problem-list retrieval system for General Medical Clinic outpatients. At the conclusion of the project, a fully operational system was implemented. This system is currently in use at the General Medical Clinic; its impact on health care delivery is the subject of an extended JHH evaluation.

BACKGROUND

The Johns Hopkins Hospital performs the services of family physician for a large portion of the local population as well as for a fairly extensive outpatient referral group from suburban hospitals through approximately 100 outpatient clinics servicing almost 100 000 patients each year. The General Medical Clinic provides ongoing care to outpatients with chronic problems that do not fall within the purview of specialty clinics such as Diabetes Management. However, General Medical Clinic patients do visit specialty clinics and, in off hours, the Emergency Room.

The General Medical Clinic treats approximately 7000 patients a year; they constitute as varied a population as any found at JHH. It was selected as the focus for this pilot effort because the availability of a computer-managed on-line Mini Record could be most effectively tested on a group of this size and makeup.

Specific objectives of the system were to:

1. Provide continuity in medical care for those patients who rely upon the General Medical Clinic as their primary source of health care or are currently being treated by more than one clinic. This should result in better follow-up for known problems.
2. Facilitate the implementation and use of a telephone inquiry service for General Medical Clinic patients. This service would provide emergency counseling, avoid unnecessary off-hour visits to the Emergency Room, and reassure patients experiencing anticipated complaints or reactions.
3. Provide the minimal information required so that a patient is not placed at undue risk either from unnecessary diagnostic procedures or

from inappropriate new prescriptions during an unscheduled encounter.

4. Assure the presence of a succinct and easily maintained patient medical-summary/problem-list in the Medical Records of all General Medical Clinic patients.
5. Evaluate the impact of computer-supported medical abstracts on patient care delivery.

DISCUSSION

The Mini Record Demonstration was performed over a period of five months in three phases: requirements definition, program and data base development, and operational demonstration. All systems analysis, computer programming, and user training were performed by APL. JHH provided medical consultation with regard to the use and contents of the Mini Record and was responsible for operational support and system evaluation. At the end of the APL-supported effort, a fully operational system and data base were transferred to JHH where it is now operational and undergoing extended evaluation.

The system maintains a Mini Record (Fig. 1) for each General Medical Clinic patient. The Mini Record contains demographic and administrative information, brief text descriptions of major medical problems and history, identification of currently prescribed medications, and an indication of visits to other outpatient clinics since the last General Medical Clinic encounter. The Mini Record is available for display from interactive terminals; a hard copy of the most recent Mini Record is also maintained in each patient's medical folder. Access to the on-line Mini Record is by patient history number or name. Terminals are located in the General Medical Clinic, the Emergency Room, and other selected areas.

Information for the Mini Record is collected from: (a) an Encounter Form, which is filled out during each General Medical Clinic visit; (b) the billing file, which records all visits to other clinics; (c) discharge summaries, which provide problem lists and medications for newly discharged patients scheduled for follow-up at the General Medical Clinic; and (d) corrections and additions to existing Mini Records submitted by physicians. Procedures have been established to assure timely and accurate records.

Figure 2 illustrates the flow for processing and using the Mini Record. General Medical Clinic pa-

THE JOHNS HOPKINS HOSPITAL
MINI RECORD

HISTORY NUMBER: 100-03-63
NAME: SMITH, MELLIE

PHONE: 301-247-3510 BIRTH: 09/08/32 SEX: F CL: OSL
PHYS: 02901 JAMES, STEPHEN PAUL FIM: OTHR SES: 5
ADDR: 1023 MCALDER CT NEXT APP: 06/29/75
BALTIMORE MD 21217 LATEST VISIT: 04/26/75

MEDICAL INFORMATION

VISITS THROUGH 05/31/75 SINCE LAST ENCOUNTER

04/26/75 ER
04/26/75 ER
05/21/75 OPWTH.
05/22/75 DIAB MAN
05/29/75 DIAB MAN
05/29/75 GI

- # 1 PATIENT DISCHARGED FROM OSLER ON 04/24/75 (04/24/75)
- # 2 SARCOIDOSIS WITH HEP INVOLVMT (04/24/75)
- # 3 MENTAL CONFUSION (04/24/75)
- # 4 AODH (04/24/75)
- # 5 RENAL INSUFF (04/24/75)
- # 6 HBP (04/24/75)
- # 7 RX: PREDNISOLONE (04/24/75)
- # 8 RX: NPH (04/24/75)
- # 9 RX: DIOXIN (04/24/75)
- # 10 RX: GUANETHIDINE (04/24/75)
- # 11 RX: MAALOX (04/24/75)
- # 12 RX: KCL (04/24/75)

Fig. 1 Mini Record of hypothetical patient.

tients are grouped so that each patient is normally assigned to a single "firm" for medical care. This "firm" provides both inpatient and outpatient care and also supports the telephone service for its patients. For all unscheduled encounters, the Mini Record is queried. In many cases, the patient and the Mini Record together should provide sufficient information to assist in treatment. Where additional information is required, the medical record is requested.

Evaluation of the Mini Record system is being performed in two phases. Based upon the APL demonstration, the initial evaluation verified (a) that the system was an effective aid to the operation of the General Medical Clinic, (b) that the system was a necessary prerequisite to establishing the desired telephone inquiry service for General Medical Clinic patients, and (c) that an extended evaluation period would be required in order to assess the impact of the Mini Record and the telephone inquiry service upon health care delivery.

The second phase of evaluation, currently in progress, is being conducted by the hospital staff and is considering the treatment of patients, the effectiveness

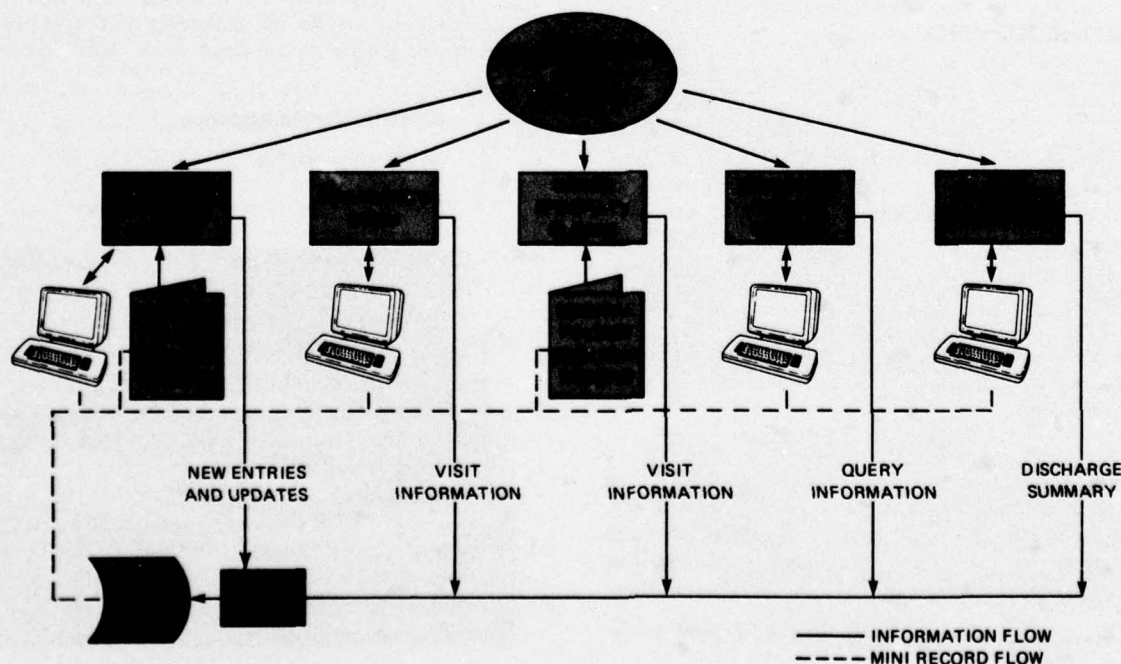


Fig. 2 Flow diagram of Mini Record system.

of the telephone inquiry service, and the net costs and benefits of the Mini Record system. To assist in this evaluation, a control group has been identified for detailed analysis. Results of the extended evaluation should be available in about 12 months.

ACKNOWLEDGEMENT

We are grateful for the assistance of the Johns Hopkins Hospital staff in this project.

Author: B. I. Blum

Support: IR&D

EVALUATION OF POWERED MEDICAL MANIPULATOR

A powered medical manipulator has been fabricated to study the man-machine control interface for highly handicapped spinal cord injury patients. Results of initial clinical testing indicate that the device may be of value in assisting such patients in some activities of daily living and work-related tasks.

BACKGROUND

One handicapped person for whom few or no assistive devices are available is the quadriplegic. He has little or no use of his arms and hands and must depend on other individuals for all of his needs. One possible solution, that of fitting a powered orthosis to one of the nonfunctioning upper limbs, has been investigated by many researchers but was found to be of little practical value because of the complex interaction with the limb. The alternative, a remote powered manipulator, appears to offer promise as a flexible machine with which severely handicapped persons can carry out personal and vocational tasks with some independence.

The scope of the five-year APL/JHMI collaborative effort to develop upper-limb powered prosthetic and orthotic systems was extended in 1974 to include aids for the spinal cord injury patient. A manipulator and an integrated work table environment was designed to provide the following required functional capabilities:

1. Handling and reading magazines and newspapers;
2. Self-feeding with a spoon or fork; and

3. Operating push-button devices such as the Touch-Tone telephone, electric typewriter, desk calculator, and tape recorder without equipment modification.

The initial experimental model configuration is shown in Fig. 1. It utilizes a multidegree-of-freedom mechanical "arm" integrated into a work table to provide a wide range of grasping capability. The manipulator provides the following motion capabilities to the patient in its stand-alone "arm" arrangement:

1. Shoulder flexion-extension,
2. Shoulder turntable,

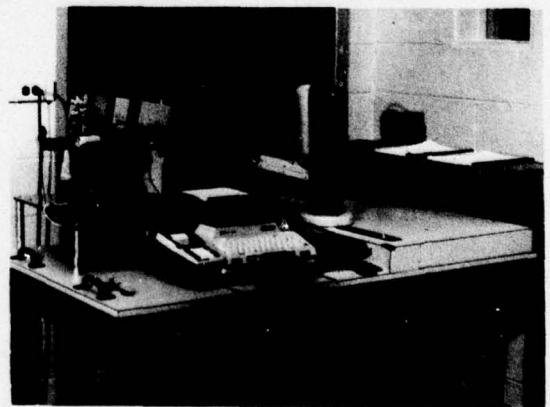


Fig. 1 Experimental model of powered medical manipulator/work table.

3. Elbow flexion-extension,
4. Wrist pronation-supination, and
5. Hook opening (can be locked in any open position).

The manipulator is controlled by first generating a pulse train of from one to four pulses to mode-enable the desired axis of motion. This is followed by proportional control of an input signal transducer that first unlocks the desired axis of motion and then positions the manipulator in its desired position. A single pulse stops the motion and locks the mechanism. The proportional control may be provided by eyebrow/eyeglass control, thumb-wheel control, or depression of a control paddle with the chin or head stick. Selection of the appropriate control mode is based on the capabilities of the individual patient. Initial clinical evaluation has included testing in all three control modes.

DISCUSSION

A powered medical manipulator, utilizing concepts and component designs from previously developed powered prosthetic systems, has been designed and fabricated. Some of the more important design constraints for the manipulator are that (a) the effort required to control the device must be within acceptable limits, (b) output motions and forces must be limited, considering the safety interface between the machine and the patient, and (c) the electromechanical design must be reliable and acceptably quiet.

The various personal and vocational devices are located on the work table to minimize manipulator motions as well as to allow maximum flexibility to the user. The typewriter/calculator/Touch-Tone telephone pad are mounted in a thin flat cart so that the manipulator can move them in or out of range of the head stick or mouth stick. The typewriter may be loaded by the manipulator by means of special vacuum fingers permanently attached to the terminal device. For patients with good head-stick or mouth-stick control, a mechanical paddle control input may be preferable to other facial control techniques, such as the eyebrow/eyeglass control mode. If the typewriter tray is moved a short distance to the rear with the manipulator, the mouth stick can also reach the Touch-Tone telephone buttons. In this instance, the manipulator would be used to pick up the telephone headset and hold it near the patient's head for normal phone conversation, and the mouth stick would be placed in a holder during the actual conversation.

Other work-related tasks include operating an electronic calculator, manipulating paper work, and handling magazines. A magazine may be removed from the rack and placed in position for reading; the pages are turned and finally the magazine is returned to its storage position in the rack. Figure 2 shows the magazine pages being turned by the manipulator.



Fig. 2 Manipulator turning magazine pages.

In addition to the described work-environment capabilities, the system can provide some self-feeding capability to the highly disabled patient. The typewriter is moved back to its storage position by the manipulator to clear the area directly in front of the patient for the feeding task. A plate is then placed in front of the patient with food in bite-sized portions or with other foods that can be picked up by a fork or spoon.

The medical manipulator has now been subjected to limited clinical testing by two patients at the Maryland Rehabilitation Center. The first patient, a 19-year-old male who used the device for about eight hours, is afflicted with rheumatoid arthritis to the extent that his musculoskeletal function is limited to a few degrees of flexion-extension of his elbows and fingers. He quickly learned to master basic control of the manipulator and could perform all of the designated tasks of the system. However, since he was studying to be an accountant and the machine could not handle large ledgers and other reference materials, he discontinued his participation in the testing.

The second patient is a middle aged male who has used the manipulator for about seven months and is continuing to develop skills in its use. This patient suffered a spinal cord injury about eight years ago and had no residual hand, wrist, elbow, or shoulder motion. He initially used eyebrow motion for control. In later clinical testing he greatly improved his per-

formance by using a head stick to control the manipulator. Since he had already developed skill in typing using the head stick, this control mode was easy for him to learn. He is continuing to test the device and is becoming proficient in some tasks of interest to him.

Results of the initial clinical testing have been promising. The sponsor has requested APL to fabricate three additional models. These units will incor-

porate additional sensors and other features, to improve the interface between the patient and the machine.

Authors: W. Seamone (APL) and G. Schmeisser, Jr. (JHMI)

Support: Veterans Administration

ELEMENTAL PHENOMENON OF VISION

The basic nature of a novel kind of visual phenomenon—suprafusion transients—has been uncovered through an abstract theory of vision that mathematically predicts physiological suprafusion responses of the eye-brain system. Retinal and cortical experiments confirm the theory and, through it, are correlated with other neural and behavioral studies. Analysis also educes potential clinical utility for the retinal (electroretinogram, ERG) suprafusion transient.

BACKGROUND

A light that fluctuates sufficiently rapidly about a constant mean luminance appears to be of a constant brightness equal to that of the mean luminance. Long ago this Talbot-Plateau law was recognized to require not only that the fluctuation be faster than a flicker fusion frequency but also that it be steady. Nevertheless, in this suprafusion regime only passing investigation has been made beyond that needed to establish the steady-state precision of the classic Talbot-Plateau law. Recently a novel technique for investigating unsteady modulation above fusion was developed, largely at APL, combining psychophysical observation, physiological experiment, and mathematical theory. A basic phenomenon proves to be the transient brightness change that is perceived when the light fluctuation waveform is abruptly changed, as by the sudden jump in waveform period depicted at the top of Fig. 1. The perception of such "suprafusion transients" was studied psychophysically earlier, and its sensory basis was formulated into an abstract theory (Ref. 1). The theory predicted the mathematical form of associated physiological responses of the visual system that have now been detected in the eye and brain of monkeys (Refs. 2 and 3). The analysis and interpretation of these retinal (ERG) and

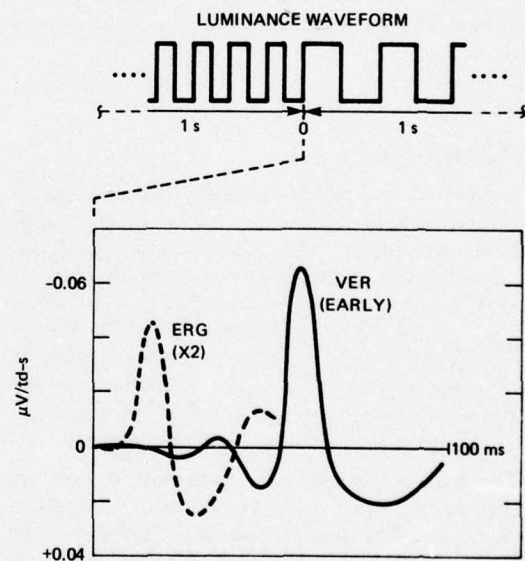


Fig. 1 Period-jump stimulus ($t_1 \rightarrow t_2$) and resulting Green's functions for retina (ERG) and cortex (VER).

cortical (visually evoked responses, VER) suprafusion transients are discussed briefly here (cf. Ref. 4).

DISCUSSION

The elemental nature of suprafusion transients is manifest in the theoretical deduction that they represent fundamental Green's functions of the visual system. For example, the waveform period-jump at the top of Fig. 1 is predicted to elicit suprafusion responses of the form

$$R_p(t) \propto (t_2 - t_1) \cdot G_p(t, 0) \quad (1)$$

in any linearizable part, P , of the system, where $t_2 - t_1$ is the period-jump and $G_p(t, 0)$ is the Green's function defined as the response of P at time t to an impulse at time 0. Equation (1) was derived, discussed, and accurately verified by human behavioral experiments (Ref. 1).

In the physiological studies (Refs. 2 and 3) the period-jump stimulus was applied to monkeys with electrodes implanted on the visual striate cortex and contact electrodes on the cornea. A principal-components analysis has extracted from the responses the hypothetical retinal (ERG) and cortical (VER) Green's functions shown in the lower part of Fig. 1. Aside from the amplitude difference and the expected time delay in transmission from retina to cortex, the two waveforms are remarkably similar.

Figure 2 illustrates the good accord between the experimental data and the theoretical prediction for the cortical responses. Since for the VER one may distinguish two main parts of the system—the traditional "on-" and "off-" brightness subsystems—we have P in Eq. (1) equal to plus or minus (say), depending on whether $t_2 - t_1$ is greater or less than 0. Then Eq. (1) predicts straight lines radiating from the origin. This prediction is satisfactorily confirmed by the data points (Fig. 2). Similar confirmation is obtained for the retinal responses.

With the theory validated, we take the ERG and VER response components in Fig. 1 as Green's functions for the retina and cortex. Then their Fourier transformations must be frequency response curves. The calculated ERG and VER transforms in Fig. 3 display reasonable correlation with other behavioral and neurophysiological response curves.

Detailed analysis now in process of the ERG transients finds a substantial component that we can only associate with amacrine cell activity in the retina. If so, the ERG suprafusion transient affords increased anatomical resolution that could be clinically useful for the diagnosis of macular dysfunction.

REFERENCES

1. J. F. Bird and G. H. Mowbray, "Analysis of Transient Visual Sensations above the Flicker Fusion Frequency," *Vision Research*, 13, March 1973, pp. 673-687.
2. R. W. Flower, J. F. Bird, and G. H. Mowbray, "Retinal and Cortical Electrophysiological Responses to Instantaneous Frequency Shifts in Light Modulated above Fusion," *Investigative Ophthalmology*, 14, January 1975, pp. 75-78.
3. G. H. Mowbray, R. W. Flower, and J. F. Bird, "Visual Cortex Responses to Abrupt Changes in the Periodicity of Rapidly Intermittent Light," *Electroencephalographic Clinical Neurophysiology*, 39, October 1975, pp. 305-312.
4. J. F. Bird, R. W. Flower, and G. H. Mowbray, "An Elemental Phenomenon of Vision—Suprafusion Transients: General Theory, Retinal-Cortical Manifestations, Potential Application," *J. Theoretical Biology*, 55, December 1975, pp. 553-557.

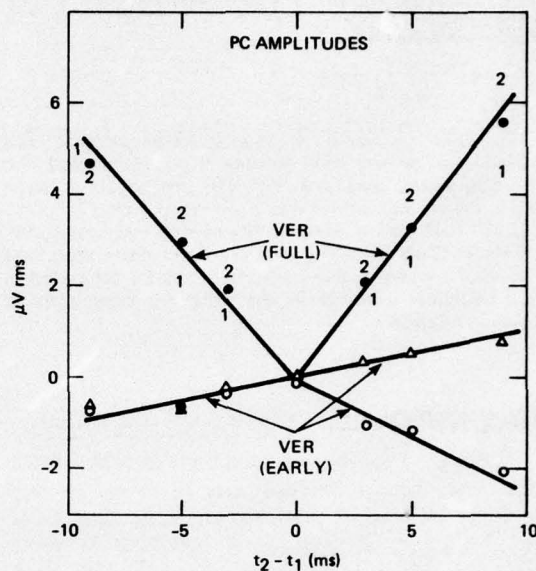


Fig. 2 Comparison of experiment (symbols) with theory (lines) for cortical responses.

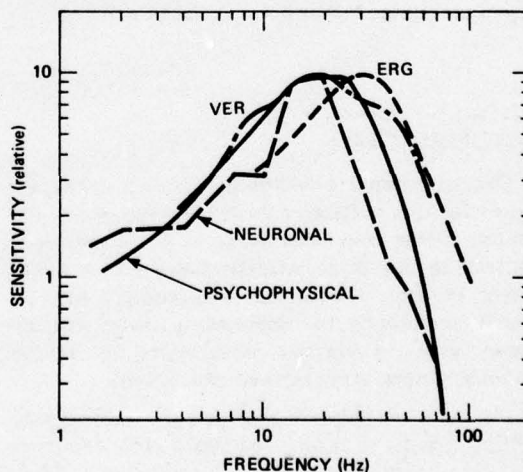


Fig. 3 Frequency response calculated from Green's functions (Fig. 1, VER and ERG) and measured by flicker perception and cellular responses.

Authors: J. F. Bird, R. W. Flower, and G. H. Mowbray

Support: NAVSEASYSOM and U. S. Public Health Service, National Eye Institute and National Institute of Neurological and Communicative Disorders and Stroke

A MONITOR FOR INTRACRANIAL PRESSURE

A cause of death in neurosurgical patients and others with severe head trauma is an undetected rise in intracranial pressure. For the protection of such patients, an instrument has been constructed for clinical use that makes possible the continuous monitoring of intracranial pressure with the least discomfort and risk to the patient. The instrument will be evaluated in neurosurgical patients in the intensive care units at several hospitals.

BACKGROUND

There are a number of conditions in which extensive brain damage or death may be caused by high levels of intracranial pressure. The early detection of rising intracranial pressure is important in severe head injuries, in acute stroke (especially with bleeding), in hydrocephalic patients, and in the postoperative care of neurosurgical patients. An intracranial pressure monitor will give early warning to the attending physicians so that pressure-relieving techniques are started before brain damage can occur.

DISCUSSION

The intracranial pressure monitoring device designed for this purpose is an implantable sensor that fits into a burr hole made in the skull. The sensor is nontoxic so that if disintegration occurs after a long period of time, the degradation products will not cause a reaction in the surrounding tissue. For this reason also, the pressure sensor does not contain batteries, copper wires, or transistor devices.

The technique makes use of an implantable capsule called a transensor, which contains a radio frequency resonant circuit (inductance and capacitance) whose natural frequency is affected by deformation of the capsule caused by pressure changes in its environment. Located outside the body (Fig. 1) but in close proximity to the transensor is an external detector, or interrogator. The interrogator radiates a frequency-modulated VHF radio signal that loses energy to the transensor when the signal frequency has a value equal to the transensor's resonant frequency. A bedside monitor connected to the sensing head records the frequency at which the energy loss occurs and converts this measurement to an intracranial pressure reading.

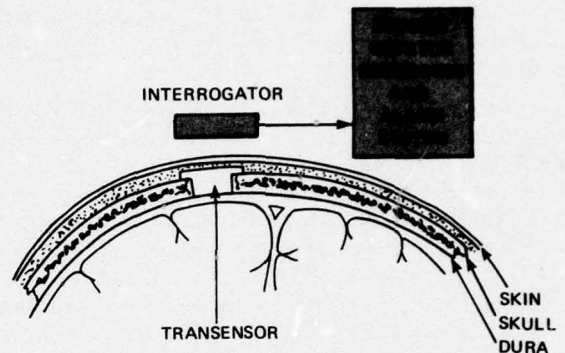


Fig. 1 Intracranial pressure-monitoring system.

Figure 2 shows the steps in assembling the transensor. In the second step (b), the gold-plated nickel bellows are glued into the ceramic half-sections with epoxy. In the third step (c), the ceramic halves are glued together, bringing the closed ends of the bellows into opposition but separated by 0.1 mm. Thus an electrical capacitance is produced. As shown in the third step (c), eight turns of wire are wrapped around the outer diameter of the ceramic case to form the inductance coil. Each end of this coil of wire is soldered to one of the bellows, the whole now making up an electrically resonant circuit. At this stage, a small vent hole is sealed, trapping a volume of air under the specified conditions of temperature and pressure. Finally in the fourth step (d), the ceramic capsule is enclosed in a plastic case that is filled with medical-grade silicone oil and sealed.

Figure 3 shows a cross section of the transensor. Pressure from a body cavity deflects the thin (0.13-mm) plastic membrane inward. The pressure inside the plastic case is transmitted by the silicone oil to the flexible bellows. The bellows are pushed closer together, increasing the electrical capacitance. This lowers the resonant frequency, which is readily detected outside the body by an interrogator coil placed near the skin over the implantation site. The pressure on the transensor is determined from the resonant frequency, a relationship known from previous calibrations.

Figure 4 shows the transensor and the mounting flange, separate and assembled. To implant the tran-

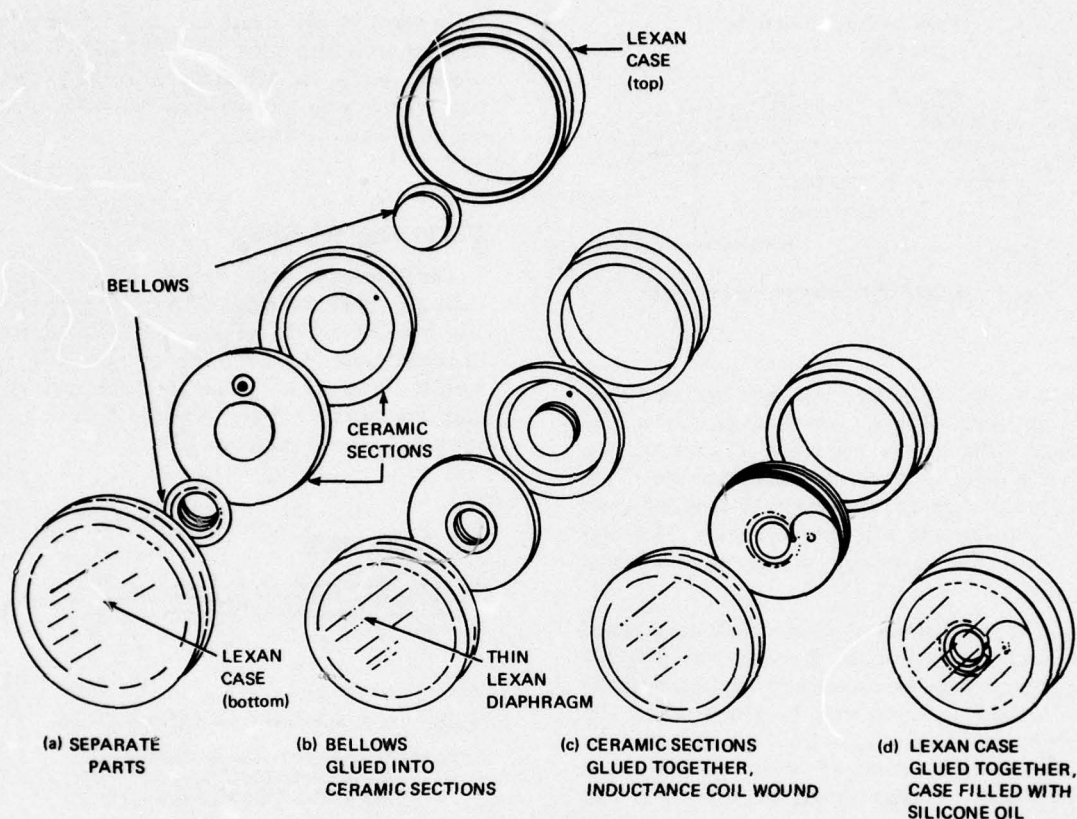


Fig. 2 Assembly of transensor.

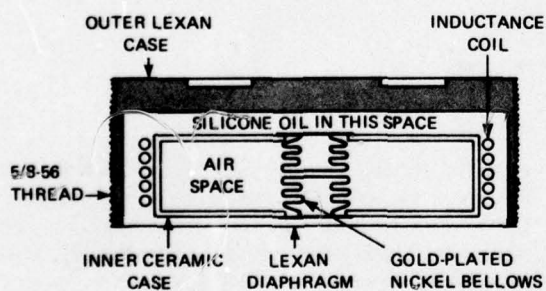


Fig. 3 Cross section of passive pressure transensor.

sensor (Fig. 5), the flange is mounted in a burr hole in the skull and secured in place with skull screws. By means of the screwdriver shown in Fig. 4, the transensor is advanced in the threaded flange until its sensing diaphragm barely touches the dura mater. The critical pressure that must be measured is the pressure of the cerebrospinal fluid in the subarachnoid space.

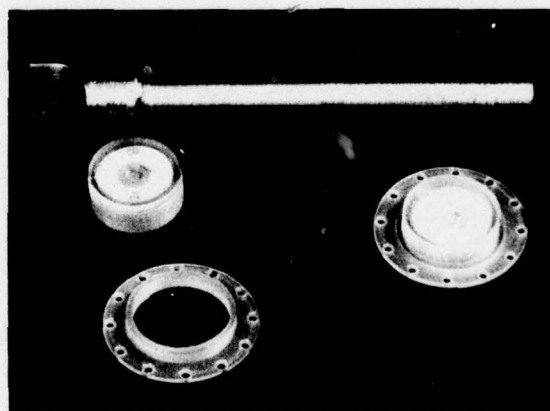


Fig. 4 Flange design for the transensor. The transensor and threaded flange are shown both separately and assembled. The screwdriver for advancing the transensor in the flange is shown in the background.

Currently, intracranial pressure is measured by placing the interrogator over the site of the transensor

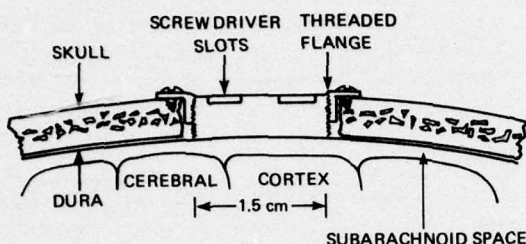


Fig. 5 Method of transensor implantation.

implant to determine the transensor RF frequency. The frequency is read on an oscilloscope display. The frequency value of the transensor is converted to a pressure reading by means of a calibration chart. The reading must then be corrected with a second chart for temperature and barometric pressure. This procedure, now done manually, will be fully automatic next year.

Clinical trials have been initiated following animal experimentation and trials. Recently, the first two patients have undergone transensor implants to monitor their intracranial pressures. Occasional spinal taps to obtain spinal fluid samples have also allowed direct monometric measurement of spinal fluid pressure. These pressure readings agreed to within 5% with

those taken by the transensor. In both patients, the pressure transducer performed well and played a significant part in the management of the patient's illness by notifying the attending physicians of excessive intracranial pressure.

FUTURE PLANS

The transensors are now being made in quantity for evaluation at several hospitals. In addition, a new bedside monitor will be designed for 24-hour recording of intracranial pressure. The monitor will have a built-in barometer to compensate for barometric pressure changes and will give an alarm if the intracranial pressure reaches a dangerous level.

REFERENCE

1. A. E. Walker, L. J. Viernstein, J. G. Chubbuck, and S. Karas, "Intracranial Pressure Monitoring," presented at meeting of the American Association of Neurological Surgeons, Miami, FL, April 1975.

Authors: L. J. Viernstein and J. G. Chubbuck

Support: U.S. Public Health Service Grant NS-11710, National Institute of Neurological and Communicative Disorders and Stroke

CALCULATIONS AND MEASUREMENTS OF SIMULATED ARTERIAL FLOWS

Calculations of pulsatile flow in a symmetric branch modeling the aortic bifurcation were carried out to elucidate the role of hemodynamic factors in atherogenesis. A water tunnel was constructed to model the computational geometry; measured velocity fields agreed well with the calculations. This validation thus permits each technique to be used to explore those aspects of blood flow to which it is best suited, with emphasis on fluid mechanical and related processes that can be involved in the development of arterial disease. These include the role of wall distensibility, particle and solute transport, and geometric effects such as arterial narrowing on fluid mechanical variables.

BACKGROUND

Much current theory on the etiology of atherosclerotic disease centers around certain hemodynamic

variables. Among the hemodynamic phenomena that have been suggested as being responsible for atherogenesis are low shear, high shear, turbulence, and flow separation. These properties of the flow are difficult or impossible to measure in vivo. Hence our approach is via computational and experimental simulation models that approximate the anatomy of interest.

DISCUSSION

Interest first centered on the aortic bifurcation, which was simulated by a symmetric Y-shaped geometry (Fig. 1). The governing equations and method of solution are described in Refs. 1 and 2. Nonlinear flow solutions for peak Reynolds numbers (based on the full width of the inlet channel) up to

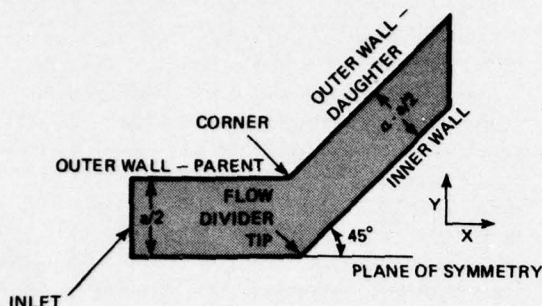


Fig. 1 The experimental region.

400 have been computed for the symmetric 90°-Y bifurcation containing an "ideal" (sinusoid plus DC) pulsatile flow. The solution yields all of the variables of the flow, including instantaneous streamlines, velocity vectors, vorticity, vorticity gradients, and wall shear. It was shown that details of the shear distribution within the branch cannot be estimated from considerations of mean shear levels proximal and distal to the segment.

Also, transient separation lasting about 20% of the cycle was computed for a short distance along the outer wall just distal to the corner. This suggests that the replenishment of blood at the intimal surface will proceed slowly in this region, to the disadvantage of the lining endothelium. If low wall shear is a part of the etiology of atherosclerosis, pulsatility exacerbates the situation at a branch. Details of these results can be found in Ref. 3.

A more realistic periodic flux waveform, recorded by Dr. L. J. Krovetz in a boy's aortic bifurcation, was used next. Typically, the ratio of the peak in vivo flux to the mean, $R = 5$, is greater than in the ideal pulsatile wave for which $R = 2$. For the larger value of R , the wall shearing stress reaches higher peaks, and there is an indication of more intense recirculation in the transient separated region along the outer wall of the branch.

Turning our attention to approximately orthogonal arterial junctions (e.g., renals and intercostals), we have also computed flow within two-dimensional orthogonal branches for an ideal pulsatile inflow. In contrast to our calculations in the Y-branch, the flow pattern in such T-branches is asymmetric and depends upon the flow partition. However preliminary comparisons indicate certain qualitative similarities within the two types of junction.

These numerical studies have demonstrated that pulsatility in general and even the detailed shape of

the flux wave have important effects on the stresses experienced by the inner (intimal) surface of the arterial wall. The results show further that there is a correlation between the sites of hemodynamic extrema and of atheromatous lesions in branches.

A water tunnel capable of producing well-defined flowfields that can validate the results of numerical computations has been designed and constructed. The tunnel can be used to generate steady or pulsatile flows at physiological Reynolds numbers. A 90°-Y model bifurcation, matching in plan geometry that used in the hemodynamic calculations, was designed so that the flow channels could be viewed vertically through glass windows by a laser doppler velocimeter (LDV) and so that surveys completely across the channels could be made without interference. The flow cross section was rectangular with a nominal inlet aspect ratio of 10 (see Fig. 2). By careful design of the test section, the flow velocity can be measured at least as close to the wall as the first computational mesh point (about 400 μm). The optical system of the LDV has been improved to the point that the spatial resolution in the lateral direction (the "important" coordinate, measured normal to the vertical walls of the channel) is much less than 100 μm . This resolution capability has been maintained in operation by mounting the entire LDV rigidly to a translation table beneath the water tunnel, so that the position of the beam intersection within the flowing fluid is known accurately.

To test the validity of the computational results, a pulsatile input was applied to the water tunnel. The

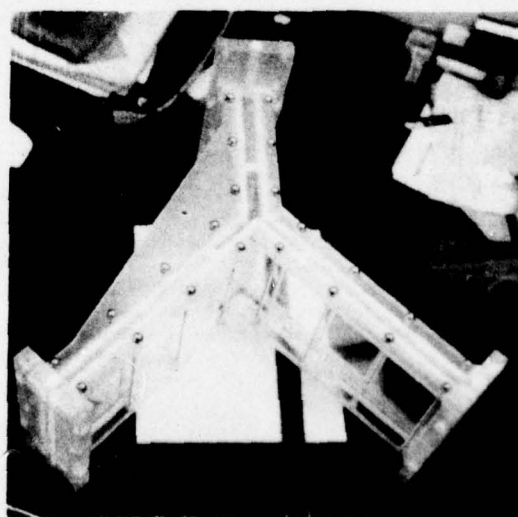


Fig. 2 The test bifurcation.

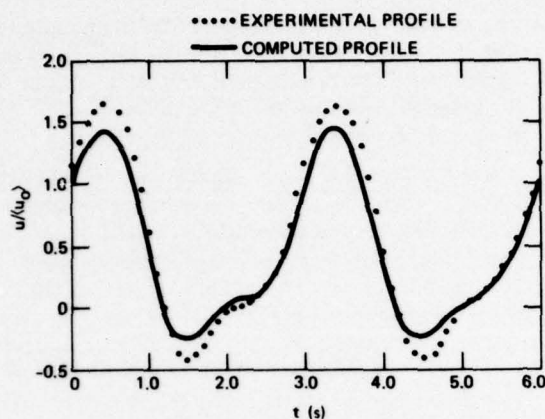


Fig. 3 Time-dependent experimental and computed velocity profiles at a point in the branch, normalized by average upstream centerline velocity. Note that the experimental area ratio is slightly less than the value used in the numerical calculations and is sufficient to explain the minor amplitude difference.

time-dependent velocity upstream of the branch at the line of symmetry was measured. By Fourier decomposition techniques, using solutions for plane parallel flow, this velocity was used to calculate the inlet flux wave for the numerical computation.

Measurements were made in the bifurcation of the velocity component parallel to the walls. Particular emphasis has been placed on the velocity very near the wall in both parent and daughter in the region of the outside corner. Agreement between experimental and computational values is good (Fig. 3), indicating that we may have confidence in the numerical analysis as well as the experimental tech-

niques. Since velocity profiles can be obtained quite close to the vessel wall, these techniques can also be used to estimate wall shear.

Since the water tunnel is three-dimensional and the computation is two-dimensional, the effect of the inlet aspect ratio on the relationship between centerline velocity and flux was examined. Fully developed unsteady parallel viscous flow (viscosity coefficient, ν) in straight rectangular ducts admits an exact flow solution in terms of separable Fourier components. Each harmonic component $e^{i\omega t}$ introduces a characteristic "viscous length," $\sqrt{\nu/\omega}$, that—along with the dimensions of the duct—determines the detailed periodic flowfield. When this analysis was applied to the experimental situation, the aspect ratio in the tunnel was large enough to permit the estimate of flux from a plane parallel solution.

REFERENCES

1. L. W. Ehrlich, M. H. Friedman, and V. O'Brien, "A Digital Simulation of Periodic Blood Flow in a Bifurcation," *Proceedings of the 25th Annual Conference on Engineering in Medicine and Biology*, Bal Harbour, FL, 1972.
2. V. O'Brien, L. W. Ehrlich, and M. H. Friedman, "Nonlinear Simulation of Unsteady Arterial Flows in a Branch," presented at the Conference of American Institute of Chemical Engineers, Philadelphia, PA, November 1973.
3. M. H. Friedman, V. O'Brien, and L. W. Ehrlich, "Calculations of Pulsatile Flow through a Branch," *Circulation Research*, 36, 1975, pp. 277-285.
4. C. B. Barger, F. F. Mark, and M. H. Friedman, "Pulsatile Flow in a Rectangular Cross-Section Bifurcation," *Proceedings of the 28th Annual Conference on Engineering in Medicine and Biology*, New Orleans, LA, 1975.

Authors: C. B. Barger, O. J. Deters, L. W. Ehrlich, F. F. Mark, V. O'Brien, and M. H. Friedman

Support: U.S. Public Health Service, National Heart & Lung Institute Grant HL-14207

CIVIL PROGRAMS

INTRODUCTION

With the encouragement of the Navy, APL conducts applied research in civil program areas where techniques and expertise developed in its defense activities can make an especially favorable contribution. In addition to the biomedical engineering and space science programs discussed in other sections, these may be categorized as transportation systems, environmental engineering, and, most recently, energy systems.

APL expertise in automation of radar signal data processing, interpretation, and presentation was applied to a prototype Harbor Vessel Traffic System developed and demonstrated for the U.S. Coast Guard, and is being utilized in continuing air traffic safety and control research for the Federal Aviation Administration. Navigation techniques and equipment developed for the military have also been applied to civil navigation problems.

APL has used its expertise in systems engineering and controls technology to assist the U.S. Department of Transportation in establishing requirements and constraints of urban mass transit systems, evaluating competitive system concepts and prototype tests, and developing control systems and techniques for the operation of large fleets of automated vehicles. These studies have been extended to other areas of transportation planning and implementation including personal vehicles and highway safety.

APL environmental engineering activities fall in two general areas: fire research and the evaluation of the environmental impact of power plant siting. The APL fire research program, initiated by the National Science Foundation and now supported by the National Fire Prevention and Control Administration, Department of Commerce, stemmed from expertise acquired in the research and development of ramjet and rocket propulsion systems for missiles. It includes basic and applied combustion research, fire prevention, fire fighting, health and safety, and public education aspects.

Since 1972, APL has provided to the State of Maryland evaluation of the environmental impact of specific sites proposed for nuclear or fossil fuel electric power plants. This work, carried out jointly by APL, The Johns Hopkins University, and the Chesapeake Bay Institute, includes evaluation of air and water pollution problems, hydrology, biological impacts, waste product disposal, radioactivity problems, noise, and other community impacts. Also included is assessment of new technologies for control and reduction of environmental impacts. Findings are made available to all interested parties (the state, the utility, and the public) and have been pronounced helpful by all concerned. Studies have now been completed on oil, coal, and nuclear fueled plants. As a result of this work, Maryland is believed to have one of the most advanced power plant siting programs in the country.

Most recently APL has begun study of alternative long-range, nondepleting energy sources and more efficient systems to meet future national requirements. Exploitations of the thermal gradient between the surface and the deep waters of the ocean (a form of solar energy storage) and of geothermal energy sources have been identified as important areas to which APL can contribute. In energy use conservation, more efficient building heating and cooling and personal transportation are considered areas of opportunity, and programs have recently been initiated.

The articles in this section provide a sample of APL's broad and increasing interests in civil programs.

MOVING WIRE TECHNIQUE STUDIES OF ABLATION, IGNITION, AND EXTINCTION OF POLYMER FLAMES

An apparatus and a group of techniques for studying polymer flammability have been developed at APL. The method yields scientific information and may also be of practical utility as a flammability test.

BACKGROUND

The combustion behavior of polymers during ignition and extinction is an important practical problem since many fires are initiated and/or fueled by natural or synthetic polymers. The complexity of solid-fuel/gaseous-oxidizer systems and the transient nature of ignition and extinction have made quantitative studies difficult. Systems are commonly studied transiently, or critical time-exposure parameters are determined.

This work describes a new method called the moving wire technique for studying these transitions. The basic concept is the exchange of transient time dependence for steady-state position dependence. This is accomplished by moving the material to be ignited relative to the laboratory coordinates. A polymer-covered wire sample is drawn across the igniting flame (see Fig. 1 insert). Positions across the flame in the direction of wire travel correspond to increasing residence times. The time at a particular point in the flame can be controlled by changing the velocity of the wire to provide flexible control of ignition and extinction phenomena. Precise measurements are possible because the time available for experiment is limited only by convenience. The use of moving systems in fixed laboratory coordinates appears to be new in the study of ignition and extinction phenomena.

DISCUSSION

Flame-piloted ignition was investigated initially. Flames provide both high temperatures and non-thermal excesses of reactive species such as atoms and radicals (Ref. 1). The apparatus could also be adapted to alternative ignition sources such as hot gas jets, radiant fluxes, or electrical arcs. Since polymers are solids, ignition requires (a) volatilization of the polymer, (b) the availability of a reactant, normally an oxidizer such as O_2 , from the air, (c) gas-phase mixing of volatilized fuel and oxidizer on the molecular level, and (d) the local availability of a sufficiently high temperature and radical concentration to initiate

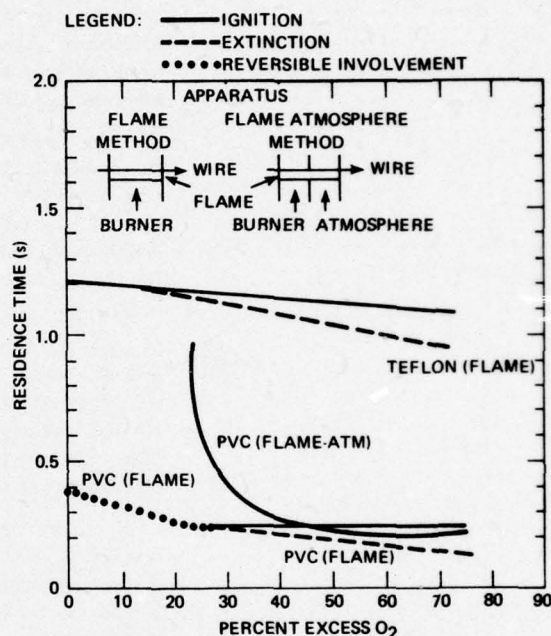


Fig. 1 Ignition, extinction, and ablation of some polymers using the moving wire technique; critical residence time behavior of two commercial polymer-covered wires, #30 gauge copper covered with Teflon and with polyvinyl chloride. Residence time at the ignition, extinction, or ablation transition is shown as a function of composition of the ignition gases. Exposure time is defined as exposed wire length divided by wire velocity.

the chain reaction processes of combustion. Flames can supply these requirements. Ignition can occur in the wake of a flame if sufficient oxygen is available there, or it can occur at the boundary between a fuel-rich flame and an oxidizing atmosphere.

These situations are simulated by two modifications of the APL apparatus (Fig. 1). The first is an isolated flame, while the second has an adjacent atmosphere. The compositions of both the flame and the atmosphere are controlled. The substrate to be ignited is in the form of a polymer-coated wire that is pulled across the flame. Wire support is desirable and necessary if the polymer softens during ignition. The drive for pulling the wire across the flame is provided by a mechanism similar to that used in tape decks. A variable-speed motor provides velocity control. The

speed is measured using an optical counter mounted on the drive shaft. Fluctuations measured with a differential rate meter are less than 0.2%. With this drive and control of composition of the flame and atmosphere, exposed length of polymer, etc., the critical transition times can be reproduced to within a few parts in a thousand.

ISOLATED BURNER EXPERIMENTS. Two types of behavior are observed, ablation-extinction transitions and ignition-extinction transitions. Ablation-extinction occurs in oxygen-poor flames and is reversible. When the wire speed is decreased, a characteristic velocity is found at which visible attack begins. The involvement length increases monotonically as velocity decreases. Extinction occurs at the same velocity at which ablation began.

Ignition-extinction behavior occurs in oxygen-rich flame atmospheres and shows hysteresis. If wire velocity is decreased, a sharp ignition point is observed. Movies show that ignition begins at the far edge of the flame and propagates back along the wire. The size of the initial polymer flame depends on the concentration of oxygen, and increases with increasing concentration. Reducing the velocity increases the involvement. Conversely, increasing wire velocity decreases involvement until extinction occurs at a critical velocity and/or flame size. The extinguishment velocity is higher than the ignition velocity so that a bistable velocity region exists (Fig. 1). Temperature measurements in the gas phase and on the polymer surface have shown that this behavior is reproducible and that the sharpness and reproducibility increase with oxygen concentration.

BURNER-ATMOSPHERE EXPERIMENTS. If a flame is bounded by an atmosphere containing a higher free-oxygen concentration, similar behavior is observed. In the flame, free oxygen is defined as the fraction of oxygen remaining after stoichiometric reaction; in the atmosphere, free oxygen is the fraction of oxygen in the incoming flow. Ignition begins at the flame/atmosphere interface but propagates along the wire into the atmosphere. If the atmosphere has a low oxygen concentration, the flame will ablatively attack

the wire prior to ignition. The behavior is similar to that observed for ablation in the isolated burner experiments. Below a minimum oxygen concentration, ignition is not observed. At higher oxygen concentrations, the ablative attack prior to ignition is reduced until, above a certain level, no flame attack is observed prior to atmospheric ignition. If the flame has a higher free-oxygen concentration than the atmosphere, ignition will occur in the flame rather than in the atmosphere, and the behavior will be the same as that of the isolated burner. Typical ablation, ignition, and extinction behaviors of polyvinyl chloride (PVC) are shown in Fig. 1.

The moving wire apparatus lends itself to a variety of measurements of the ablation-ignition-extinction behavior of polymers. The processes can be characterized by measurements of temperature and composition of the gas and polymer as a function of position. Such measurements should be interpretable in terms of rates of elementary processes of heat transfer and reaction. This interpretation will require a quantitative model, which APL is attempting to develop. Preliminary studies suggest that ignition is governed principally by surface temperature.

The complete understanding of moving wire experiments will require extended experimental and theoretical studies, but the resulting increase in understanding of ignition and extinction should prove worthwhile. Such work should help provide a better, more scientific understanding of flammability tests and of realistic polymer fire hazard situations.

REFERENCE

1. R. M. Fristrom and A. A. Westenberg, *Flame Structure*, McGraw-Hill, New York, 1965.

Authors: R. M. Fristrom, C. Grunfelder, and L. W. Hunter

Support: National Fire Prevention and Control Administration through National Science Foundation RANN Program, Grant GI-44088X

EVALUATION OF RADAR PROCESSING SUBSYSTEM

The Radar Processing Subsystem (RPS) of the Automated Radar Terminal System III (ARTS III) has been analyzed to determine the feasibility of the proposed design, optimum operating parameters, and design simplifications that would reduce complexity without impairing performance. A system configuration is recommended that significantly simplifies the original design without sacrificing performance.

BACKGROUND

ARTS III is the term used to indicate the current evolutionary configuration of the Automated Radar Terminal System. The function of this system is to detect and track aircraft within 60 nmi of an air terminal while minimizing false contacts caused by clutter. The system is automated; all detection and tracking of aircraft is done by system equipment and not by an operator.

The radar display provides an air traffic controller with the positions and velocities of aircraft within the coverage region while suppressing clutter returns. This allows the controller to devote his full attention to ensuring adequate aircraft separation and maintenance of flight rules. Since the radar environment varies with weather conditions, ARTS III is adaptive. The ability of the system to detect aircraft while rejecting clutter is a function of the intensity of the radar return from natural phenomena.

In order to assist in aircraft tracking, major aircraft are equipped with radar beacons. When the aircraft is illuminated by a coded radar pulse, the beacon transmits a coded message back to the radar. Because of variations in aircraft attitude relative to the radar, it is possible to receive a radar return from an aircraft with no beacon return, and vice versa. In the ideal case, both a radar return from the body of the aircraft and a beacon return are received and used to generate a track for that aircraft.

The RPS is comprised of the Radar Data Acquisition Subsystem and the associated radar software of the Data Processing Subsystem of ARTS III (Fig. 1).

The RPS receives linear moving target indicator (MTI) and logarithmic video signals from the Airport Surveillance Radar (ASR) and processes this information to develop target position reports. These radar position reports are correlated with target position reports provided by the Beacon Data Acquisition System (BDAS) to yield a composite target track file for each contact in the ARTS III coverage area.

DISCUSSION

The baseline RPS configuration is shown in Fig. 2. There are two inputs, logarithmic video and linear MTI video from the ASR. The output of the RPS is an estimate of the position (range and azimuth) of each radar contact.

Comparators Q_0 and Q_1 convert log video into a binary signal by comparing the input voltage from the radar receiver to a variable threshold based on the observed level of receiver noise. Whenever the threshold is exceeded, the output goes from 0 to 1. A "1" signifies a first-threshold crossing and is called a hit. The threshold of Q_0 is set to a higher value than that of Q_1 by the addition of an offset to the variable component. The variable threshold is set by feeding the output of Q_1 into a noise meter, which measures the noise level over a large portion of the radar coverage area.

The binary outputs of the comparators are fed into hit processing blocks that check for minimum and maximum pulse length to ensure that the length of the first threshold crossing is characteristic of a return from a real contact.

The clutter monitor and clutter mapping blocks perform spatial and temporal integration of the comparator outputs on a zone basis. Each zone is 2.8° in azimuth by 2 nmi in range, encompassing about 1000 radar resolution cells. The clutter mapping system measures the intensity of clutter in each of the 4096 zones within the radar coverage area (360° by 60 nmi).

Rank quantizers Q_2 and Q_3 convert log normal video and linear MTI video, respectively, into binary signals by performing a rank order test on the input video signal. The rank order test compares the relative amplitudes of the radar video in 25 adjacent radar resolution cells. The voltage in the center cell is compared to the voltage in each of the 24 other cells. Each time the voltage in the center cell is greater than the voltage in one of the other cells, the rank of the center cell is increased by 1. If the voltage in the center cell is greater than the voltage in each of the other cells, the rank of the center cell is 25. If the voltage in the target cell is greater than the voltage in 23 of the 24 other cells, the rank of the center cell is 24. The rank computed for the center cell is compared to a rank threshold, generally set to 23 or 24. If the threshold is exceeded, a threshold crossing is declared for the center cell. This test is performed sequentially so that all cells from 1 to 60 nmi are

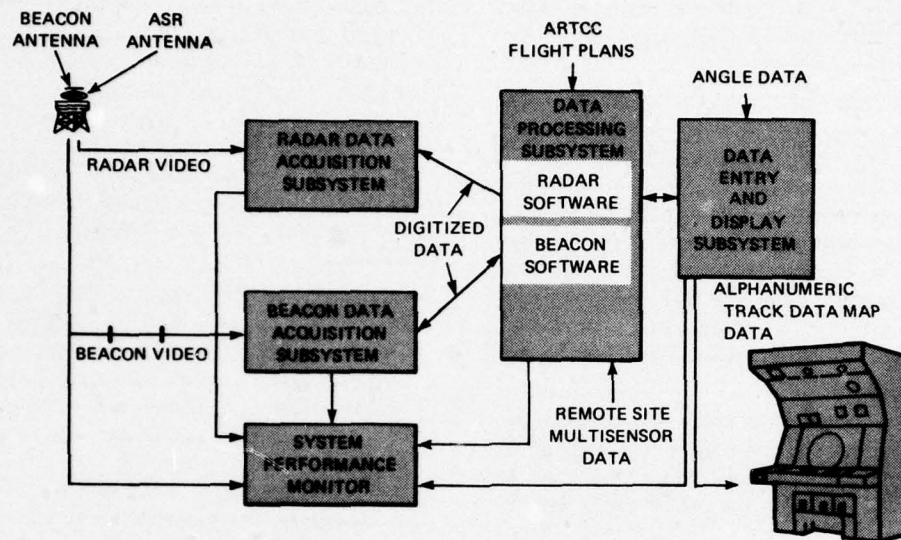


Fig. 1 Terminal automation.

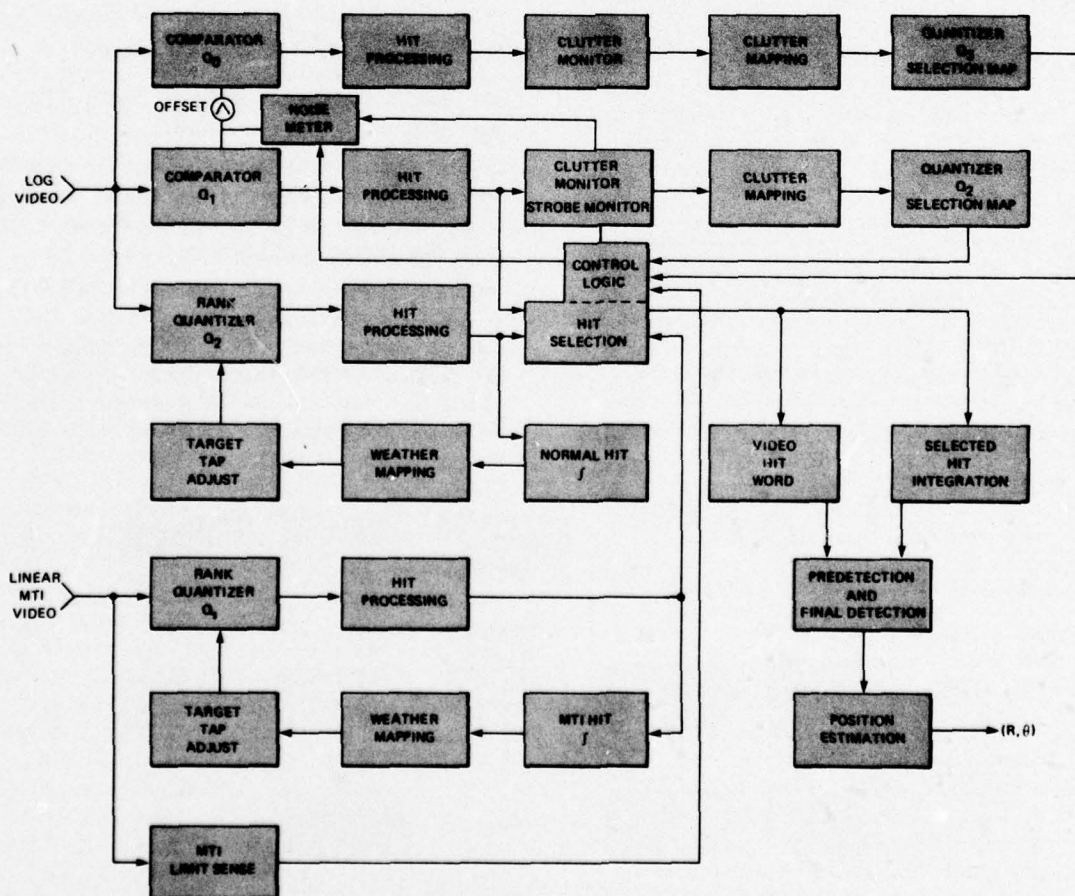


Fig. 2 Baseline RPS configuration.

compared to the 24 cells nearest in range once per scan, resulting in a constant false alarm rate at the output of the rank quantizers.

The hit processing blocks for the rank quantizers function in the same manner as those for the comparators Q_0 and Q_1 . Rank quantizers Q_2 and Q_3 drive two weather maps via scan-to-scan integration of the output of a sequential observer (up-down counter) monitoring the outputs of the quantizers. The weather maps are used to control the output false alarm rate of the quantizers by biasing the rank order test procedure as a function of an estimate of the degree of azimuthal video correlation present between adjacent radar sweeps.

The strobe monitor determines the presence of transient electromagnetic interference, while the MTI limit-sensing module determines if the MTI video is limiting (i.e., video output is at the saturation level).

The output of only one of the three quantizers (Q_1 , Q_2 , or Q_3) is fed to the final detection block at any one time. The choice is determined by the hit selection block, on the basis of the combined outputs of the strobe module, the MTI limit module, and the two quantizer selection maps. In the presence of receiver noise, comparator Q_1 is selected; in light clutter, normal rank quantizer Q_2 is selected; in medium clutter, MTI rank quantizer Q_3 is selected; and if MTI video is limiting, rank quantizer Q_2 is selected.

The video selected by the hit selection block is integrated in azimuth by a two-level second threshold. The first level, called a predetector, uses an up-down counter similar to the one used for weather mapping to check for azimuthally correlated groups of radar cells containing first-threshold crossings. When a predetection occurs, the radar software examines a row of 17 azimuthally adjacent radar cells centered on the

location of the predetection and counts the number of cells that contain a first-threshold crossing. If 8 or more of the 17 cells contain a first-threshold crossing, a target detection is declared (this is called an 8/17 second threshold). The radar software then proceeds to determine the range and azimuth of the centroid of the target. The centroid location is passed to another portion of the ARTS III Data Processing Subsystem for correlation with target reports received from the BDAS.

The baseline RPS configuration (Fig. 2) was simulated in NELIAC programming language for use on a Univac 1230 computer. The computer simulation was designed to use standard Burroughs variable quantizer recorder tapes of digitized ASR video as the input. A concurrent analytic simulation effort was undertaken to select suitable values for the various unspecified parameters contained in the system configuration and to measure system performance as influenced by these parameters. The results of this parallel effort were used to evaluate various features of the system, and several configuration modifications were developed.

The first modification is essentially a simplification of the baseline RPS design. The second uses two separate target detection channels. The third presents the basic characteristics of an all-digital RPS as a guide to future development work.

SIMPLIFIED RPS. Figure 3 shows the simplified RPS configuration. Either of two video formats may be selected for target processing: log normal or linear MTI. Both are processed by a rank quantizer.

The hit processing blocks function in the same manner as in the original system design. The final detection block consists of an azimuth sliding window that looks at 17 azimuthally adjacent radar cells and counts the number of cells that contain a hit. This number is compared to a threshold on a real-time

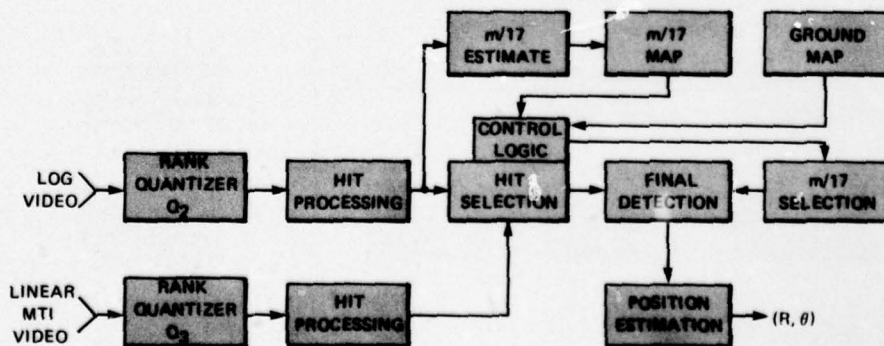


Fig. 3 Recommended simplified RPS configuration.

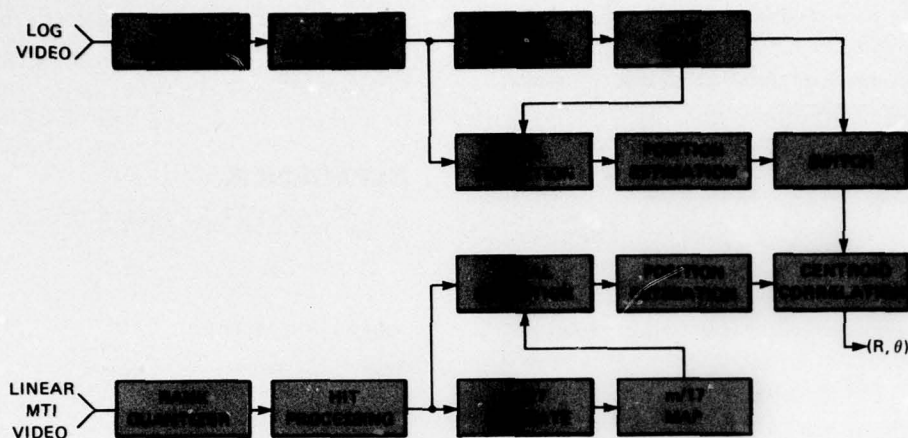


Fig. 4 Proposed modified RPS configuration.

basis. This threshold m is variable and is set by the $m/17$ estimation block, which estimates the azimuthal correlation present in each zone (2.8° by 2 nmi) within the radar coverage area. (If $m = 9$, then at least 9 of the 17 adjacent cells must contain a hit in order to pass the second threshold.)

The second threshold for each zone is stored in an $m/17$ map, which has a storage location for a second-threshold value for each of the 4096 zones that constitute the coverage area. This map is also used to determine which quantizer will be selected. A ground map indicates areas where MTI video will always be selected in order to eliminate radar returns from large stationary objects (buildings, mountains, etc.).

This system configuration represents a considerable savings in hardware, software, and complexity over the baseline configuration, without sacrificing system performance.

MODIFIED RPS. Figure 4 shows the proposed modified RPS configuration. Again the two basic video formats are available for processing, but instead of selecting one of the video formats as the input to the final detection block, both formats are processed in parallel through two independent final detection blocks. Three maps are required (two $m/17$ maps and one ground map not shown in the figure), since the second-threshold m estimates used in the final detection are independent for the log normal and linear MTI video input channels. For certain values of azimuthal clutter correlation, no value of second threshold will keep the number of false centroids reported per scan under the saturation level of the centroid processing algorithm. Hence, a "switch" function is inserted in the normal video path after the

position of the centroid has been determined. The switch prevents further normal video centroids from being passed to the radar software when the value of m selected for normal video exceeds 16/17 (16 hits in 17 azimuthally adjacent cells). This limiting value is an engineering estimate; it may prove advantageous to lower this limit after further study or operational usage.

The radar software (centroid correlation block) receives position estimates from either or both position estimation blocks and combines them into a single report for track processing by the ARTS III radar software.

The primary advantage of this configuration is that the problem of which quantizer output should be selected is eliminated. The determination of the proper second threshold to be used is put on a more rational basis, and problems associated with quantizer switching are eliminated.

FUTURE RPS DEVELOPMENT. During the current effort to improve and simplify the existing RPS design, it is appropriate to consider the type of system that will be desirable in the next generation design. Such consideration will permit a broader perspective of alternative designs and will lessen the probability of future development becoming prematurely locked into a particular design philosophy. The most obvious trend in radar processors and sensors is toward all-digitized systems whose basic features are:

1. Use of digital MTI as well as digital log video;
2. Simultaneous processing of both video channels;

3. Estimation of multilevel, mean-level azimuthal correlation;
4. Use of microprocessor technology to reduce cost and complexity;
5. Greatly reduced input/output and processing requirements on the general-purpose computer (less program maintenance);
6. Effective operation in correlated clutter environments; and
7. Improvement in target resolution and accuracy.

Such a system presents a new design philosophy and is currently under investigation for use in various Department of Defense programs. It represents a first

attempt at configuring such processing for FAA needs and should be viewed as an indication of possible future trends.

REFERENCE

1. R. M. Barnes and P. J. Voss, *Radar Processing Subsystem Evaluation, Final Report*, APL/JHU FP8-T-013, November 1975.

Author: P. J. Voss

Support: Department of Transportation, Federal Aviation Administration

DAT—A MOBILE DATA ACQUISITION SYSTEM

A mobile Data Acquisition Trailer (DAT) was designed and constructed to provide a highly sophisticated and versatile test control and radar data acquisition facility that can be operated at a host radar site. Thus, information concerning the performance of the radar/beacon sensor and the characteristics of the targets it sees, whether real or spurious, can be obtained. The DAT enables this task to be accomplished irrespective of the degree of automated radar data processing currently operating at the host site, and has minimal impact on the normal operations of the host facility.

BACKGROUND

APL is working to improve the quality of data derivable from radar/beacon sensors and is investigating optimal methods of processing data from one or several sensors. The performance of the task requires more detailed knowledge of the information provided by the sensors, including:

1. The number of aircraft detected by the radar system;
2. The number of aircraft equipped with beacon transponders and detected by the beacon interrogation system;
3. The number of false detections declared by the sensors as a result of precipitation or land interference, sensor noise, radio interference, etc.; and

4. Detailed information on sensor output in the immediate vicinity of targets (aircraft or false detections) of interest.

These data can be analyzed to determine the aircraft detection capability of a radar/beacon site, to determine the characteristics of spurious data, and to examine the difference between true and spurious detections in order to devise methods of minimizing false detections. In addition, the capability of simultaneous data collection from several noncollocated sensor sites is desirable.

APL's experience in the research and development phases of U.S. Navy search and fire control radar system programs, and its development of the U.S. Navy AN/SYS-1 Target Information Processing System, were applicable in the design and construction of the DAT.

DISCUSSION

The DAT equipment is shown in Fig. 1. The DAT was designed to operate with two-dimensional radar/beacon search sensors or a tracking radar. Sensor inputs are recorded directly on a wideband recorder and simultaneously processed in one of several available modes for storage on digital magnetic tape. Simultaneous data collection at several sites is accomplished by placing wideband video recorders at each

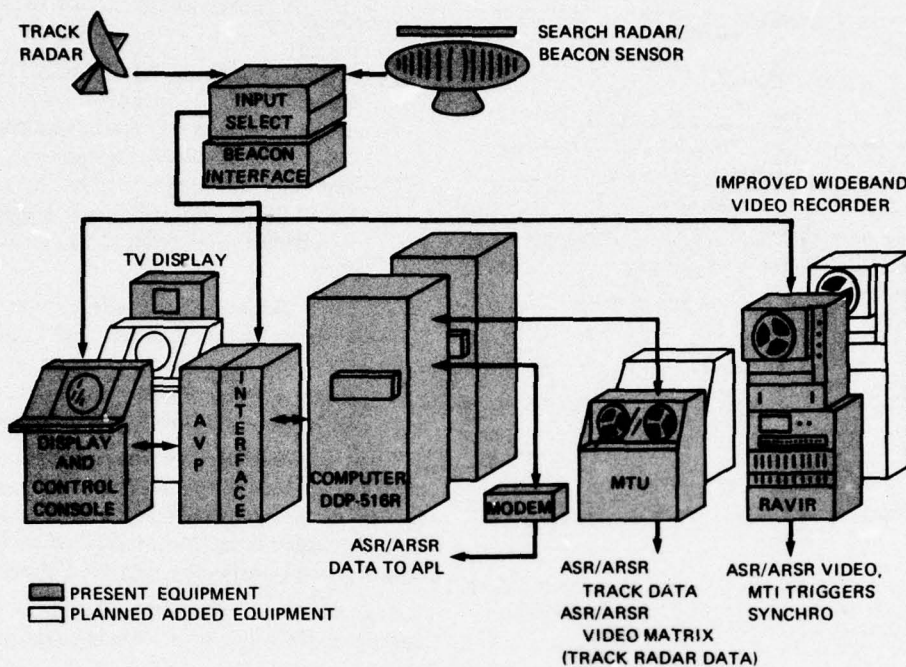


Fig. 1 DAT data collection equipment.

site, coordinating recording via the DAT control and communications system, and then playing the recordings through the DAT system for digital processing.

The input select unit chooses the desired DAT input from the available data sources and provides conditioning for all signals to be processed. Signals selected from either live inputs or prerecorded analog tape playback are fed to the appropriate interfaces where they are amplified, conditioned, coded, and formatted prior to distribution to the video processor, computer, displays, and recording equipment.

The Adaptive Threshold Video Processor (AVP) receives radar video or beacon video and provides target detections to the computer for target tracking. Radar data require dual processing before a target is declared. The first process derives a threshold from an analog sum, in range, of video samples prior to and following the target. When the target amplitude exceeds the first threshold, a first-threshold detection is declared. The second process is an azimuth correlation (M/N) performed on first-threshold-declared targets. This requires that M first-threshold crossings must occur out of N radar dwells at the same range before a second-threshold crossing is declared. When this occurs, the range of the detected target is sent to the computer. The sensitivity of both processes is selectable at the Display and Control Console.

A beacon target is declared when beacon video passes a first threshold of pulse width and spacing criteria and then the M/N azimuth threshold. An additional feature of the AVP provides video amplitude quantizing when a data collect matrix is generated by the computer.

The computer (Honeywell DDP-516R) has been programmed to provide four basic modes of digital data collection:

1. **Tracking**—The computer accepts targets declared by the AVP, performs scan-to-scan correlation, and classifies target tracks as fixed or moving, with a capacity of 256 of each. Track-position and velocity data are stored on digital magnetic tape. A typical moving track scenario generated by this mode is shown in Fig. 2.
2. **Hooked Track**—The computer performs the same functions as in the tracking mode. In addition, a target of interest may be selected (hooked) from the Display and Control Console, causing a computer-generated data matrix (40 samples in range by 63 samples in azimuth) to be centered around the target. Quantized video amplitude data generated by the AVP in this matrix are collected by the computer and stored with the normal track

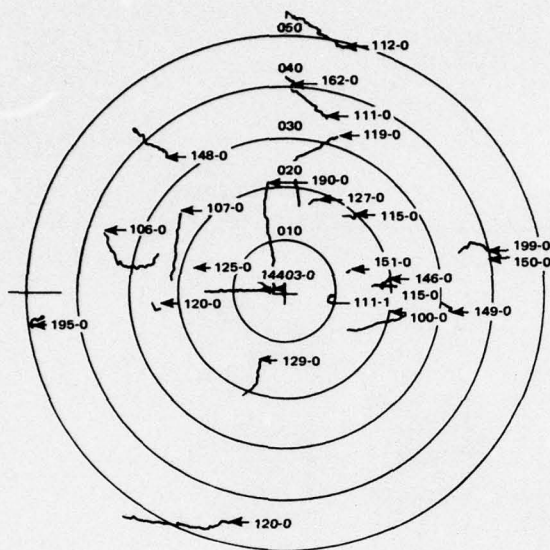


Fig. 2 Scenario of selected tracks seen by radar during a 5-min interval (rings signify 10-nmi intervals).

data. A portion of typical matrix data is shown in Fig. 3.

3. Video Quantizing—This mode provides for the collection of quantized video over a large area of interest. A matrix generated by the computer is manually positioned at the Display and Control Console. The matrix contains either 80 or 160 samples in range and up to 125 dwells in azimuth and is stored on digital tape.
4. Track Radar—This mode accepts track radar measured range, azimuth, and video amplitude data and uses the track radar coordinates to center a search radar data matrix. Data from both radars are stored on digital tape.

Computer-controlled modem communications with APL can be used to transmit real-time track data for immediate analysis and display. Another computer function provides on-site verification of DAT-generated digital magnetic tape data via TV display.

Data from the tracking mode can be analyzed to determine the number of aircraft in the sensor space,

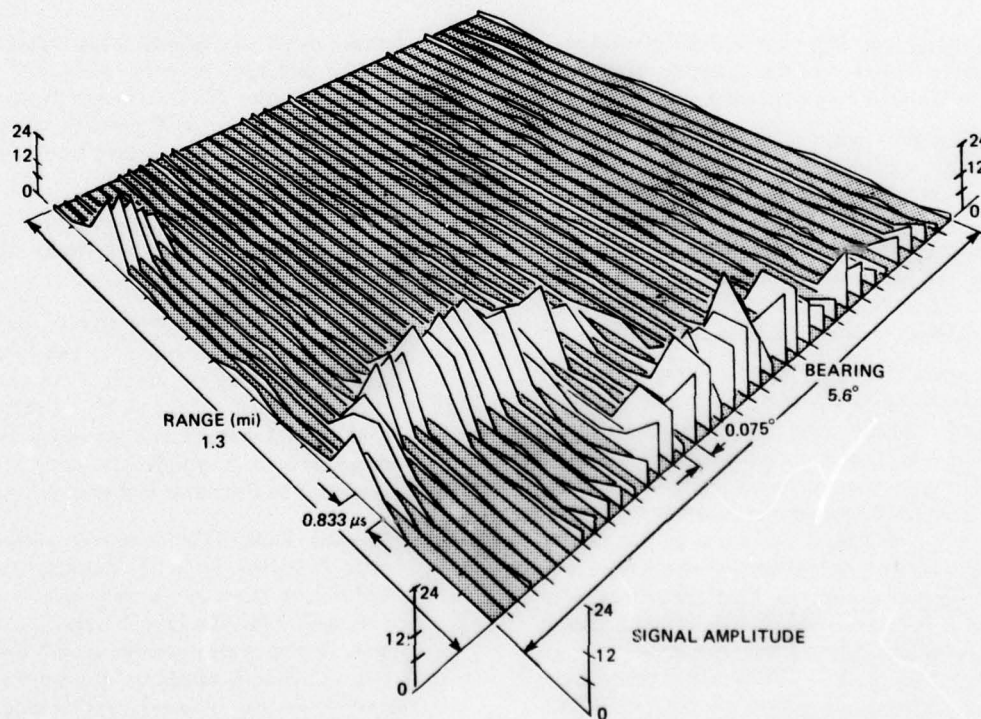


Fig. 3 A portion of the data collect matrix for search radar video from bird targets.

regions of the space where the sensor is blind (by flying a controlled test aircraft through the sensor space and determining the regions where it is not detected), the probability of detecting aircraft within the sensor space, and various data regarding an aircraft or group of aircraft within the sensor space (position, speed, and heading).

Data from the video quantizing mode can be used for detailed analysis of the video in the immediate vicinity of targets of interest. Useful parameters that can be determined include the range and azimuth correlation of the video, the mean amplitude of target signals, and other statistical data. This information can be used to develop new methods of detecting aircraft in the video and reducing false detections.

The hooked track mode provides all of the tracking mode data plus a reduced video quantizing capability. It has the advantage of accurately centering a computer positioned data matrix about a target as it moves through the sensor space and thus provides a detailed track life history of the motion and video signature of a target.

The track radar mode can be used in accuracy studies by comparing data from the track and search sensors. Also, since the tracking radar provides continuous data on a target, the characteristics of target video as a function of time can be described more accurately.

The analog recorder used in the DAT is the AN/SPH-1 Radar Video Recorder/Reproducer Set (RAVIR), which was designed and developed by APL for the U.S. Navy. When recording live data, it provides a fail-soft mode of data collection in the event of a failure in one of the digital processing components. Furthermore, if data must be collected at several noncolocated sites, only a recorder need be installed at the remote sites since the recorded analog tapes can be digitally processed in the DAT.

The Display and Control Console serves as the primary means of monitoring and controlling the performance of the processing equipment. By means of plan position indicator display and switching features, a wide variety of data can be displayed. It has the capability of identifying aircraft equipped with beacon transponders and selectively displaying their positions. The console, combined with the communications system (not shown in Fig. 1) enables the DAT to be a data collection command post while controlling test aircraft and mobile land units. Because the DAT is a self-contained unit (and self-supporting, if required), and because of the minimal equipment installation required at remote sites in multisite tests, the DAT can coordinate large-scale data collection efforts with minimal impact on the operations and procedures of the sensor user.

The DAT has been used in several data analysis efforts by the U.S. Navy and Federal Aviation Administration. One such effort involved the analysis of the radar video of birds (Fig. 3) in order that they not be mistaken for aircraft or obscure the detection of aircraft during periods of heavy bird migration. Every mode of DAT data collection was used in this task, and subsequent analysis resulted in several recommended methods of rejecting bird-generated false detections. Another effort involved the collection of data at several sensor sites that had overlapping coverage. The DAT controlled simultaneous data collection at each site and, by analysis of tracking mode information, APL was able to quantify the benefits achievable by processing the combined data from several noncolocated sensors.

Author: E. L. Brickner

Support: Federal Aviation Administration

SMALL-CAR STUDY

A study has been completed, in conjunction with the Center for Metropolitan Planning and Research of The Johns Hopkins University, that addressed the problems associated with the transition to a smaller private automobile. The results should be helpful in guiding policy for energy conservation in private automobile usage.

BACKGROUND

In examining ways to alleviate the world energy shortage, the private automobile has been singled out as one of the most likely targets for energy conservation, mainly because of its relatively large and ineffi-

cient use of energy. Various methods are available to improve the fuel efficiency of the private automobile. This study focuses on a very promising method to decrease curb weight and, implicitly, size.

Three questions arose at the outset of the investigation: How small is small? How do you sell such a car? What effects will result from a major shift to small cars? Although we have no firm answers to any of these questions, the study has raised a number of more restrictive questions that can lead to a better understanding of the problems associated with an orderly transition toward a smaller private automobile.

DISCUSSION

How SMALL IS SMALL? Since fuel economy improves as weight is reduced, the question really is: How small a car will satisfy safety, emission, comfort, aesthetic, and performance criteria acceptable to the consumer and to current/proposed government regulations? Three small cars weighing 2000, 1500, and 1000 lb, delivering 25, 35, and 45 mi/gal, respectively, are addressed. The findings suggest that cars weighing 1500 lb or less would be acceptable with respect to performance and comfort. A major shift to such cars by 1977 could save approximately 1 million barrels of oil per day by 1980.

Since several foreign cars weighing less than 2000 lb are already in growing use for both urban and highway travel, it seems clear that a small, limited-performance vehicle weighing less than 1500 lb would be acceptable for urban use. The most important problem is safety. A major shift to small cars could lead to a 15% increase in fatalities or serious injuries unless it is accompanied by the institution of safety measures such as improvement in and more extensive use of passenger restraint systems, improved structural design, and strict enforcement of speed limits.

Future emission goals also represent an unknown, in that enforcement of the presently scheduled reduction of the NO_x emission standard in 1978, the real need for which is being questioned, could nullify efforts to conserve fuel and hold car prices down. In this area, it is suggested that the current California standards be adopted as the Federal standards and that further reduction not be considered for a period of five years.

There do not appear to be any technological reasons why a small, low-emission, economical, and safe private automobile with a curb weight of less than 1500 lb cannot be mass-produced. To accomplish this

objective will require substantial design effort and the introduction of specific legislative incentives and constraints.

How Do YOU SELL IT? Current automotive industry marketing is directed toward making the consumer aware of fuel economy as evidenced in recent advertisements. The methods considered in this report are specifically directed toward those that can be formulated into legislation by the Federal Government. An attempt to compile from current literature what is known regarding price elasticities (i.e., a measure of the effect of a price change on demand for a product) has shown that the pertinent long-run elasticities vary over a considerable range so that the long-run market response to increased costs due to taxes and/or rebates cannot be predicted with great certainty. It is felt that a shift to small cars, through Government policy, might best be effected in the short run by tax/rebate policies designed to raise exponentially the original investment cost of automobiles as their fuel economy declines, and that large increases in the cost of gasoline must occur to effect a significant reduction in gasoline consumption.

WHAT EFFECT WILL RESULT FROM A MAJOR SHIFT TO SMALL CARS? A major conversion to small cars would improve traffic conditions and alleviate parking problems. If systems of parking segregated by size are instituted, a potential for twofold increases in both on-street and off-street parking capacities is foreseen. Other effects on the national economy are difficult to assess, and a meaningful analysis would require better data than are currently available. A "first approximation" analysis indicates that effects on the suppliers of raw materials for new cars could be great—e.g., an 8% reduction in total steel sales. A previous study led to the conclusion "that 1 percent change in new car weight results in a greater than 1 percent change in auto manufacturing employment" (Ref. 1). For these reasons, we recommend that a detailed study be initiated using such economics methods as input-output analysis in order to account for the interrelationships of the various economic sectors.

SAFETY. Three fundamental factors are involved in determining the crashworthiness of a vehicle:

1. A definable upper limit on the short-term deceleration forces that can be sustained by a *properly restrained* human body,
2. A required stopping/crushing distance proportional to the square of the initial velocity, and
3. A difference in the weights of two colliding vehicles that will amplify the deceleration forces imposed on the lighter vehicle.

The last factor is often used to explain away the safety hazards to small-car occupants; i.e., there wouldn't be a problem if everyone drove small cars. However, the first two factors refute this claim because (a) the human body can stand only a certain level of deceleration, which, for a given vehicle speed, dictates the required crush distance, and (b) present small cars have inadequate crush distance available within their frames for the speeds at which they travel.

Accident statistics show that the risk of driver injury when two subcompact cars collide is more than twice as great as when two full-size cars collide. Nevertheless, the risk of injury for the small-car driver is only one-fourth to one-half as great when he collides with another small car as with a large car.

A significant improvement in small-car safety can be achieved by addressing all three of the fundamental factors listed above and by taking action in the following areas:

1. **Passenger Restraint Systems** – Improvements in use and effectiveness of restraint systems are even more important for small cars than for large cars. For a 2000-lb car, injury rates can be halved by effective passive restraint systems such as automatically activated belts or air bags. The technology is available to produce effective and acceptable passive restraint systems. It is recommended that legislation be passed to require manufacturers to provide them.
2. **Speed Limits** – The "safe" speed for a 2000-lb car is 10 to 15 mi/h less than that of a 4000-lb car, assuming that passenger restraint systems are used. The national speed limit of 55 mi/h must be maintained and enforced and a further reduction in speed to 45 to 50 mi/h should be imposed on urban expressways where small-car traffic is heavy.
3. **Improvements in Small-Car Structural Design** – Small-car structures must be designed to some degree of crashworthiness. It is recommended that a 30-mi/h barrier crash be the goal, with emphasis on passenger safety rather than damage reduction. The structure must provide adequate crush distance. Additionally, it is recommended that the structure of large cars be limited in front-end stiffness so as to reduce their aggressiveness to the smaller cars.

COMFORT. Anthropometric studies suggest that an automobile with interior dimensions adequate to provide a commonly accepted level of comfort for the middle 90% of the riding public can be designed for automobile weights as low as 1500 lb. Maximum comfort and convenience, on the other hand, cannot be obtained without significant changes in extant compartment configurations. Further reductions in vehicle weight, to 1000 lb for instance, can be expected to reduce the percentage of the riding public that will accept the comfort level; however, no quantitative estimates have been formulated.

MARKETING AND POLICY CONSIDERATIONS. Selection of an optimal policy to effect a shift to small-car ownership depends heavily on empirical information about the price and income-elasticities of demand for gasoline, and the cross-elasticities between new and used cars and between cars and other modes of transit. Recent empirical studies provide a very wide range of estimates, none of which includes price increases as large as those recently experienced in the U.S. We therefore have very little hard evidence from which to work in estimating the effects of alternative mandatory and price (tax) policies.

On the basis of recent observations, the price-elasticities of demand for gasoline are relatively low, even in the long run, and tax policies must incorporate fairly large price increases in gasoline and in cars having low fuel economy, together with careful subsidy and rebate schemes, to effect a significant reduction in gasoline consumption without adverse effects on income. A shift to small cars can best be effected by tax policies designed to raise exponentially the original investment cost of automobiles as their fuel economy declines. Such a policy will have strong employment and income impacts that must be cushioned by redistribution of the tax revenues through other programs.

REFERENCE

1. S. Wildhorn, B. K. Burright, J. H. Enns, and J. F. Kirkwood, *How to Save Gasoline: Public Policy Alternatives for the Automobile*, Rand Corporation, Santa Monica, CA, R-1560-NSF, October 1974.

Authors: L. L. Perini, R. A. Makofski, J. F. George, R. M. Hanes, and F. F. Mark (APL), and A. Levy and K. Lyall (CMPR)

Support: IR&D

SUPPORTING DEVELOPMENT

INTRODUCTION

APL conducts a vigorous program of exploratory and advanced development in support of improved missile and defense systems. Identifying critical problems that may limit the effectiveness of weapon systems and applying new science and technology to provide solutions in a timely fashion can both increase the technical options available and improve the expertise of the APL staff for advanced system development. APL has long been in the forefront of aerodynamics, structures, propulsion, controls, and guidance technology and design for missile systems. Advanced development tasks in such areas as remote sensor technology and computer applications to data and systems management are also conducted to support APL's mission.

The items presented here are only a small sample of this class of work, selected for technical interest and possible applicability in nondefense areas. Nap-of-the-Earth Radar is a concept that may be potentially applicable to civil flight safety. Electronic beamsteering increases the capability of a parametric sonar for high-resolution ocean bottom surveys. The earth's electrostatic field may provide a simple, cheap system for obstacle sensing and avoidance for pilotless or small piloted aircraft under certain adverse visibility conditions, e.g., at night or in fog or low cloud cover. The error correction encoder/error correction decoder technique is generally applicable to high-density, multitrack, magnetic tape recording and reproduction.

NAP-OF-THE-EARTH RADAR (NOTER)

The Nap-of-the-Earth Radar (NOTER) described herein was developed as a demonstration of proof of principle. The project was based on a feasibility study of meeting requirements for helicopter terrain scanning and wire detection with a 95-GHz radar. Terrain avoidance and the avoidance of collision with unseen wires is a critical issue with military helicopter operations.

BACKGROUND

NOTER was intended to be capable of integration with any of the terrain imaging systems currently in advanced state of development by the U.S. Army to provide a day and night capability of nap-of-the-earth flight. At the time the development was undertaken, APL was aware of the Army's laser terrain warning system (LOTAWS) program. The objective of the NOTER program was to provide an alternate, near-term technique for evaluation. The Army subsequently decided to devote all its efforts to the laser approach.

A most pressing problem for military helicopter operations is the danger of collision with unseen wires. Army strike reports (Ref. 1) list collisions even with wires whose locations were known, as well as those intentionally or unintentionally deployed in a tactical environment. Discussions with operational personnel at the time of the feasibility study indicated that even very small, soft wires can disable a helicopter. The development of the effective air-defense systems now deployed worldwide makes very-low-altitude flight mandatory, which in turn necessitates the employment of wire detection and avoidance systems.

DISCUSSION

A study indicated that a radar system in the 95-GHz region could detect small wires, even in adverse weather conditions. To assemble and demonstrate such a system with available components was reasonably straightforward. Although components are currently somewhat expensive because of limited demand, the system has the potential of modest production cost. NOTER has no critical alignment and maintenance features and, accordingly, is well-adapted to the helicopter's harsh vibration and operational environment. Millimeter wave radar systems are basically compact, lightweight, and reliable and can be mounted on a helicopter as small as the Cobra. The operational char-

acteristics and general specifications of NOTER are listed in Tables 1 and 2.

TABLE 1
OPERATIONAL CHARACTERISTICS

Detect Army field wire (1/8-in. twisted pair) at range of 2 km and S/N of ≥ 10 dB
Detect #22 wire at range of 1 km and S/N of ≥ 10 dB
Covert operation as a result of limited range and pencil-beam RF propagation
Useful in moderately foul weather (e.g., fog, medium rainfall)
Field of view: 4° elevation by 200° azimuth
Automatic pilot alert system via visual indicator
Display: variable persistence CRT giving both pictorial rendition of entire field of view and analog display of range to wires or other objects.
Human interface: no special interpretive operator training required

TABLE 2
GENERAL SPECIFICATIONS

Frequency: 95 GHz
Transmitter: Amperex DX-287 magnetron
Peak power: 5kW
PRF: 2 kHz
Pulse length: ≥ 100 ns
Average power: ≈ 1.0 W
Antenna size: 18-in. diameter
Antenna type: Cassegrainian
Antenna scan: Palmer (via nutating subreflector)
Radar beamwidth: 9.4 mrad
Scan time: ≈ 1 s for total field of view
Range resolution: ≈ 50 ft
Display: CRT variable persistence (Tektronix 605)
Operational environment: airborne/helicopter
Size: nose pod ≈ 6 ft³
Weight: nose pod ≈ 85 lb; display/processor ≈ 50 lb
Power: ≈ 1.5 kW, prime

The current system has an easily comprehended visual pilot display with an audio/flashing-light warning system, and requires little or no operator training. The system consists of a nose pod weighing 85 lb with a volume of 6 ft³ (Fig. 1). The nose pod contains a scanning parabolic dish antenna, the 95-GHz magnetron, a klystron local oscillator, and the balance of the radar components (Fig. 2). The radar per-

OPERATOR'S CONSOLE
WITH AUXILIARY DISPLAY

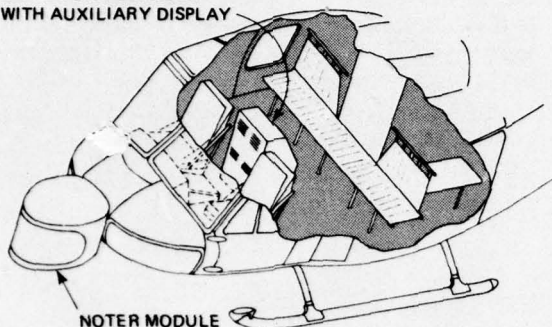


Fig. 1 UH-1 helicopter with NOTER.

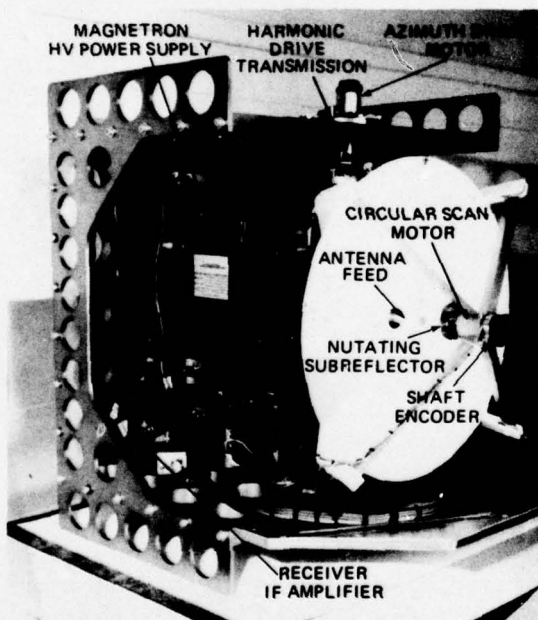


Fig. 2 Front view of radar.

forms a Palmer scan through an angle of 4° by 200° centered around the helicopter velocity vector. This is required so that a near-broadside aspect of the wire is always presented, irrespective of the relative geometry. Figure 3 shows the visibility of several different-sized wires in angle from broadside for various antenna diameters.

Figure 4 is a plan view plot of the total NOTER azimuth scan (200°) used in procuring a radar image of object space and of the radar's instantaneous field

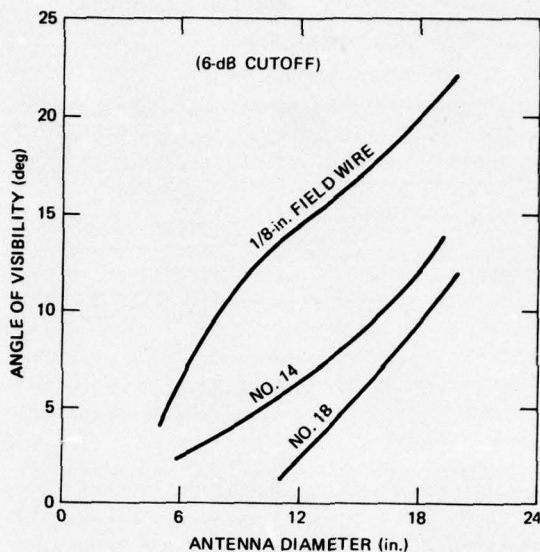


Fig. 3 Angular visibility of wire.

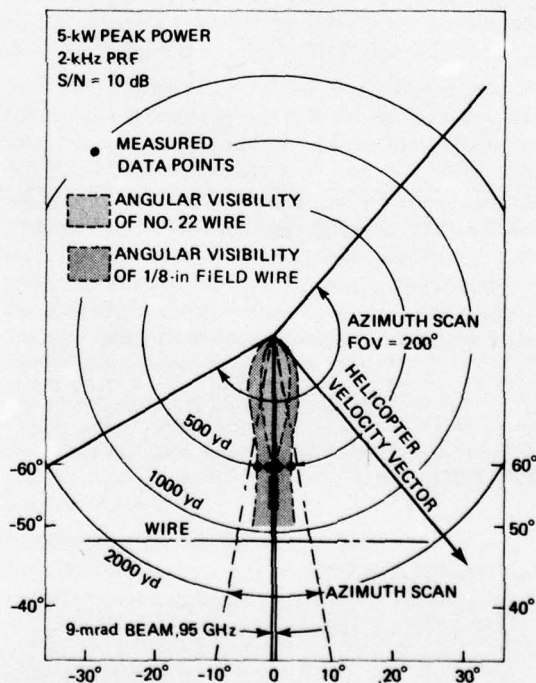


Fig. 4 Wire detection range versus angular incidence of radar beam.

of view. The angular visibility of a wire with respect to orthogonal radar beam impingement varies inversely with range and directly with wire size.

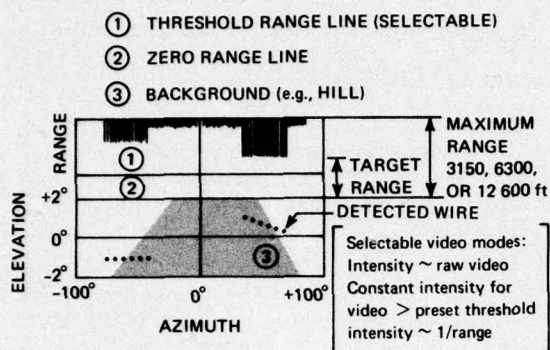


Fig. 5 NOTER display.

Figure 5 is a rendition of what the operator might see on the system's variable persistence display. The lower half of the display represents a pictorial view of object space. The upper half of the screen displays range to wires or objects shown in the pictorial posi-

tion of the display. A variable range threshold line is available for easy interpretation of object returns and proximity. The display, associated electronics, and power supplies are located within the helicopter.

The radar has been bench-tested with limited field tests at APL, and operates as designed. Flight operational field testing depends upon the support of the military services.

REFERENCES

1. W. P. Christian and A. W. Kuhns, *Wire Strike Mishap Analysis Report*, U.S. Army Board for Aviation Accident Research, Fort Rucker, AL, Report No. 71-2.

Authors: F. W. Schenkel and A. Finkel

Support: Defense Advanced Research Projects Agency
Tactical Technology Office

ELECTRONIC BEAMSTEERING FOR A PARAMETRIC SONAR

An innovative digital beamsteering and signal-generation system for a parametric sonar has been designed, fabricated, and tested by APL. In-water testing of the system demonstrated its versatility and marked the first time, to our knowledge, that a parametric sonar has been steered electronically over such a wide range of angles.

BACKGROUND

For the past several years, the Development Engineering Division of the Naval Oceanographic Office (NAVOCEANO) has been developing a parametric sonar for high-resolution bathymetric surveillance. In order to stabilize the sonar beam on a spot at the bottom of the ocean as the survey ship pitches and rolls, it was desirable to develop an electronic beamsteering system for the sonar capable of steering in two dimensions. Thus, in the fall of 1973 NAVOCEANO requested the assistance of APL in devel-

oping portions of a beamsteering and signal-generation system for the sonar.

APL subsequently has designed and fabricated an experimental digital beamsteering and signal-generation system and simultaneously designed and procured a 61-element transducer array (Fig. 1) from Gould, Inc., to be used for demonstrating the system. Fabrication of the array and the associated beamsteering electronics was completed in Fiscal Year 1975. Successful in-water tests of the integrated system were conducted in June 1975.

DISCUSSION

In a parametric sonar, the nonlinear compressibility of water or another medium is utilized to generate difference frequencies between two or more high-frequency transmitted sonar beams. The advantage of this arrangement is that the beamwidth at the differ-

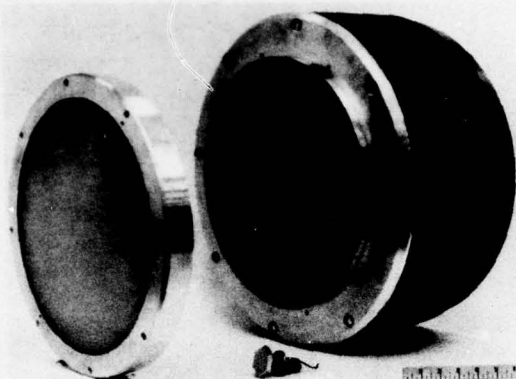


Fig. 1 Sixty-one element experimental array; faceplate and individual element are shown.

ence frequencies can be made as narrow as that of the transmitted higher-frequency beams.

The sound pattern in the water consists of regions of high-pressure fluctuations where there is constructive interference of the two signals and regions of little sound intensity where there is destructive interference. These regions propagate along the beam at the velocity of sound. In the regions where the sound intensity is high, the average density of the water, averaged over several cycles, is reduced from the ambient because of the nonlinearity of the compressibility of the water. Consequently, there is a pattern of moving density changes that correspond to the density and pressure variations of the desired low-frequency (or secondary) beam. The pattern generates the actual transmitted low-frequency beam, and it is easy to see why the beamwidth is the same as that of the higher-frequency beam.

Recognizing that the sound envelope pattern in the water determines the characteristics of the low-frequency beam, an innovative technique was devised at APL to create this envelope pattern in the water by modulating a *single* carrier frequency on and off. In this way, the beamsteering and the beam modulation are separate functions. It is not necessary to have a linear system transmit two frequencies through the beamsteering and power amplifier circuits to generate the sound in the water. It is necessary only to use a single high-frequency sonar beam steered in the desired direction and then to modulate the transmitting amplifiers to generate the sound pattern desired in the water. This permits the use of efficient amplifiers and simplified beamsteering circuits for a phased array, since the beam direction may be determined by phase

control (and this for a single frequency) rather than time-delay control. Only the pulse shaping at the desired difference frequency need be done with time-delay modulation control.

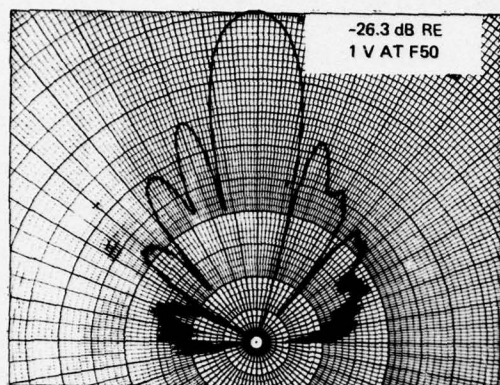
Once the principles of the APL signal-generation and beamsteering techniques were established, the techniques were implemented using digital electronics. A square wave was used for the high-frequency drive signal so that it could be represented solely by a series of 1's and 0's in digital logic. For the same reason, pulsewidth modulation rather than amplitude modulation was used to modulate the drive signal. During pulsewidth modulation, the power amplifiers are turned on and off with a varying duty cycle so that the distribution of sound energy in the seawater closely approximates that obtained with amplitude modulation.

Implementation of the beamsteering was achieved by passing the drive signal through a two-dimensional matrix of shift registers controlled by two variable-frequency clocks. The phase of the drive signal differed between each port of the shift-register matrix by a known and controllable amount. The phase-delayed signals from each port of the shift-register matrix were then applied to the proper elements of the array to steer the beam in pitch and roll.

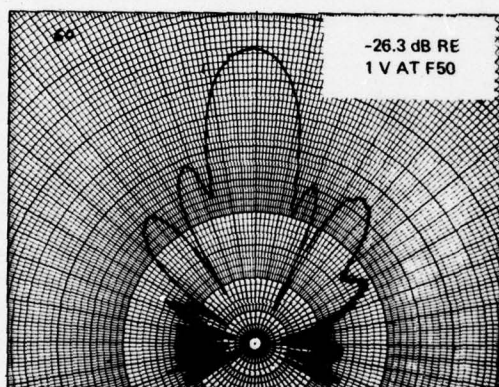
After a preliminary checkout of the 61-element array and the supporting electronics, a series of in-water tests was conducted at the Millstone Test Facility of NUSC near New London, CT. The APL digital signal generator was compared with a conventional sinusoidal signal generator, array beam patterns were measured at various frequencies, and nonlinear mixing was demonstrated. The APL signal generator produced the equivalent of two high-frequency sound beams in the water (Fig. 2). Furthermore, as desired, the patterns did not differ significantly from those obtained with a simple sine-wave drive. Finally, the APL beamsteering system was shown to function well by steering the primary beams in fine increments between $\pm 75^\circ$. A typical beam pattern is shown in Fig. 3 for a roll steering angle of 30° .

Beam patterns were also recorded at the difference frequency during the tests even though the maximum available range at Millstone was too short to allow full development of the nonlinear beam. Nevertheless, the beam patterns of the nonlinear beam shown in Fig. 4 display the narrow beamwidth characteristic of parametric patterns. Electronic beamsteering of the difference frequency was also demonstrated during the tests, as was chirping of the difference frequency by varying the modulation frequency of the carrier.

Based on the Millstone tests, the unique techniques devised at APL for signal generation and beamsteer-



(a) 24.2-kHz PATTERN

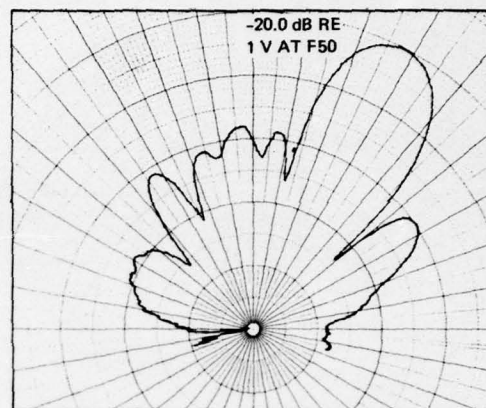


(b) 19.2-kHz PATTERN

Fig. 2 Broadside beam patterns obtained with modulated signal generator.

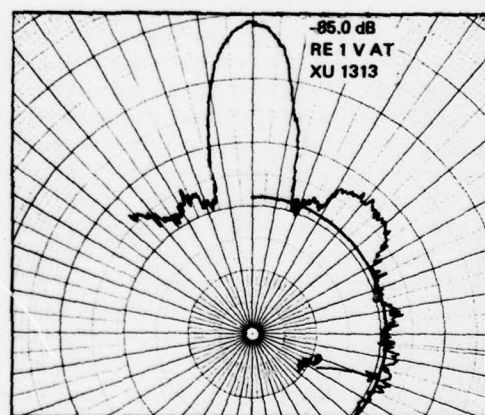
ing of a parametric sonar were shown to work well in practice as well as in principle. The system provided good quality steerable sonar beams at both primary frequencies, thus resulting in a well-developed steerable nonlinear beam in the water.

Author: M. L. Dwarkin, J. W. Follin, Jr., R. E. Miller, and D. W. Stowe



30° ROLL-STEERING ANGLE

Fig. 3 Roll-steering beam pattern obtained with unmodulated signal generator.



VDC = 85.0 V

Fig. 4 Difference-frequency beam pattern obtained during high-power modulated operation of signal generator.

Support: Naval Ocean Research and Development Activity (Code 351), formerly NAVOCEANO (Code 6222)

THE EARTH'S ELECTROSTATIC FIELD AS AN OBSTACLE SENSOR

The perturbations in the atmospheric electric field in the vicinity of orographic protrusions, as computed by Poisson's equation, have been experimentally verified for a limited range of parameters. These atmospheric field perturbations can be used, at least for a limited group of vehicles and protrusions, for terrain avoidance in "fair-weather" conditions.

BACKGROUND

Using relatively simple electronics and servomechanisms as an autopilot, M. L. Hill (Ref. 1) showed that it was possible to fly a remotely piloted vehicle (RPV) along the equipotential contours that exist in the atmosphere, parallel to the earth's surface. This "electrostatic stabilization" of flight over level terrain has been shown to be possible whenever the so-called "fair-weather" electric atmospheric field exists, typically about 90% of the time. Since the conductivity of the ground (or any orographic protrusion) is so much greater than that of the atmosphere, the boundary condition for the Poisson's equation describing the atmospheric potential is that the value of the potential at the earth's surface and over the surface of any protrusion is a constant conventionally taken as zero. Thus in the vicinity of all protrusions, natural or man-made, the atmospheric field will be distorted compared with the field that would exist for a flat earth. The possibility of utilizing the atmospheric electric field for obstacle avoidance depends upon the detection and use of these spatial disturbances.

DISCUSSION

The first-order attempt at a model for the atmospheric electric field posits a conducting layer at about 50 km altitude that is maintained at a positive potential relative to the earth of about 300 000 V by thunderstorm pumping. The spherical capacitor formed by the electrosphere and the earth is discharged by fair-weather leakage current densities of about 2×10^{-12} A/m². Under fair-weather conditions, the current density, J , is constant with altitude and the conductivity, λ , increases with altitude. Since $J = \lambda E$, where E is the electric field, the electric field has a divergence, $\nabla \cdot E = \rho/\epsilon_0$, where ρ is the charge density. Thus the atmospheric potential, ϕ , is given by Poisson's equation

$$\nabla^2 \phi = -\rho/\epsilon_0.$$

If it is assumed that the conductivity is a simple exponential function of the altitude, z , of the form $\lambda = \lambda_0 e^{\beta z}$, it can be shown (Ref. 2) that the atmospheric potential is a solution of

$$\nabla^2 \phi + \beta \frac{\partial \phi}{\partial z} = 0. \quad (1)$$

Computer and analytic solutions of Eq. (1) are discussed in Refs. 2 and 3. Figure 1 shows a computer solution of Eq. (1) for a 15-m wall (Ref. 3). It shows the contours of constant potential under the realistic assumption that the electric field strength at the surface of the earth is 100 V/m. These contours show the typical behavior of the electric field near a protrusion; as one approaches the wall, the horizontal component of the atmospheric field increases from zero. The vertical component decreases as one approaches the wall near the ground but is much higher than the unperturbed field directly above the wall. Figure 2 shows an analytic calculation, also from Ref. 3, of the potential contours near a cross section of South Mountain, Maryland. The horizontal component of the electric field is 5.5 V/m measured at a distance five times the mountain height at an altitude one-half the mountain height.

The computations all assume an idealized fair-weather atmospheric field with a vertical scale factor β , as contained in Eq. (1), of 2.5×10^{-4} m⁻¹. In the study of atmospheric electricity, the term fair weather refers to occasions when the electric field vector is

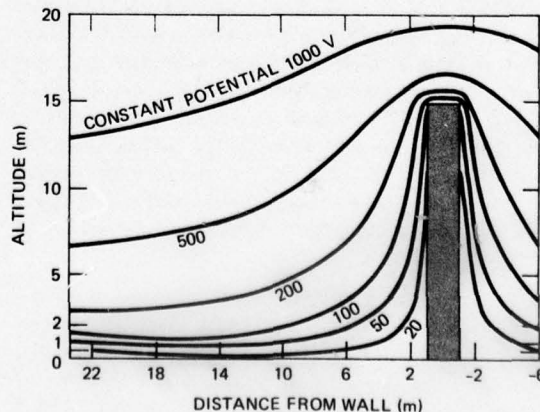


Fig. 1. Potential contours about a wall 15 m high.

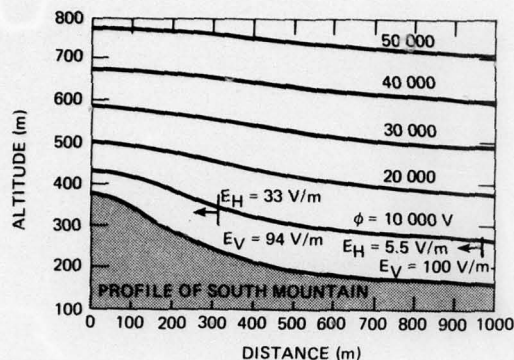


Fig. 2 Equipotential surfaces near South Mountain.

pointed toward the earth and there is no precipitation or electrical storm activity in the area. However, during times of meteorological fair weather, the atmospheric field can reverse and is always subject to significant fluctuations. These fluctuations are discussed in Ref. 4; their possible effects on obstacle avoidance are discussed in Ref. 3. As Ref. 3 shows, the fair-weather field exists at least 90% of the time over much of the earth, and fluctuations in the horizontal component of the field are rare near ground level.

The measurement of the atmospheric electric field or potential is difficult because the atmospheric resistivity is typically $5 \times 10^{13} \Omega/\text{m}$. For the experimental work reported here, three methods of measuring the atmospheric field were used (Ref. 3). For ground-based measurements, a very high impedance voltmeter, coupled to the atmospheric field with a radioactive equalizer, and a field mill were used. The field mill measures the electric field by means of the relationship $E = \sigma/\epsilon_0$ where σ is the bound charge on a conductor that is periodically exposed to the atmospheric field. Measurements from a Cessna 337 aircraft used both the high-impedance voltmeter and the low-impedance electric field-sensing circuit described in Ref. 1. All of these instruments are difficult to use. From an aircraft, there is the additional problem caused by the charging of the aircraft surface relative to the ambient atmosphere. Methods of minimizing or eliminating these difficulties are discussed in Ref. 3.

As discussed in Ref. 3, ground-based measurements of field perturbations about obstacles are best carried out using a field mill. Figure 3 shows the change in the vertical and horizontal components of the atmospheric field as a stepladder covered with a conducting mesh is moved toward a field mill

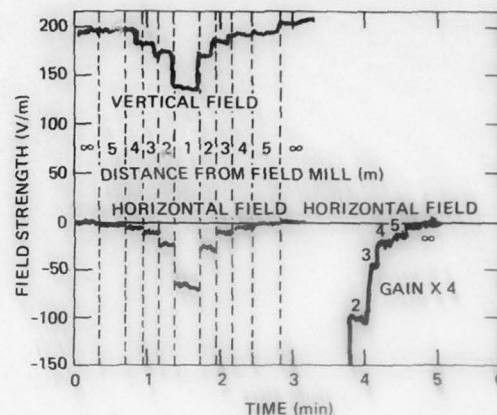


Fig. 3 Vertical and horizontal electric field versus time; measurements made with a field mill at various distances in front of a 2.4-m ladder covered with conducting mesh.

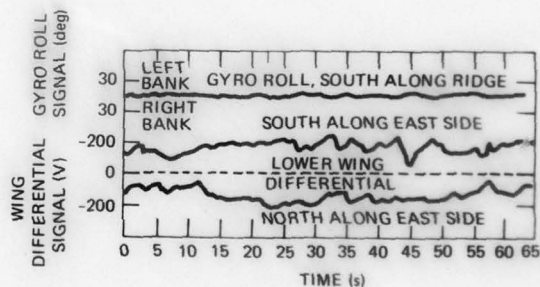


Fig. 4 Lower wing differential signal versus time; flights south and north along South Mountain at 1300 ft.

mounted 1 m above the earth. The results conform with those predicted from Fig. 2.

Figure 4 shows the potential difference measured wingtip to wingtip for an instrumented Cessna 337 aircraft flying parallel to South Mountain. Measured horizontal gradients of 15 to 20 V/m agree well with the predictions of Fig. 2 for a flight path just below the mountain peak and 200 to 300 ft from the slope. Since a variation in the horizontal field of 5 V/m can be detected, field disturbances for this type of mountain can be detected at horizontal distances of five times the mountain height for horizontal flight paths lying below the peak of the ridge.

REFERENCES

1. M. L. Hill, "Introducing the Electrostatic Autopilot," *Astronautics and Aeronautics*, 22-31 November 1972.
2. W. A. Hoppel, "Altitude Variations in the Electric Potential Resulting from Orographic Features," *Pure and Applied Geophysics*, 84, 1971, pp. 57-66.
3. C. S. Leffel, Jr. and M. L. Hill, *Use of the Atmospheric Electric Field for Terrain Avoidance*, APL/JHU TG 1271, April 1975.

4. H. Israel, *Atmospheric Electricity, I and II*, U.S. Department of Commerce, National Technical Information Service, Springfield, VA, 1973.

Author: C. S. Leffel, Jr.

Support: Defense Advanced Research Projects Agency

ERROR CORRECTION ENCODER/ ERROR CORRECTION DECODER

A high-density digital tape recording/reproducing system planned for use in one of APL's programs has an inherent bit error rate (BER) on the order of 10^{-6} . APL designed and developed an Error Correction Encoder (ECE) and an Error Correction Decoder (ECD) that reduce the effective BER to a value on the order of 10^{-11} . The lowered BER is achieved by generating coded information (parity bits) from the input data, recording that information on tracks that would otherwise be unused, and then, on playback, decoding the information and using it to correct errors in the data.

BACKGROUND

In the process of recording high-density pulse coded modulation (PCM) data on magnetic tape and subsequently playing back the data, the tape recorder/reproducer and the tape itself may introduce errors. Such errors are caused by the practical limits of tape recorder performance and minute imperfections in the magnetic tape. The measure of these errors, the BER, is the number of errors that occur in a given number

of bits. The high-quality, 14-track tape recorder/reproducer planned for use in an APL program records data at a density of 30 kilobits per inch and has a BER on the order of 10^{-6} . In this program, data will sometimes be received from only 8 or 12 input channels, thus leaving six or two tape tracks free for error correction information.

An innovative encoding and decoding technique was derived for accomplishing error correction by using the otherwise free tracks. The technique has been implemented in the ECE and the ECD. The ECE and the ECD will lower the overall BER to 10^{-11} .

DISCUSSION

Figure 1 is a simplified block diagram of the system in which the ECE and the ECD are designed to operate. For simplicity, control lines are omitted. Fourteen data channels (0 to 13) can be accommodated although error correction is possible only if 8

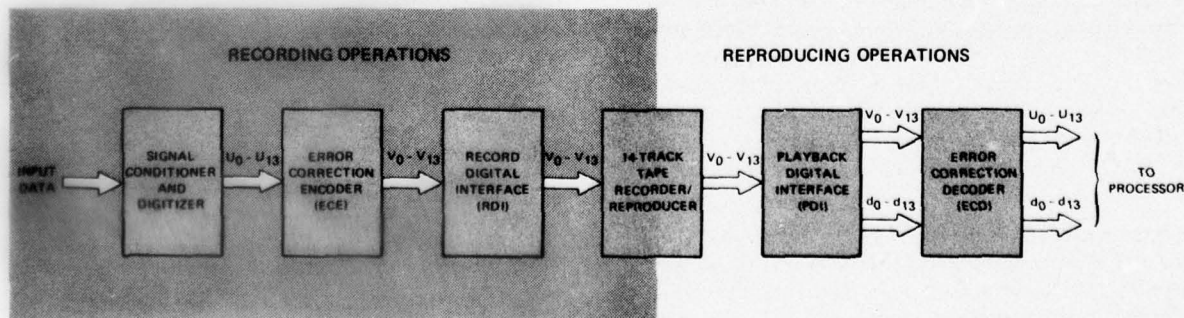


Fig. 1 Simplified block diagram of high-density digital tape recording/reproducing system.

or 12 are used. The record digital interface converts the data to a recording code and controls the tape recorder speed synchronization. The playback digital interface controls the tape recorder playback speed, synchronizes and deskews the data, and checks the data for dropouts by means of signal monitoring electronics. As a result of this last operation, the playback digital interface generates data quality information (d_0 to d_{13}) on a line-for-line, bit-for-bit basis.

The ECE and the ECD operate at rates up to 10 MHz. Several different modes are available, depending on the number of active input channels (8, 12, or 14) and the method of correction. (If all 14 channels of input data are present, then the ECE and ECD merely pass the data straight through.)

The addition of an external multiplexer and demultiplexer would allow handling data at 120 MHz from a single input channel, but would require a 42-track tape recorder/reproducer for subsequent recording.

RECORDING OPERATIONS. If eight channels of input data are present (14,8 mode), six modulo-2 adder circuits in the ECE generate 6 parity bits for each 8-bit word. In this case, the data appear in channels U_3 to U_{10} and the parity bits in channels U_0 to U_2 and U_{11} to U_{13} . Each 14-bit word from the ECE is complete in itself and independent of adjacent words.

If 12 channels of input data are present (14,12 mode), nine modulo-2 adder circuits in the ECE operate on a block of four contiguous words, generating 8 parity bits that are packed 2 in each word. The bits across four contiguous words in a single track constitute a byte. In this case, the data appear in channels U_1 to U_{12} and the parity bits in channels U_0 and U_{13} . Each 14-bit word from the ECE is not independent in itself (so far as parity is concerned), but rather the four-word block is an independent unit.

REPRODUCING OPERATIONS. On playback, the ECD can use the data and parity bits to detect errors

TABLE 1
ECE/ECD CORRECTION CAPABILITIES

Mode and Technique	Type of Data Errors Corrected
(14,8) Error correction	Three adjacent track errors Two adjacent track errors Two track errors separated by one good track Single track errors Double errors, parity tracks 0 and 13 (no error indication)
(14,8) Erasure correction	Single track error, where the track number matches the data-quality line indicating "bad data" or matches one of two data-quality lines indicating "bad data" Any two track errors where the track numbers match the data-quality lines indicating "bad data"
(14,12) Error correction	Byte errors on any single data track (a byte error can be one of the 15 non-zero combinations of the four bits)
(14,12) Erasure correction	Single byte errors on any single data track, where the track number matches the data-quality line indicating "bad data" or the track number matches either one of two data-quality lines indicating "bad data" Two byte errors on any two tracks where the track numbers match the data-quality lines indicating "bad data"

and correct the data by an "error correction" technique that is essentially the reverse of the encoding operation performed by ECE. Alternatively, the ECD can use the data-quality information from the playback digital interface, which indicates tracks or bit positions likely to contain erroneous data, to correct the data by an "error erasure" technique. A summary of the correction capabilities is given in Table 1.

Authors: P. J. Luke, J. L. Machamer, and W. A. Becraft

Support: U.S. Navy

RESEARCH

INTRODUCTION

APL requires thorough, up-to-date competence in the most recent advances in basic knowledge, which can only be maintained by carrying out creative research in the frontier areas of physical science. Applied research and development programs draw continually on advances in knowledge and understanding of basic physical phenomena but are often constrained by their product or application orientation from contributing broadly to the advancement of this knowledge. The APL Research Center provides this capability through innovative work in selected areas most pertinent to the APL technical programs. These comprise principally the mechanisms whereby matter and energy interact at the atomic or molecular and quantum levels, and their application to both microscopic and macroscopic physical and biological processes. In general, this research is aimed at void areas between the often highly idealized research problems characteristic of universities and the specific application or product-oriented research characteristic of industrial laboratories. Much of the work is multidisciplinary in order to fill the gaps between the traditional scientific disciplines.

The productivity, originality, and quality of this work are attested by more than 50 publications per year in leading professional journals and by many invited presentations. Only a small sample of this work is presented herein. Other research areas not covered here or elsewhere in this volume include applied mathematics, lasers, microwaves, and solid-state physics.

ORGANIC CONDUCTORS

Recent discoveries of several organic compounds with metallic properties at room temperature are of great potential technological significance. However, materials previously studied have been characterized by a sharp metal-to-insulator transition at temperatures above those where a transition to a superconducting state might be expected to occur. A new organic conductor, hexamethylene-tetraselenafulvalinium tetracyanoquinodimethanide (HMTSF-TCNQ), has been discovered that remains metallic to temperatures below 1°K.

BACKGROUND

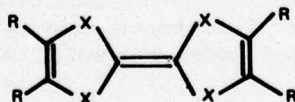
The original development of the salt of tetrathiofulvalene and 7,7,8,8-tetracyanoquinodimethane (TTF-TCNQ) raised the electrical conductivity of the organic metallic state by two orders of magnitude (Ref. 1). Since that development, related organic compounds of high conductivity have also been synthesized in this and other laboratories (Table 1). The possibility of creating organic compounds with superconducting properties at relatively high tem-

peratures has been precluded by the occurrence of metal-to-insulator transitions in all materials studied previously.

DISCUSSION

The newly discovered salt HMTSF-TCNQ is an addition to the class of quasi-one-dimensional conductors based upon the prototype TTF-TCNQ, but its properties represent a radical departure from those of previous compounds (Ref. 2). It is the first organic material to continue conducting as the temperature, T , approaches 0°K, with conductivity on the order of $10^3 \Omega^{-1}\text{cm}^{-1}$ at 1°K. This behavior is in sharp contrast to the other materials in Table 1 whose electrical conductivity, σ , is characterized by some σ_{max} at some temperature T_m and then a sharp drop below some critical temperature T_0 . Its room-temperature conductivity of $2200 \Omega^{-1}\text{cm}^{-1}$ is the highest of any known organic material.

TABLE 1
ORGANIC SEMIMETALS; 1:1 TCNQ SALTS OF



COMPOUND	R	X	σ_{RT} ($\Omega^{-1} \text{cm}^{-1}$)	$\sigma_{\text{max}}/\sigma_{RT}$	T_m
TTF	-H	S	500	20	59
DMTTF	2-H,2-CH ₃	S	50	25	~50
TMTTF	-CH ₃	S	1000	1	100
	-CH ₃	S	350	15	60
HMTTF	-CH ₂ CH ₂ CH ₂ -	S	500	4	80
TSF	-H	Se	800	12	40
DTDSF	-H	2S,2Se	500	7	64
TMTSF	-CH ₃	Se	1000	6	71
HMTSF	-CH ₂ CH ₂ CH ₂ -	Se	2000	No transition	

The molecular structure of HMTSF-TCNQ is illustrated in Fig. 1. The new donor molecule is the logical extension of the tetramethyl analogs TMTTF (Ref. 3) and TMTSF, which become insulating at low temperatures. However, the larger nonplanar molecule HMTSF is incompatible with the crystal structure of TMTSF-TCNQ. This leads to a disordered structure along one principal direction perpendicular to the stacking axis. The higher molecular symmetry, reduced coupling between conducting chains, and lack of three-dimensional long-range order suggest natural rationalizations for suppression of the insulating state.

From a room-temperature value of $2200 \Omega\text{-cm}^{-1}$, the resistivity $\rho(T)$ drops rapidly as the sample is cooled (Fig. 2). However, below 110°K , the curve flattens and passes through a broad minimum between 45° and 75°K , where the conductivity is about

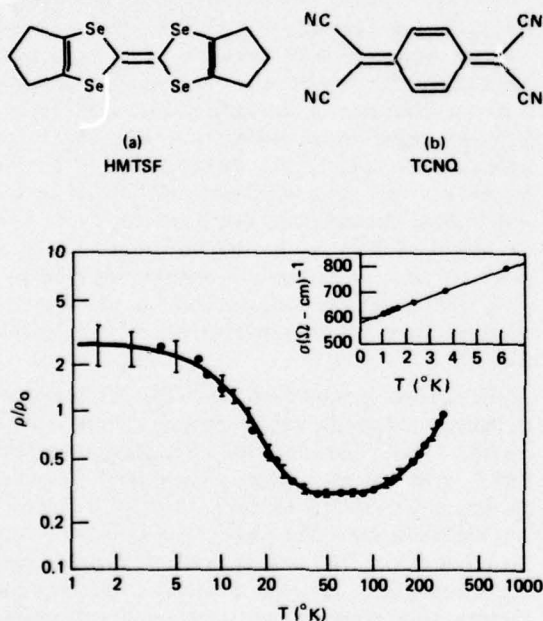


Fig. 2 Normalized DC resistivities (solid line) of nine samples and microwave resistivities (•) of two additional samples of HMTSF-TCNQ. (Inset: DC conductivity of typical crystal near $T = 0^\circ\text{K}$)

3.4 times the room-temperature value. With further cooling the resistivity rises again, but extrapolation from $T = 1^\circ\text{K}$ to $T = 0$ (inset) yields values still in the metallic range.

In close agreement with the DC results is the normalized microwave resistivity at 10 GHz, presented

in Fig. 2 for two additional crystals (Refs. 4 and 5). The microwave dielectric constant remains large and negative, as for a metal, throughout the temperature range. No electron spin resonance signal is observable in this compound at any temperature.

The resistivity appears to consist of at least two distinct contributions. Above 100°K , the normalized curves are highly reproducible; below 45°K , variations are substantially greater where conduction is presumably limited by impurities and lattice defects. The simplest assumption is that $\rho(T)$ is the sum of an intrinsic part that decreases and an "impurity" part that increases as the temperature is lowered, forming a minimum at their crossing point. Recent data for the quasi-one-dimensional inorganic polymer $(\text{SN})_x$ invite similar analysis (Ref. 6).

The intrinsic resistivity of HMTSF-TCNQ above 110°K is described by

$$\rho(T)/\rho(300^\circ\text{K}) = a + bT^\gamma \quad (1)$$

where $a = 0.264$, $b = 8.84 \times 10^{-7}$, and $\gamma = 2.39$. The other compounds in this class obey a similar relation with values for γ of 2.33 (TTF-TCNQ), 2.34 (TMTTF-TCNQ), and 2.4 (TMTSF-TCNQ). From the trend in the coefficient b , which decreases with molecular weight, it appears that the second term in Eq. (1) is phonon dominated. For a simple one-dimensional metal, the usual one electron-phonon interaction yields a resistivity proportional to T . The large value for γ found in these materials is not a general feature of one-dimensional metals but rather is a feature of two-band organic systems.

HMTSF also forms a conducting salt with the electron acceptor 11,11,12,12-tetracyano-2,6-naphthoquinodimethane (TNAP). Preliminary DC and microwave measurements indicate that HMTSF-TNAP remains metallic to 1°K and displays a resistance minimum at a somewhat higher temperature and lower conductivity than does HMTSF-TCNQ.

REFERENCES

1. J. Ferraris, D. O. Cowan, U. Walatka, and J. H. Perlstein, *J. Am. Chem. Soc.*, **95**, 1973, p. 948.
2. A. N. Bloch et al., *Phys. Rev. Letters*, **34**, 1975, p. 1561.
3. J. P. Ferraris, T. O. Poehler, A. N. Bloch, and D. O. Cowan, *Tetrahedron Letters*, **27**, 1973, p. 2553.
4. A. N. Bloch, J. P. Ferraris, D. O. Cowan, and T. O. Poehler, *Solid State Comm.*, **13**, 1973, p. 753.
5. T. O. Poehler et al., *Bull. Am. Phys. Soc.*, **20**, 1975, p. 440.
6. R. L. Greene, P. M. Grant, and G. B. Street, *Phys. Rev. Letters*, **34**, 1975, p. 89.

Author: T. O. Poehler

Support: NAVSEASYSOM

PHOTOEXCITED TRIPLET MECHANISM OF CHEMICALLY INDUCED ELECTRON SPIN POLARIZATION

A detailed study has been made of the role of photoexcited triplet-state molecules in the production of electron-spin-polarized radicals during the photodecomposition of carbonyl compounds. The predicted dependence of the electron spin polarization on the relative orientations of the electric vector of a polarized photoexcitation light source and the magnetic field has been observed, thus confirming the triplet mechanism.

BACKGROUND

Chemically induced magnetic polarization is the generic name for a number of recently discovered processes whereby free-radical reactions in liquids yield abnormal populations of the nuclear spin states of the diamagnetic products and reactants, and abnormal populations of the electron spin states of the free-radical intermediates (Ref. 1). The polarizations, which are readily observed by nuclear-magnetic-resonance and electron-spin-resonance spectroscopy, yield information about very rapid individual steps in the overall reaction mechanism that are difficult to study directly.

The origin of the strong electron spin polarizations produced by photodecomposition of aromatic carbonyl compounds is of interest, since these systems have both practical and theoretical importance as photochemical models. One possibility was the combined effects of chemical bonding interactions and magnetic interactions between two radicals (radical pair mechanism, or RPM); the other was the production of polarization in a photoexcited triplet-state molecule that then reacted to give a spin-polarized radical pair (triplet mechanism, or TM) (Ref. 2). A definitive experimental test of these two mechanisms was suggested by detailed analysis of the TM using a time-dependent quantum mechanical formulation to account for rotation of the molecule during the evolution of the electron spin states. This led to several interesting conclusions, the most notable being that the electron spin polarization depends on the relative orientation of a polarized photoexciting light and the external magnetic field (Ref. 3). Shortly after preprints of Ref. 3 were sent to scientists working in the field, the predicted light-polarization dependence was observed in the photodecomposition of various quinones by A. J. Dobbs and K. A. McLauchlan at Oxford University, England (Ref. 4) and J. K. S.

Wan and his co-workers at Queens University, Ontario, Canada (Ref. 5). This not only confirmed the TM as the source of the electron spin polarization in the systems but gave considerable information about the electronically excited states involved and their chemical reactivity, which must be considerably faster than was believed from earlier wet-chemistry experiments.

DISCUSSION

In the electronic ground states of most molecules, all electron spins are paired (singlet spin states), each pair forming one chemical bond. If an electron pair bond is broken, each of the resulting free-radical fragments has one unpaired electron. The magnetic moment associated with the spin of this unpaired electron may be parallel or antiparallel to an external magnetic field; thus, a free radical has a doublet electron spin state. In an excited electronic state of a molecule, the spin of the excited electron may be paired with the spin of its original partner in the fully paired ground state (excited singlet) or may be antipaired with it. In the latter case, the total magnetic moment of the two electrons may be parallel, antiparallel, or perpendicular to the external magnetic field, and the resulting state is a triplet spin state.

The electron spin state cannot change during photoexcitation, and so the singlet excited state is formed initially. Usually, however, the corresponding excited triplet state lies at a lower energy level than the singlet, and there is a tendency to slide "downhill" into the triplet state. The change in electron spin state (intersystem crossing, or ISC) is effected by the spin-orbit interaction, i.e., the interaction between the electron spin magnetic moment and the magnetic field produced by its orbital motion in the electrostatic field of the molecule. The interaction is naturally spin selective; however, since the starting singlet state is nonmagnetic, the initial triplet polarization must also be field independent and therefore resides in the purely intermolecular interaction between the magnetic moments of the two electron spins and the associated zero-field triplet spin states. After the "birth" of the triplet, the magnetic moments of these spins begin to interact with the magnetic field. Provided the magnetic field is strong enough, the

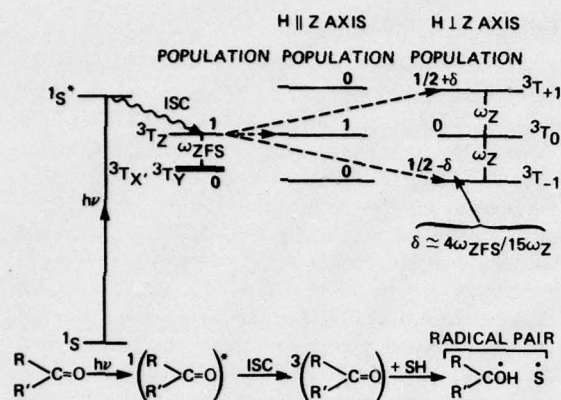


Fig. 1 Schematic description of the triplet mechanism of electron spin polarization.

purely intermolecular initial polarization is partially transferred to a polarization with respect to the magnetic field and the associated triplet Zeeman spin states.

The strength of the magnetic field is important because the rate of transfer of the polarization is determined by the rate at which the spin magnetic moments begin to precess about the magnetic field, thereby competing with the loss of the intermolecular polarization by random rotational motions of the molecules that average to zero the dipolar interaction between the electron magnetic moments. Finally, the chemical reaction of the triplet molecule transfers the polarization to a pair of doublet radicals. The last step must occur rapidly (within 10^{-8} s); otherwise, the modulation of the dipolar interaction by the random motions of the triplet molecule destroys the spin polarization by disorienting the steady precession of the spin magnetic moments about the magnetic field.

This process is indicated schematically in Fig. 1 where ω_{ZFS} is the spin-spin interaction energy; T_x , T_y , and T_z are the zero-field triplet spin states; ω_Z is the energy of interaction with the external magnetic field; and T_1 , T_0 , and T_{-1} are the Zeeman spin states in a strong magnetic field. Since the zero-field and Zeeman spin states are the same for some but not all orientations of the molecule with respect to the magnetic field, the amount of polarization that can be transferred from zero-field to Zeeman spin states depends on the initial orientation of the triplet molecule. This orientation can be partially controlled by using polarized light, which will excite only those molecules whose transition dipole moment has a component in the direction of the light polarization. This leads to a dependence of the observed polarization on the relative orientations of the light-polarization axis and the external magnetic field.

REFERENCES

1. A. R. Lepley and G. L. Closs, Eds., *Chemically Induced Magnetic Polarization*, John Wiley, New York, 1973.
2. S. K. Wong, D. A. Hutchinson, and J. K. S. Wan, "Chemically Induced Electron Polarization. II. A General Theory for Radicals Produced by Photochemical Reactions of Carbonyl Compounds," *J. Chem. Phys.*, 58, No. 3, 1 February 1973, pp. 985-989.
3. F. J. Adrian, "A Possible Test of the Photoexcited Triplet Mechanism of Chemically Induced Electron Spin Polarization: Dependence of the Spin Polarization on Polarized Light Orientation," *J. Chem. Phys.*, 61, No. 11, 1 December 1974, pp. 4875-4879.
4. A. J. Dobbs and K. A. McLauchlan, "Chemically Induced Electron Spin Polarization from Photolysis with Plane Polarized Light," *Chem. Phys. Letters*, 30, No. 2, 15 January 1975, pp. 257-258.
5. B. B. Adeleke, K. Y. Choo, and J. K. S. Wan, "Chemically Induced Electron Polarization. VI. Dependence of the Spin Polarization of 1,4-Benzosemiquinone and 9,10-Anthra-semiquinone Radicals in the Orientation of the Exciting Polarized Light," *J. Chem. Phys.*, 62, No. 9, 1 May 1975, pp. 3822-3823.

Author: F. J. Adrian

Support: NAVSEASYS COM

REACTION RATES OF H AND O WITH METHYL HALIDES

Rate constants for reactions of the type $H + CH_3X \rightarrow HX + CH_3$ and $O + CH_3X \rightarrow OH + CH_2X$ (where X is Br, Cl, or F) have been measured over the temperature range of 300 to 1000°K. These reactions are

important as prototypes in the basic understanding of flame inhibition by halogen compounds and may also be of interest in the chemistry of the stratosphere perturbed by such compounds.

BACKGROUND

Among the many substances that have been used as chemical inhibitors of flame propagation, some of the best are relatively simple compounds that contain halogen atoms, particularly bromine. The usual assumption is that such materials function as "radical traps," i.e., converting or diverting free atoms and radicals such as H, O, OH, etc. from their crucial role as chain carriers in the fast reactions upon which the combustion process depends. The more detailed understanding of such a mechanism will depend heavily on reliable knowledge of the rates of the various radical-inhibitor reactions. In another area, there has been much recent concern over the effects of species such as the chlorofluorocarbons and methyl halides on the stratospheric ozone layer, which is so vital to life on earth. The reaction rates of these species with simple atmospheric atoms and radicals (particularly O and OH) are of prime importance in assessing these effects.

For a number of years, the chemical kinetics research program at APL has been actively involved in measuring such atom-molecule reaction rates over a wide temperature range and under well-defined conditions. The basic apparatus (Fig. 1) consists of a fast-flow system in which atoms are generated by a microwave discharge in a small concentration of parent gas (H_2 or O_2) heavily diluted with an inert gas such as helium. The gases are pumped down a quartz reactor past a movable injector through which a stable reactant gas is added, and then to an electron spin resonance (ESR) cavity for atom detection and a quadrupole mass spectrometer inlet for stable species detection. The position of the movable injector determines the reaction time and allows the rate constant of the reaction to be measured. The reactor can be uniformly heated or cooled over a 200 to 1000°K range.

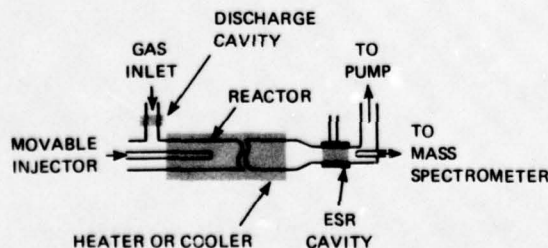


Fig. 1 Schematic of fast flow reactor.

DISCUSSION

For the present reactions, it was desirable to operate the apparatus with the concentration of H or O atoms in large excess over that of the CH_3X added through the movable injector. The mass spectrometer was then used to monitor the decay of CH_3X as a function of reaction time with an essentially constant atom concentration, thereby considerably simplifying the data analysis. Results for the rate constant of the reaction $H + CH_3X \rightarrow HX + CH_3$ are presented in Arrhenius form in Fig. 2 as the plotted lines through the experimental points (squares and circles). The differences in reactivity of CH_3Br , CH_3Cl , and CH_3F are immediately apparent and reflect the increasing C-X bond energy in that series. The greater effectiveness of CH_3Br as a flame inhibitor is also clearly indicated, since its appreciably larger rate constant permits the much more efficient removal of H atoms from the reaction zone. A subsequent fast step $H + HBr \rightarrow H_2 + Br$ means that two H atoms are effectively recombined to H_2 with the substitution of relatively unreactive CH_3 and Br. The tendency for the plots to curve somewhat upward at the high-temperature end may be an indication that the alternate reaction path $H + CH_3X \rightarrow CH_4 + X$ begins to contribute slightly under these conditions.

The triangular points in Fig. 2 are data obtained directly from the addition of CH_3Br as a trace flow from a "point" source in an actual H_2 - O_2 flame at temperatures in the 900 to 1100°K range. These data were from an entirely different experiment performed at APL (Ref. 1). The flame experiment was carried out using a mixture that was very H_2 rich, so that the concentrations of O and OH were greatly suppressed compared with H, and the contributions of $O + CH_3X$ and $OH + CH_3X$ were minimized. The agreement within a factor of 2 or 3 between the two experiments on $H + CH_3Br$ in the overlapping temperature range is satisfactory and tends to corroborate some of the assumptions made in the flame experiment. Even more striking is the agreement shown in Fig. 3, where data obtained as ratios of rate constants are presented from the two types of experiment. As ratio data, certain inherent errors in both techniques tend to cancel out, and the agreement is excellent. This is one of the very rare examples of a direct check on kinetic data obtained in an actual flame by an independent method at the same temperature.

Similar experiments were carried out on the reaction $O + CH_3X \rightarrow CH_2X + OH$ where X is Br or Cl. The O atom reactions differ fundamentally from the foregoing H reactions since the O reactions involve the abstraction of H from CH_3X while the $H + CH_3X$ reactions are halogen (X) abstractions. Thus

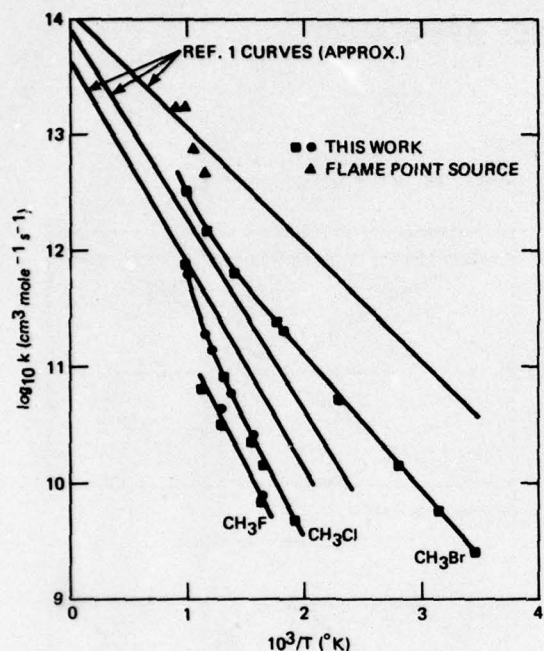


Fig. 2 Arrhenius plot of rate constants for $\text{H} + \text{CH}_3\text{X}$.

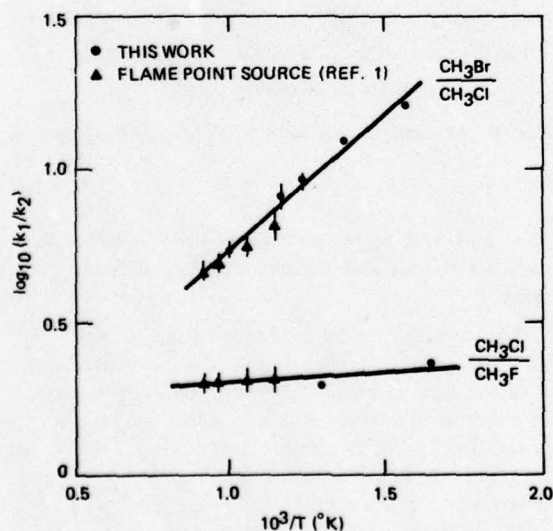


Fig. 3 Ratios of rate constants for $\text{H} + \text{CH}_3\text{X}$.

the $\text{O} + \text{CH}_3\text{X}$ reactions would not be expected to be effective flame inhibitor steps since they only result in the replacement of O by the still more reactive OH

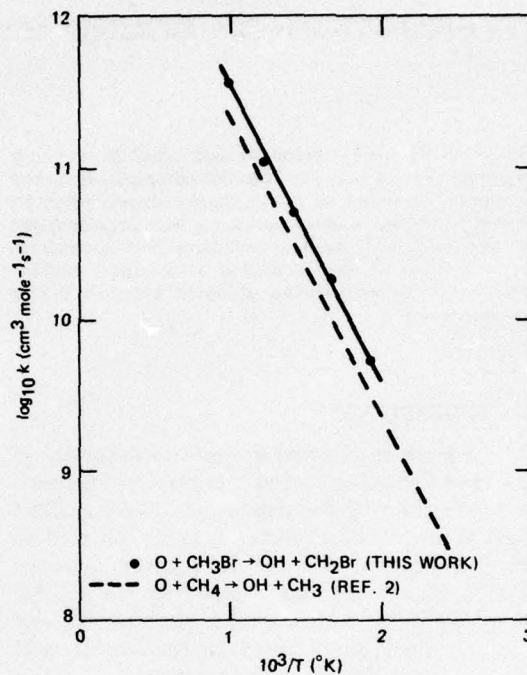


Fig. 4 Arrhenius plot of rate constants for $\text{O} + \text{CH}_3\text{Br}$.

radical. Results for the $\text{O} + \text{CH}_3\text{Br}$ rate constant are plotted as the solid line in Fig. 4. Also shown (the dashed line) are earlier data from APL (Ref. 2) on the reaction $\text{O} + \text{CH}_4 \rightarrow \text{CH}_3 + \text{OH}$. This is also a simple H abstraction step, and the similarity in slope (i.e., the activation energy) in the two cases is clear.

Results for both $\text{H} + \text{CH}_3\text{X}$ and $\text{O} + \text{CH}_3\text{X}$ reactions have been published (Refs. 3 and 4).

REFERENCES

1. L. W. Hart, C. Grunfelder, and R. M. Fristrom, "The Point Source Technique Using Upstream Sampling for Rate Constant Determinations in Flame Gases," *Combustion and Flame*, **23**, 1974, pp. 109-119.
2. A. A. Westenberg and N. deHaas, "Reinvestigation of the Rate Coefficients for $\text{O} + \text{H}_2$ and $\text{O} + \text{CH}_4$," *J. Chem. Phys.*, **50**, 1969, pp. 2512-2516.
3. A. A. Westenberg and N. deHaas, "Rates of $\text{H} + \text{CH}_3\text{X}$ Reactions," *J. Chem. Phys.*, **62**, 1975, pp. 3321-3325.
4. A. A. Westenberg and N. deHaas, "Reaction Rates of $\text{O} + \text{CH}_3\text{Br}$ and $\text{O} + \text{CH}_3\text{Cl}$," *J. Chem. Phys.*, **62**, 1975, pp. 4477-4479.

Authors: A. A. Westenberg and N. deHaas

Support: National Science Foundation RANN Grant GI-34288X

ATTENUATION OF SOUND BY RIGID SPHERES

An acoustic cavity technique was used to measure separately the viscous and thermal components of the attenuation of sound by rigid spheres. Experiments on spheres of known size in various gases provided, for the first time, a rigorous quantitative test of theoretical predictions of the individual attenuation components. Good agreement was obtained between theory and experiment.

BACKGROUND

The absorption of sound by particles suspended in a gas is an interesting process that plays an important role in determining the stability of solid-propellant rocket motors. Theory (Refs. 1 to 3) predicts an acoustic attenuation that can be resolved into two terms: a viscous component caused by the relative motion of the gas with respect to the particles, and a thermal component caused by irreversible heat transfer between the gas and the particles.

Despite extensive previous experimental studies on the attenuation of sound by particles of various sizes in suspensions and emulsions, a rigorous quantitative verification of the theoretical predictions for the individual components of attenuation had not been obtained. Under typical experimental conditions the particles are subjected simultaneously to both viscous and thermal damping effects, so that the individual effects are not separable. In the experiments reported here (Ref. 4), spheres of known size were suspended in an acoustic cavity so that they could be selectively subjected to either viscous or thermal damping, thereby permitting the two components of attenuation to be measured independently.

DISCUSSION

The principle of the method can be understood by considering the standing wave patterns (Fig. 1) for a cylindrical acoustic cavity excited in the fundamental and second harmonic longitudinal modes. At positions corresponding to velocity antinodes, particles would be subjected only to viscous damping, while at velocity nodes (pressure antinodes), they would be subjected only to thermal damping. For example, if a particle were translated along the axis of the cavity excited in the second harmonic mode, it would be subjected to maximum thermal damping at $X = 0$, $L/2$, and L ; to maximum viscous damping at

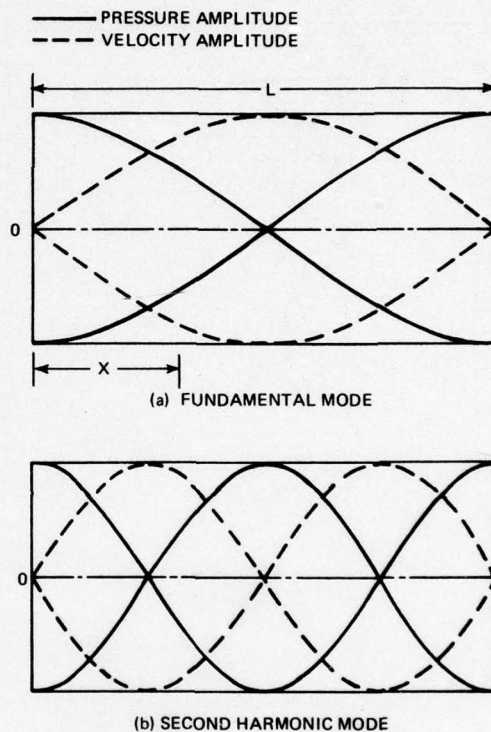


Fig. 1 Acoustic cavity excited in longitudinal modes.

$X = L/4$ and $3L/4$; and to readily calculable mixtures of viscous and thermal damping at other positions.

The acoustic cavity arrangement is shown schematically in Fig. 2. Standing waves are generated by a piston-type vibration generator. The small change in cavity damping produced by one or more spheres suspended by the translating rod is measured. To do this, the acoustic driver (vibration generator) is programmed to excite a particular mode for a prescribed time, typically 10 ms, allowing the energy in that mode to build up. The driver is then turned off, causing an exponential free decay of the acoustic pressure, P , in accordance with the expression $P = P_0 e^{-\alpha t}$, where P_0 is the pressure at time $t = 0$, and α is the decay constant in nepers per second (Np/s). In order to obtain accurate measurements of the decay constant, a special electronic system had to be designed (Ref. 4). With this system, changes

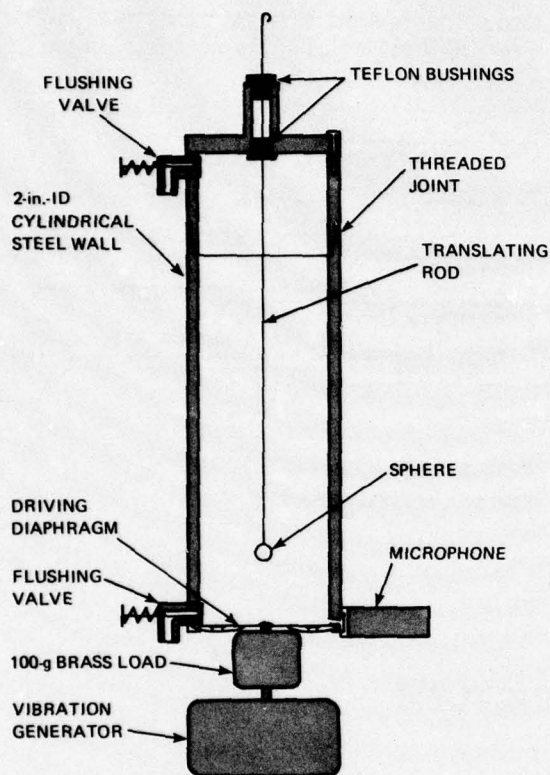


Fig. 2 Acoustic cavity arrangement for attenuation measurements.

in the decay constant of about 0.002 Np/s, representing about 0.01% of the empty cavity damping, could be readily observed.

Experiments were carried out on rigid spheres having diameters of 0.794 cm (5/16 in.) and 0.953 cm (3/8 in.) in argon, nitrogen, and dichlorodifluoromethane (Freon-12). These gases were selected in order to cover a wide range in the relative influence of viscous to thermal damping.

Experimental data for the damping produced by a single 0.953-cm-diameter ball bearing in argon are shown in Fig. 3. The cavity was excited in the second harmonic mode at a frequency of 1.1195 kHz. Curve A shows the cavity damping produced by the ball bearing and the translating rod, curve B shows the damping produced by the translating rod alone, and curve C shows the difference between curves A and B and gives the attenuation produced by the ball bearing alone. The solid curve is the attenuation predicted by theory. The data are in good quantitative agreement with theoretical calculations for both vis-

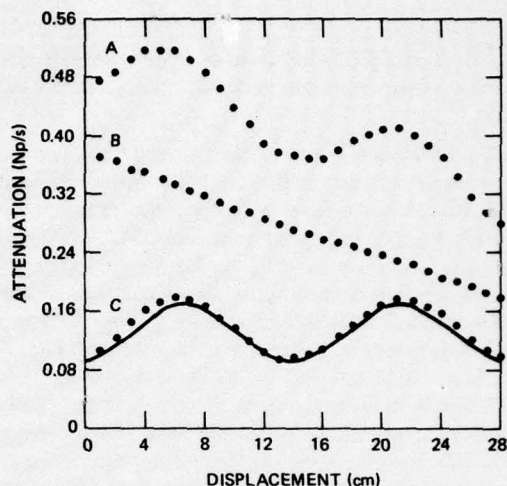


Fig. 3 Experimental data for the damping of a single 0.953-cm-diameter sphere in argon.

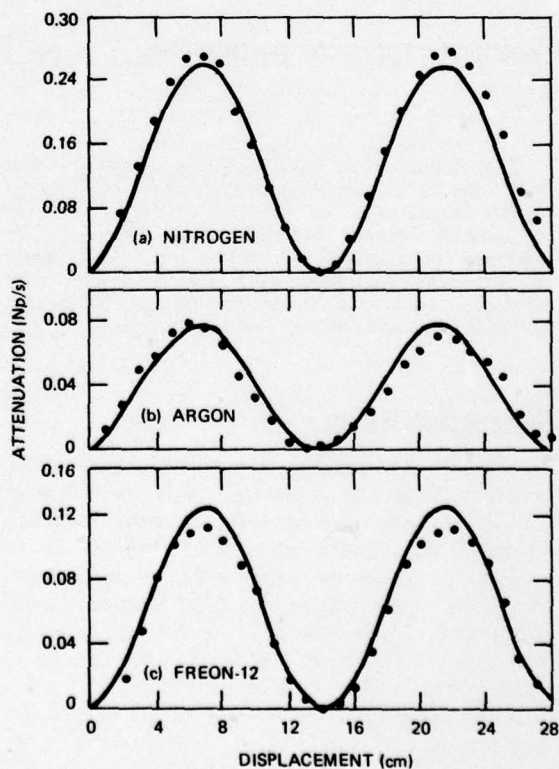


Fig. 4 Comparison of experiment with theory for the difference between viscous and thermal attenuation for spheres in various gases.

cous and thermal attenuations. The sinusoidal variation of attenuation with distance is as expected, with maxima at velocity antinodes and minima at velocity nodes.

The difference between the viscous and thermal components of attenuation can be measured with good precision, without requiring the cavity to be opened. Results for spheres in nitrogen, argon, and Freon-12 are given in Fig. 4. Figure 4a shows the variation in attenuation with displacement for three 0.953-cm ball bearings in nitrogen, Fig. 4b for a single 0.953-cm ball bearing in argon, and Fig. 4c for three 0.953-cm ball bearings in Freon-12. The theoretically calculated values in each case are shown as solid curves. The experiments cover a wide range in the relative importance of thermal to viscous damping, ranging from 0.544 for argon, to 0.322 for nitrogen, to 0.0975 for Freon-12. The agreement between

theory and experiment is very good and provides quantitative verification of the theoretical analysis.

REFERENCES

1. P. S. Epstein and R. R. Carhart, "The Absorption of Sound in Suspensions and Emulsions. I. Water Fog in Air," *J. Acoust. Soc. Am.*, 25, 1953, pp. 553-565.
2. J. C. F. Chow, "Attenuation of Acoustic Waves in Dilute Emulsions and Suspensions," *J. Acoust. Soc. Am.*, 36, 1964, pp. 2395-2401.
3. S. Temkin and R. A. Dobbins, "Attenuation and Dispersion of Sound by Particulate Relaxation Processes," *J. Acoust. Soc. Am.*, 40, 1966, pp. 317-324.
4. S. N. Foner and B. H. Nall, "Attenuation of Sound by Rigid Spheres: Measurement of the Viscous and Thermal Components of Attenuation and Comparison with Theory," *J. Acoust. Soc. Am.*, 57, 1975, pp. 59-66.

Authors: S. N. Foner and B. H. Nall

Support: NAVSEASYS COM

MOLECULAR ENERGIES AND STRUCTURE

The diagrammatic many-body perturbation theory has been formulated through third order and applied to the calculation of electron pair correlation energies of several diatomic molecules. The high accuracy achieved indicates that this technique should be useful for the determination of other correlation-dependent properties such as electronic spectra, photoionization potentials, polarizabilities, and susceptibilities.

BACKGROUND

Chemical reactions play an important, fundamental, and pervading role in nature and in man's use of nature in such areas as fuels, synthetic materials, chemical lasers, and interactions of chemicals in the atmosphere. A deeper understanding of the intimate details of the underlying chemical reactions would enable much progress to be made in terms of energy efficiencies, new improved materials, and redesign of existing processes to optimize certain desirable products. In many cases, knowledge of the energy and structure of an unstable chemical intermediate is required but cannot be obtained through experimental means. Thus, it is necessary to develop theoretical approximations that are accurate and reliable. The theory must first be applied to fairly elementary systems in order to determine the suitability of the method. Then

the methods can be extended systematically to more complex and difficult problems. The present work indicates that the diagrammatic many-body perturbation theory offers a very promising approach to these chemical problems.

DISCUSSION

The many-body perturbation theory had been developed originally for nuclear physics. Later it was used successfully to describe the electronic structure of atoms. Current work (Refs. 1 through 4) brings these methods to bear on molecular systems. The essential difficulty with molecules is that the electrons are distributed among several nuclear centers. This problem has been overcome in the present work by the use of basis sets of Slater-type atomic orbitals located on all nuclear centers.

Preliminary applications have been made to the calculation of pair-correlation energies in the diatomic hydrides LiH, BH, and HF (Ref. 1) and NaH (Ref. 2), using small basis sets. More extensive calculations have been carried out (Refs. 3 and 4) using quite large basis sets consisting of 46 orbitals for the closed-shell first-row diatomic hy-

drides. Even though the first-order perturbation expansion yields 99.62% of the energy of the HF molecule, this energy is so large that the remaining 0.38%, called the correlation energy, represents an error of over 225 kcal/mole, which is orders of magnitude greater than the tolerable level required for "chemical accuracy" (about 1 to 10 kcal/mole). To obtain this degree of accuracy, higher orders in the perturbation expansion need to be considered (Ref. 5).

In the many-body approach, the correlation energy is developed in terms of diagrams representing various types of interelectronic interaction. All the relevant diagrams are presented in Fig. 1. The second-order correlations are derived from diagrams A and B in the figure. Diagrams C and D are of the third-order "particle-ladder" type, and diagrams E and F are the corresponding third-order "hole-ladder" terms. The third-order "ring" diagrams G through N represent "hole-particle" interactions. Finally the third-order diagrams Q through T represent the interaction between excited state orbitals and an arbitrary potential (Ref. 6).

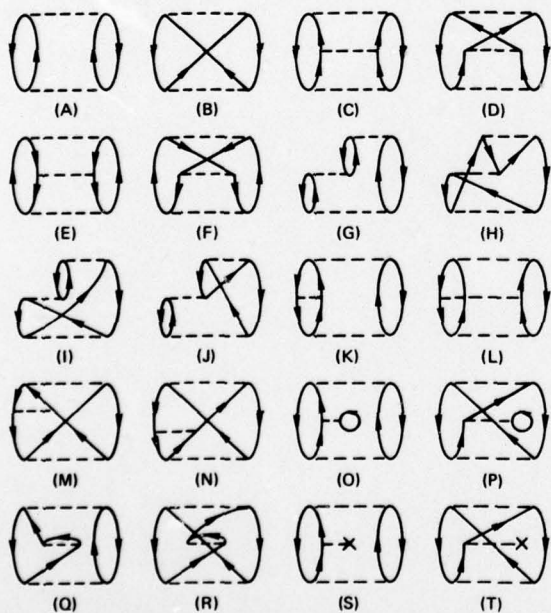


Fig. 1 All second-order (A and B) and third-order (C through T) energy diagrams contributing to the correlation energy of molecular systems in the many-body perturbation theory.

The perturbation expansions make use of all possible N -electron determinantal wave functions that can be constructed from a given basis set. Through third order, this collection of excited-state determinants consists of double excitations from the reference

state, i.e., determinants formed from the reference determinant by deleting orbitals i and j and replacing them with orbitals a and b , for all unique combinations of the indexes i, j, a , and b . The total possible number of these double excitations arising from the 46 orbital basis sets (Refs. 3 and 4) is 22 968 for LiH, 54 825 for BH, and 149 445 for HF. However, because of the spin and spatial symmetry orthogonalities of the molecular orbitals, the number of determinants entering the perturbation expansions with nonzero interactions is reduced to 2396 for LiH, 5355 for BH, and 14 377 for HF. One of the powerful attributes of the diagrammatic perturbation method (Ref. 5) is that all of these nonzero interactions can be efficiently taken into account. This is in striking contrast to other methods for handling the electron correlation problem, where it is feasible to include the effects of only a small subset of these interactions.

All of the nonzero determinantal states have been used to calculate the various correlation energy corrections indicated in Fig. 1. For each of the closed-shell first-row diatomic hydrides, this work recovers more than 94% of the experimental correlation energy when the diagrams of Fig. 1 are calculated with pair restrictions and include selections of higher-order diagrams via denominator shifts. For the HF molecule in particular, 97% of the correlation energy is recovered, representing 99.99% of the total energy with a residual error of only about 6 kcal/mole. For the LiH and BH molecules, the residual errors are about 3 and 5 kcal/mole, respectively.

The application of the many-body perturbation theory has been able to produce energy results that are within chemical accuracy for these systems. This work provides the most accurate numerical determination of correlation energies ever obtained for these systems. Moreover, the results are amenable to a pair-by-pair analysis, which permits an understanding of the various interaction processes.

REFERENCES

1. R. J. Bartlett and D. M. Silver, "Correlation Energy in LiH, BH, and HF with Many-Body Perturbation Theory Using Slater-Type Atomic Orbitals," *Intern. J. Quant. Chem.*, **S8**, 1974, pp. 271-276.
2. R. J. Bartlett and D. M. Silver, "Pair-Correlation Energies in Sodium Hydride with Many-Body Perturbation Theory," *Phys. Rev.*, **A10**, 1974, pp. 1927-1931.
3. R. J. Bartlett and D. M. Silver, "Many-Body Perturbation Theory Applied to Hydrogen Fluoride," *Chem. Phys. Letters*, **29**, 1974, pp. 199-203.
4. R. J. Bartlett and D. M. Silver, "Many-Body Perturbation Theory Applied to Electron Pair Correlation Energies. I. Closed-Shell First-Row Diatomic Hydrides," *J. Chem. Phys.*, **62**, 1975, pp. 3258-3268.
5. R. J. Bartlett and D. M. Silver, "Some Aspects of Diagrammatic Perturbation Theory," *Intern. J. Quant. Chem.*, **S9**, 1975, pp. 183-198.
6. D. M. Silver and R. J. Bartlett, "Modified Potentials in Many-Body Perturbation Theory," *Phys. Rev.*, **A13**, 1976, pp. 1-12.

Author: D. M. Silver

Support: NAVSEASYS COM

JHU EVENING COLLEGE CENTER AT APL

MASTER'S DEGREES AWARDED AT APL EVENING COLLEGE CENTER

As early as 1958, a few technical courses, but no degree programs, were offered after regular working hours at the Applied Physics Laboratory. These courses were taught by APL staff members under sponsorship of the Evening College of The Johns Hopkins University. In 1963, as a result of increasing staff interest in expanding the advanced education opportunities at APL and the rapidly increasing number of persons in the adjacent area desiring advanced technical courses, a Center of the Evening College of the University was authorized at APL.

In the fall of 1964, the APL Evening College Center formally began operation. A program leading to the Master of Science in Electrical Engineering was instituted, and all courses were opened to the public. One hundred and sixteen individuals completed 149 registrations for the six courses offered. (Some individuals registered for more than one course.) In 1965, the courses offered increased to 11, the number of individuals enrolled to 193, and class registration to 241.

Since 1965, ad hoc committees of APL scientists and engineers have from time to time proposed and helped to implement four additional master's degree programs to fill perceived needs of the APL staff and the neighboring technical community. These programs lead to Master of Science degrees with majors in numerical science (first offered in 1966), applied physics (1967), space technology (1967), and computer science (1971).

Class enrollment grew steadily to about 600, involving more than 400 individuals by 1967. Both totals remained nearly constant through 1974, but 1975

brought a new record high class enrollment of 696, with 494 individual students.

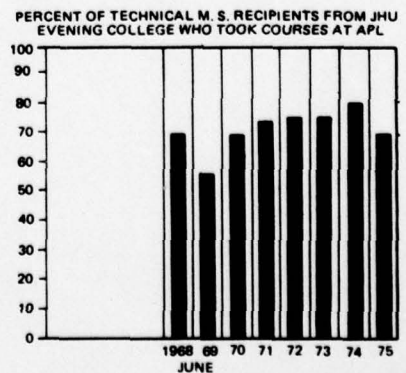
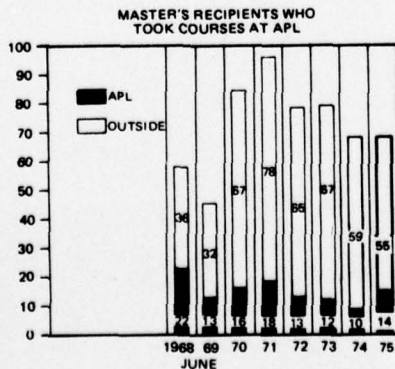
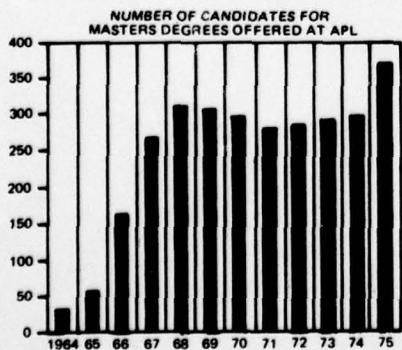
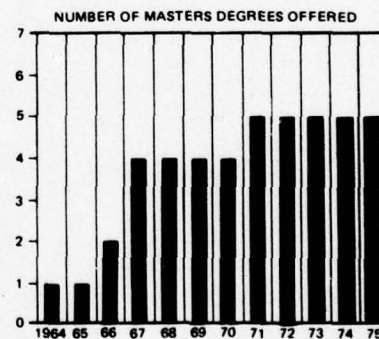
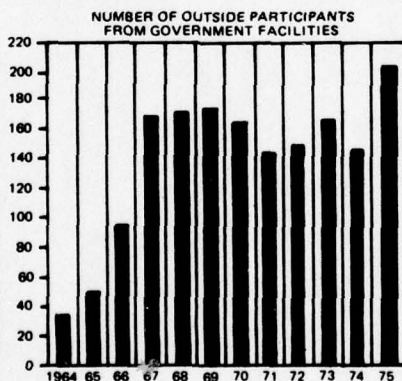
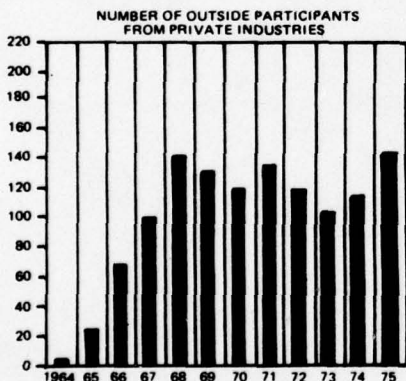
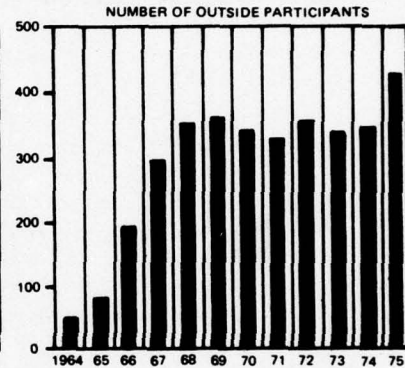
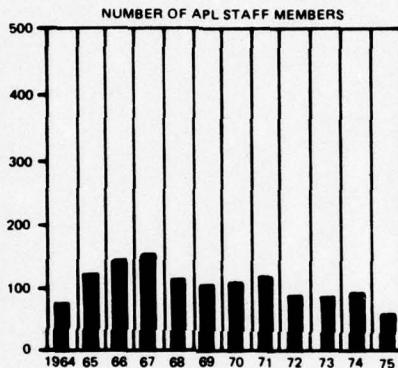
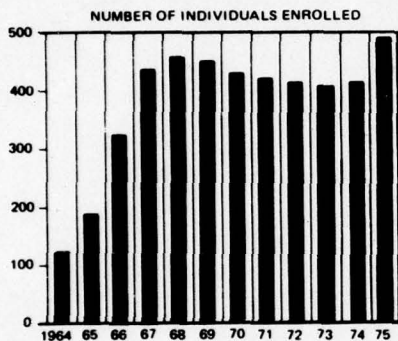
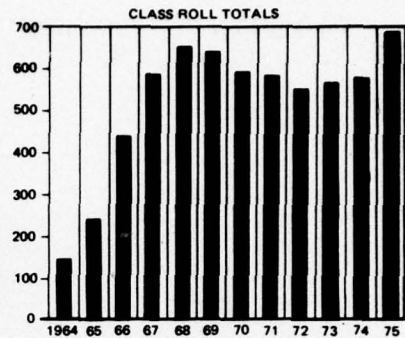
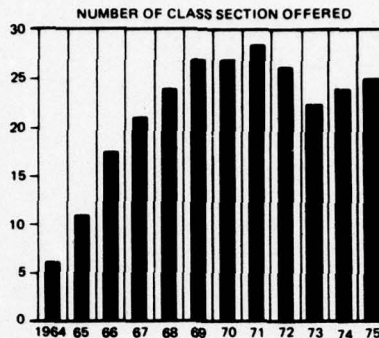
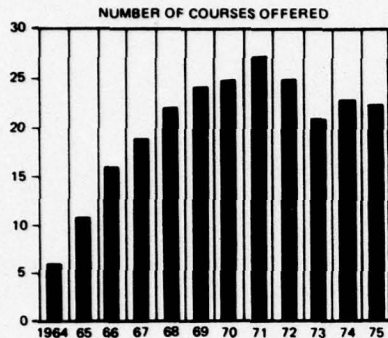
In June 1968, The Johns Hopkins University granted the first degrees awarded for the completion of programs offered by the Evening College Center. Since then, the University has granted a total of 577 master's degrees to students of the Center. These degrees constitute 71% of all master's degrees in technical areas granted during that period by the Evening College of The Johns Hopkins University and cover five academic areas of specialization:

- Numerical science 249,
- Electrical engineering 224,
- Computer science 60,
- Applied physics 23, and
- Space technology 21.

The APL Evening College Center program serves not only APL staff members desiring advanced scientific education but also the entire technical community of the Washington-Baltimore area, including nearby Virginia. The ratio of outside participants to APL staff members enrolled has risen steadily and 86% of the students now come from outside APL.

The Center is especially fortunate in its faculty. Most of the instructors are highly qualified members of the APL Senior Staff; thus the students benefit by having research-minded teachers who are involved with the subjects they teach and understand the needs of part-time students who work in research and development organizations.

THE JHU EVENING COLLEGE CENTER AT APL FALL TERM DATA EXCEPT WHERE NOTED



PUBLICATIONS

PUBLICATIONS IN PROFESSIONAL JOURNALS

1 July 1974–30 June 1975

- Adrian, F. J., "A Possible Test of the Photoexcited Triplet Mechanism of Chemically Induced Electron Spin Polarization: Dependence of the Spin Polarization on Polarized Light Orientation," *J. Chem. Phys.*, 61, No. 11, 1 December 1974, pp. 4875–4879.
- , Bowers, V. A. and Cochran, E. L., "ESR Spectrum and Structure of NaO_3 ," *J. Chem. Phys.*, 61, No. 12, 15 December 1974, pp. 5463–5465.
- Armstrong, J. C. (APL), Akasofu, S.-I. (University of Alaska) and Rostoker, G. (University of Alberta), "A Comparison of Satellite Observations of Birkeland Currents with Ground Observations of Visible Aurora and Ionospheric Currents," *J. Geophys. Res.*, 80, No. 4, 1 February 1975, pp. 575–586.
- Arnold, A., Rowland, J. R. and Konrad, T. G. (APL) and Richter, J. H., Jensen, D. R. and Noonkester, V. R. (Naval Electronics Laboratory Center), "Simultaneous Observations of Clear Air Convection by a Pulse Radar, an FM-CW Radar, an Acoustic Sounder, and an Instrumented Aircraft," *16th Radar Meteorology Conference*, 22–24 April 1975, Houston, TX, pp. 290–295.
- Avery, W. H., "Moving-Way Transportation Concepts," *Proceedings of Workshop on Moving Way Transportation Systems*, Center for Continuing Education, Northeastern University, Boston, MA, 30 July 1974, pp. 165–184.
- and Blevins, R. W., "Accelerating Walkway," *Proc. First Internat. Conf. Transp. Res.*, Bruges, Belgium, June 1973; *College d'Europe and Transp. Res. Forum*, Chicago, IL, 1974, pp. 573–579.
- Bargeron, C. B., "Measurement of a Continuous Distribution of Spherical Particles by Intensity Correlation Spectroscopy: Analysis by Cumulants," *J. Chem. Phys.*, 61, No. 5, 1 September 1974, pp. 2134–2138.
- Bartlett, R. J. (The Johns Hopkins University) and Silver, D. M. (APL), "Correlation Energy in LiH, BH, and HF with Many-Body Perturbation Theory Using Slater-Type Atomic Orbitals," *Internat. J. Quantum Chem. Symp.*, No. 8, 1974, pp. 271–276.
- and ———, "Many-Body Perturbation Theory Applied to Electron Pair Correlation Energies. I. Closed-Shell First-Row Diatomic Hydrides," *J. Chem. Phys.*, 62, No. 8, 15 April 1975, pp. 3258–3268.
- and ———, "Many-Body Perturbation Theory Applied to Hydrogen Fluoride," *Chem. Phys. Letters*, 29, No. 2, 15 November 1974, pp. 199–203.
- and ———, "Pair-Correlation Energies in Sodium Hydride with Many-Body Perturbation Theory," *Phys. Rev.*, A10, No. 6, December 1974, pp. 1927–1931.
- Benson, R. C., Benard, D. J. and Walker, R. E., "Vibrational Relaxation of N_2 and CO_2 (001) by Alkali Metal Atoms," *J. Chem. Phys.*, 61, No. 5, 1 September 1974, pp. 1652–1657.
- Binck, H. J. and Zouck, J. H., "A Microprocessor Applied to Supervisory Control," *Instrumentation Tech.*, 22, No. 1, January 1975, pp. 45–52.
- Bird, J. F., "Neural 1/f Noise and Membrane Models," *Biophys. J.*, 14, No. 7, July 1974, pp. 563–565.
- Blevins, R. W., "Moving Walks," *Proceedings Seminar on Bicycle/Pedestrian Planning and Design*, Disney World, FL, 12–14 December 1973, pp. 463–482.
- Bloch, A. N. and Cowan, D. O. (The Johns Hopkins University) and Poehler, T. O. (APL), "Design and Study of One-Dimensional Organic Conductors. II. TTF-TCNQ and Other Organic Semimetals," *Energy and Charge Transfer* (K. Masuda and M. Silver, Eds.), Plenum Press, New York, 1974, pp. 167–173.
- , ———, Bechgaard, K., Pyle, R. E. and Banks, R. H. (The Johns Hopkins University) and Poehler, T. O. (APL), "Low Temperature Metallic Behavior and Resistance Minimum in a New Quasi-One-Dimensional Organic Conductor," *Phys. Rev. Letters*, 34, No. 25, 23 June 1975, pp. 1561–1564.
- Blum, N. A. and Feldman, C., "Mossbauer Investigation of Amorphous and Polycrystalline Tellurium," *J. Phys.*, 35, December 1974, p. c6–401.
- and ———, "Mossbauer Study of Amorphous and Crystalline Tellurium," *Solid State Commun.*, 15, No. 6, 15 September 1974, pp. 965–968.
- Bohandy, J., Kim, B. F. and Jen, C. K., "An ESR Study of Vanadyl Porphin," *J. Magnetic Resonance*, 15, 1974, pp. 420–426.
- Bramhall, J. N., "Bibliography on Walsh and Walsh Related Functions," *Applications of Walsh Functions and Sequence Theory*, Institute of Electrical and Electronics Engineers, Inc., New York, 1974, Ch. 20, pp. 416–460.
- Brown, N. J. and Fristrom, R. M. (APL) and Sawyer, R. F. (University of California, Berkeley), "A Simple Premixed Flame Model Including an Application to H_2 + Air Flames," *Combustion and Flame*, 23 October 1974, pp. 269–275.
- Brown, S. J., Jr., "Design Considerations for Vehicle State Control by the Point-Follower Method," *Personal Rapid Transit II. Progress Problems Potential*, University of Minnesota, February 1974, pp. 381–389.
- Castella, F. R. and Dunnebacke, F. G., "Analytical Results for the x, y Kalman Tracking Filter," *IEEE Trans. Aerospace and Electronic Syst.*, AES-10, No. 6, November 1974, pp. 891–895.
- Caywood, W. C. and Rubinstein, N., "Ride Quality and Guideway Roughness Measurements of the TRANSPOT '72 Systems," *High Speed Ground Transp. J.*, 8, No. 3, 1974, pp. 213–225.
- Charles, H. K., Jr. and Feldman, C., "Switching Times in Amorphous Boron, Boron plus Carbon, and Silicon Thin Films," *J. Appl. Phys.*, 46, No. 2, February 1975, pp. 819–830.
- Cote, A. J., Jr., "Concepts for Future Vessel Traffic Systems," *Navigation*, 21, No. 4, Winter 1974–1975, pp. 310–319.

- and Schultheis, A. C., "Keeping a Watchful Eye on Harbor Traffic," *Electronics*, 47, No. 22, 31 October 1974, pp. 82-86.
- Dugger, G. L. (Ed.), "Proceedings, Third Workshop on Ocean Thermal Energy Conversion, Houston, Texas, May 8-10, 1975," APL/JHU SR 75-2, August 1975.
- , Olsen, H. L., Shippen, W. B., Francis, E. J. and Avery, W. H., "Ocean Thermal Power Plants," *APL Technical Digest*, January-March 1975.
- , —, —, —, and —, "Tropical Ocean Thermal Power Plants and Potential Products," AIAA Paper No. 75-617, April 1975.
- Edwards, P. B., "Effective Utilization of Professional Manpower in Educating Part Time Students," 1974 International Conference on Frontiers in Education, 15-19 July 1974, London, IEE Conference Pub. No. 115, pp. 374-377.
- , "Upgrading Unskilled Employees," *Training and Development J.*, 28, No. 10, October 1974, pp. 34-38.
- Ehrlich, L. W., "Digital Simulation of Periodic Fluid Flow in a Bifurcation," *Computers and Fluids*, 2, No. 3/4, December 1974, pp. 237-247.
- Ekstrom, J. L., "Doppler Processing Using Walsh and Hard-Limited Fourier Transforms," *Proc. IEEE*, 63, No. 1, January 1975, pp. 202-203.
- , "MTI Clutter Locking for Arbitrary Clutter Spectral Shapes," *IEEE Trans. Aerospace and Electronic Syst.*, AES-10, No. 6, November 1974, pp. 873-874.
- Fehlner, L. F. and McCarty, T. A., "How to Harvest the Full Potential of Loran-C," *Navigation*, 21, No. 3, Fall 1974, pp. 223-233.
- Feldman, C. and Charles, H. K., Jr., "Electrothermal Model of Switching in Amorphous Boron and Silicon Thin Films," *Solid State Commun.*, 15, No. 3, 1 August 1974, pp. 551-554.
- Flower, R. W., "Choroidal Angiography Using Indocyanine Green Dye: A Review and Progress Report," *Ophthalm. Digest*, 36, July 1974, pp. 18-27.
- , Bird, J. F. and Mowbray, G. H., "Retinal and Cortical Electrophysiological Responses to Instantaneous Frequency Shifts in Light Modulated above Fusion," *Invest. Ophthalm.*, 14, No. 1, January 1975, pp. 75-78.
- Foner, S. N. and Nall, B. H., "Attenuation of Sound by Rigid Spheres: Measurement of the Viscous and Thermal Components of Attenuation and Comparison with Theory," *J. Acoust. Soc. Am.*, 57, No. 1, January 1975, pp. 59-66.
- Friedman, M. H., "A Physical Description of the Pathogenesis, Histopathology and Treatment of Corneal Epithelial Edema," *J. Theoret. Biol.*, 45, 1974, pp. 153-169.
- , "Shear Profiles and Diffusion in Idealized Flows through a Y-Branch," *Proceedings Specialists Meeting, Fluid Dynamic Aspects of Arterial Disease* (R. M. Nerem, Ed.), sponsored by the National Science Foundation and Ohio State University, Columbus, OH, 19-20 September 1974, pp. 1-4.
- , O'Brien, V. and Ehrlich, L. W., "Calculations of Pulsatile Flow through a Branch: Implications for the Hemodynamics of Atherogenesis," *Circulation Res.*, 36, February 1975, pp. 277-285.
- Fristrom, R. M., "Chemistry, Combustion, and Flammability," *J. Fire and Flammability*, 5, October 1974, pp. 289-320.
- , "Fire Research in the United States," *Revue Energie Primaire*, X, No. 1, 1974, pp. 2-6.
- , "Flame Sampling for Mass Spectrometry," *Internatl. J. Mass Spectrom. and Ion Phys.*, 16, 1975, pp. 15-32.
- , "Some Activities of the Committee on Fire Research of the National Academy of Sciences/National Research Council of the United States of America," *Archives of Combustion Processes (Archiwum Procesow Spalania)*, 5, No. 3, 1974, pp. 349-352.
- Gasparovic, R. F. and Tubbs, L. D., "Influence of Reference Source Properties on Ocean Heat Flux Determination with Two-Wavelength Radiometry," *J. Geophys. Res.*, 80, No. 18, 20 June 1975, pp. 2667-2671.
- Gibson, R. E., "Centennial of Gibbs' Thermodynamics—Concluding Remarks," *J. Washington Acad. Sci.*, 64, No. 3, 1974, pp. 213-217.
- Goldhirsh, J. and Robison, F. L., "Attenuation and Space Diversity Statistics Calculated from Radar Reflectivity Data of Rain," *IEEE Trans. Antennas and Prop.*, AP-23, No. 2, March 1975, pp. 221-227.
- Gray, E. P., "Some Further Studies of Radiofrequency Supplemented Mirror Confinement," *Proceedings of the U.S.-Australian Workshop on Plasma Waves, February 1975*, Paper No. 8, Texas Technical University, 1975, pp. 8.1-8.4.
- Guier, W. H. (APL), Friesinger, G. C. (Vanderbilt University Medical School) and Ross, R. S. (Johns Hopkins School of Medicine), "Beat-by-Beat Stroke Volume from Aortic-Pulse-Pressure Analysis," *IEEE Trans. Biomed. Eng.*, BME-21, No. 4, July 1974, pp. 285-292.
- Halpin, B. M. (APL), Radford, E. P. (The Johns Hopkins University) and Fisher, R. and Caplan, Y. (The Medical Examiners Office, State of Maryland), "A Fire Fatality Study," *Fire J.*, May 1975, pp. 11-14.
- Hart, L. W., Grunfelder, C. and Fristrom, R. M., "The 'Point Source' Technique Using Upstream Sampling for Rate Constant Determinations in Flame Gases," *Combustion and Flame*, 23, No. 1, August 1974, pp. 109-119.
- Haug, A. (APL) and Graves, R. D. and Überall, H. (Catholic University of America), "Normal-Mode Theory of Underwater Sound Propagation from Directional Multipole Sources," *J. Acoust. Soc. Am.*, 56, No. 2, August 1974, pp. 387-391.

- , —, and —, "Normal-Mode Theory of Underwater Sound Propagation from Stationary Multipole Sources: Results from Realistic Sound-Speed Profile," *J. Acoust. Soc. Am.*, 57, No. 5, May 1975, pp. 1052-1061.
- Hill, M. L. (APL) and Hoppel, W. M. (Naval Research Laboratory), "Comment on 'Wind Effects on Electrostatic Autopilots'," *J. Aircraft*, 11, No. 12, December 1974, pp. 781-782.
- Hinman, E. J. and Pitts, G. L., "Practical Safety Considerations for Short-Headway Automated Transit Systems," *Personal Rapid Transit II. Progress Problems Potential*, University of Minnesota, February 1974, pp. 375-380.
- Hochheimer, B. F., "Lasers in Ophthalmology," *Laser Applications in Medicine and Biology*, 2 (M. L. Wolbarsht, Ed.), Plenum Publishing Corp., New York, 1974.
- and Flower, R. W., "Angiography of the Cervix," *Johns Hopkins Medical J.*, 135, No. 6, December 1974, pp. 375-382.
- Hunter, L. W., "On Infinite Order Sudden Approximations for an Arbitrary Potential Energy," *J. Chem. Phys.*, 62, No. 7, 1 April 1975, pp. 2855-2859.
- Hyvarinen, L. and Hochheimer, B. F., "Filter Systems in Fluorescein Angiography," *Recent Advances in the Technical Aspects of Fluorescein Angiography*, 14, No. 3 (W. H. Haining, Ed.), Little, Brown & Co., Boston, 1974, pp. 49-61.
- Jette, A. N., "Coupling Constants of the Fine and Hyperfine Interaction in the $c^3\pi_u$ Metastable State of H_2 ," *J. Chem. Phys.*, 62, No. 11, 1 June 1975, pp. 4579-4580.
- , "Spin-Other-Orbit and Spin-Spin Interactions in the Metastable $c^3\pi_u$ (1s, 2p) State of H_2 ," *J. Chem. Phys.*, 61, No. 3, 1 August 1974, pp. 816-819.
- and Miller, T. A. (Bell Laboratories), "Fine Structure in Rydberg States of the H_2 Molecule," *Chem. Phys. Letters*, 29, No. 4, 15 December 1974, pp. 547-550.
- Katz, I., "Active Microwave Sensing of the Atmosphere from Satellites," *16th Radar Meteorology Conference*, 22-24 April 1975, Houston, TX, pp. 246-252.
- , "Rain Cell Statistics Experiment," *16th Radar Meteorology Conference*, 22-24 April 1975, Houston, TX, pp. 378-380.
- Kilgus, C. C., "Shaped-Conical Radiation Pattern Performance of the Backfire Quadrifilar Helix," *IEEE Trans. Antennas and Prop.*, AP-23, No. 3, May 1975, pp. 392-397.
- Kim, B. F., Bohandy, J. and Jen, C. K., "Optical Fluorescence Spectra of Porphins in Organic Crystalline Hosts," *Spectrochimica Acta*, 30A, November 1974, pp. 2031-2040.
- Kohl, J. W., "Response of Various Thin-Film Scintillators to Low-Energy Particles," *Nuclear Instr. and Methods*, 125, No. 3, 15 April 1975, pp. 413-417.
- Konrad, T. G. and Howard, J. C., "Multiple Contrail Streamers Observed by Radar," *J. Appl. Meteorol.*, 13, No. 5, August 1974, pp. 563-572.
- and Kropfli, R. A., "Statistical Models of Rain Cells Derived from Radar Observations," *16th Radar Meteorology Conference*, 22-24 April 1975, Houston, TX, pp. 381-386.
- Krimigis, S. M., Sarris, E. T. and Armstrong, T. P., "Observations of Jovian Electron Events in the Vicinity of Earth," *Geophys. Res. Letters*, 2, 1975, p. 561.
- Kues, H. A. and Luty, G. A., "Dyes Can Be Deadly," *Laser Focus*, 11, No. 5, May 1975, pp. 59-61.
- Kuttler, J. R., "A Remark on the Paper 'A Maximum Principle for Fourth Order Ordinary Differential Equations' by Chow, Dunninger, and Lasota," *J. Diff. Equations*, 17, No. 1, January 1975, pp. 44-45.
- , "Direct Methods for Computing Eigenvalues of the Finite-Difference Laplacian," *SIAM J. Numer. Anal.*, 11, No. 4, September 1974, pp. 732-740.
- Makofski, R. A., Cusick, R. T. and Mooring, E. E., "Results of the Testing of the Dulles Prototype Systems," *Proc. First Internatl. Conf. Transp. Res.*, Bruges, Belgium, June 1973; *College d'Europe and Transp. Res. Forum*, Chicago, IL, 1974, pp. 521-533.
- and Rand, R. C., "Advanced Urban Transportation Systems," *Connecticut Transportation Symposium*, sponsored by the Connecticut Department of Transportation and the Connecticut Section of the American Institute of Aeronautics and Astronautics, University of Hartford, 8 May 1971.
- Mark, F. F., Barger, C. B. and Friedman, M. H., "Experimental Investigation of Laminar Flow in a Rectangular Cross-Section Bifurcation," *Proc. ASME 1975 Biochem. Symp.*, Troy, NY, 23 June 1975, pp. 7-10.
- McCullough, E. A., Jr. (Utah State University) and Silver, D. M. (APL), "Reaction Path Properties at Critical Points on Potential Surfaces," *J. Chem. Phys.*, 62, No. 10, 15 May 1975, pp. 4050-4052.
- Meyer, R. A. (APL) and Brunsting, A. (Auburn University), "Light Scattering from Nucleated Biological Cells," *Biophys. J.*, 15, No. 3, March 1975, pp. 191-203.
- and Haase, S. F. (APL) and Poduslo, S. E. and McKhann, G. M. (Johns Hopkins School of Medicine), "Light-Scattering Patterns of Isolated Oligodendroglia," *J. Histochem. and Cytochem.*, 22, No. 7, 1974, pp. 594-597.
- Monchick, L., "The Ehrenfest Theorem and Gas Transport Properties," *Physica*, 78, No. 1, 15 November 1974, pp. 64-72.
- , "Time Delays and Diffusion Controlled Reactions," *J. Chem. Phys.*, 62, No. 5, 1 March 1975, pp. 1907-1912.
- Moorjani, K., Blum, N. A. and Feldman, C., "Comments on the Determination and Analysis of Optical Constants of Thin Silicon Films," *Amorphous and Liquid Semiconductors*, 1 (J. Stuke and W. Brenig, Eds.), Taylor & Francis Ltd., London, 1974, pp. 563-566.
- and Tanaka, T. (Catholic University of America), Sokoloski, M. M. (Harry Diamond Laboratories) and Bose, S. M. (Drexel University), "Numerical Aspects of the Two-Sites Coherent Potential Approximation," *J. Phys.*, 35, No. 5, May 1974, pp. C4-153 to C4-156.

- Nall, B. H., "Time and Space Resolution of Bulk Acoustic Waves Generated Concomitantly with Rayleigh Surface Waves by an Integral Transducer," *J. Appl. Phys.*, 46, No. 5, May 1975, pp. 1884-1892.
- Newton, R. R., "The Authenticity of Ptolemy's Eclipse and Star Data," *Quart. J. Roy. Astronom. Soc.*, 15, No. 2, June 1974, pp. 107-121.
- , "The Obliquity of the Ecliptic Two Millennia Ago," *Monthly Notes Roy. Astronom. Soc.*, 169, No. 2, November 1974, pp. 331-342.
- O'Brien, C. J., "Explain the System or Perish," *IABC News*, 4, No. 7, January 1975, pp. 1 and 6.
- O'Brien, V., "Stokes Drag for Arbitrary Bodies," *Canad. J. Chem. Eng.*, 51, December 1974, pp. 793-794.
- , "Unsteady Separation Phenomena in a Two-Dimensional Cavity," *AIAA J.*, 13, No. 3, March 1975, pp. 415-416.
- , "Wall Shear in Unsteady Branching Flow," *Proceedings Specialists Meeting, Fluid Dynamic Aspects of Arterial Disease* (R. M. Nerem, Ed.), sponsored by the National Science Foundation and Ohio State University, Columbus, OH, 19-20 September 1974, pp. 9-11.
- and Ehrlich, L. W., "Unsteady Blood Flow through a Branch," 27th ACEMB Meeting, Marriott Hotel, Philadelphia, PA, 6-10 October 1974, p. 281.
- Paddison, F. C. and Stone, A. M., "Transportation in the Arctic," *Polar Deserts and Modern Man* (T. L. Smiley and J. H. Zumberge, Eds.), The University of Arizona Press, Tucson, AZ, 1974, Ch. 12, pp. 125-149.
- Parker, J. G., "A Study of the Role of Vibration-Vibration Exchange on the Collisional Deactivation of Vibrationally Excited Singlet Molecular Oxygen," *J. Chem. Phys.*, 62, No. 6, 15 March 1975, pp. 2235-2239.
- and Ritke, D. N., "On the Mechanism for Collisional Deactivation of Vibrationally Excited Singlet Molecular Oxygen," *J. Chem. Phys.*, 61, No. 8, 15 October 1974, pp. 3408-3413.
- Perini, L. L., "Compilation and Correlation of Stagnation Convective Heating Rates on Spherical Bodies," *J. Spacecraft and Rockets*, 12, No. 3, March 1975, pp. 189-191.
- , "Economical Scheme for Estimating Orbital Lifetimes," *J. Spacecraft and Rockets*, 12, No. 6, June 1975, pp. 323-324.
- Pirkle, J. C., Jr. (The Johns Hopkins University) and Poehler T. O. and Sigillito, V. G. (APL), "Numerical Procedure for a Pulsed DF-CO₂ Transfer Laser," *J. Comp. Phys.*, 15, No. 2, June 1974, pp. 293-298.
- and Sigillito, V. G. (APL), "Analysis of Optically Pumped CO₂ Laser," *Appl. Optics*, 13, No. 12, December 1974, pp. 2799-2805.
- Pisacane, V. L., McConahy, R. J., Pryor, L. L., Whisnant, J. M. and Black, H. D., "Orbit Determination from Passive Range Observations," *IEEE Trans. Aerospace and Electronic Syst.*, AES-10, No. 4, July 1974, pp. 487-491.
- Poehler, T. O. (APL) and Bloch, A. N., Ferraris, J. P. and Cowan, D. O. (The Johns Hopkins University), "Far Infrared Photoconductivity of TTF-TCNQ," *Solid State Commun.*, 15, No. 2, 15 July 1974, pp. 337-340.
- , Walker, R. E. and Leight, J. W., "High-Pressure Chemical Waveguide Laser," *Appl. Phys. Letters*, 26, No. 10, 15 May 1975, pp. 560-561.
- Potemra, T. A., "Ionizing Radiation Affecting the Lower Ionosphere," *ELF-VLF Radio Wave Propagation*, D. Reidel Publishing Co., Dordrecht-Holland, 1974, pp. 21-37.
- , "The Use of VLF Propagation Measurements for Studies of Magnetospheric and Meteorological Influences on the Lower Ionosphere," *Methods of Measurements and Results of Lower Ionosphere Structure*, Akademie-Verlag, Berlin, 1974, pp. 119-126.
- , Iijima, T. and Favin, S., "Field-Aligned Currents in the North and South Auroral Regions Measured with TRIAD," *EOS*, 56, 1975, p. 617.
- Powell, W. R., "Absorber for Solar Power," *Appl. Optics*, 13, No. 10, October 1974, pp. 2430-2435.
- Richter, J. H., Jensen, D. R. and Noonkester, V. R. (Naval Electronics Laboratory Center) and Konrad, T. G., Arnold, A. and Rowland, J. R. (APL), "Clear Air Convection: A Close Look at Its Evolution and Structure," *Geophys. Res. Letters*, 1, No. 4, August 1974, pp. 173-176.
- Roelof, E. C., "Comment on 'Propagation Anisotropies of Solar Flare Protons and Electrons at Low Energies in Interplanetary Space by R. K. Pyle,'" *J. Geophys. Res.*, 79, No. 19, 1 July 1974, pp. 2931-2935.
- , Cronyn, W. M., McIntosh, P. S. and Shawhan, S. D., "Solar Wind and Energetic Particle Events of June 20-30, 1974, Analyzed Using Measurements of Interplanetary Radio Scintillations at 34.3 MHz," *Space Research XVI*, M. H. Rycroft (Ed.), Akademie-Verlag (Berlin), 1975.
- , Cuperman, S. and Sternlieb A. (Tel Aviv University), "On the Correlation of Coronal Green-Line Intensity and Solar Wind Velocity," *Solar Phys.*, 41, No. 2, April 1975, pp. 349-366.
- Roesler, W. J., Williams, M. B., Ford, B. M. and Waddell, M. C., "Comparisons of Synchronous and Quasi-Synchronous PRT Vehicle Management and Some Alternative Routing Algorithms," *Personal Rapid Transit II. Progress Problems Potential*, University of Minnesota, February 1974, pp. 425-438.
- Rowland, J. R. and Arnold, A., "Vertical Velocity Structure and Geometry of Clear Air Convective Elements," *16th Radar Meteorology Conference*, 22-24 April 1975, Houston, TX, pp. 296-303.
- Sager, D. G., "Analysis of TSO Performance on the IBM 360/91," *Proc. SHARE, XLIII*, August 1974, pp. 1070-1097.
- Sigillito, V. G., "Exponential Decay of Functionals of Solutions of a Pseudoparabolic Equation," *SIAM J. Math. Anal.*, 5, No. 4, August 1974, pp. 581-585.
- Silver, D. M., "Hierarchy of Symmetry Conservation Rules Governing Chemical Reaction Systems," *J. Am. Chem. Soc.*, 96, No. 19, 18 September 1974, pp. 5959-5967.

- and Karplus, M. (Harvard University), "Valence-Bond Approach to Conservation of Symmetry in Concerted Reactions," *J. Am. Chem. Soc.*, 97, No. 10, 14 May 1975, pp. 2645-2654.
- Somers, R. M. and Poehler, T. O. (APL) and Wagner, P. E. (University of Maryland), "Microwave Time Domain in Fabry-Perot Emission Spectrometer," *Rev. Sci. Instr.*, 46, No. 6, June 1975, pp. 719-725.
- Spohn, W. G., "On the Derived Cuboid," *Can. Math. Bull.*, 17, No. 4, 1974, pp. 575-577.
- Staff of Space Department (APL) and Staff of Guidance and Control Laboratory (Stanford University), "A Satellite Freed of All but Gravitational Forces: 'TRIAD I'," *J. Spacecraft and Rockets*, 11, No. 9, September 1974, pp. 637-644.
- Sugai, I., "Exact Geodetic Latitude of Subvehicle Point," *J. Astronaut. Sci.*, XXII, No. 1, July-September 1974, pp. 55-63.
- Taylor, C. (USN) and O'Brien, C. J. (APL), "Steering by Satellite," *Naval Aviation News*, October 1974, pp. 14-17.
- Tossman, B. E. and Thayer, D. L., "Interactions between SAS-C Spacecraft Nutations and Spin Control System," *AIAA Mechanics and Control of Flight Conference*, Anaheim, CA, 5-9 August 1974, AIAA Paper No. 74-902, pp. 1-15.
- , Williams, C. E. and Brown, N. K., "SIMCON—An Advancement in the Simulation of Physical Systems," *AFIPS Conference Proceedings*, Fall Joint Computer Conference, Houston, TX, 37, 1970, pp. 399-405.
- Venkatesan, D. and Mathews, T. (University of Calgary), Lanzerotti, L. J. (Bell Laboratories), Fairfield, D. H. (NASA Goddard) and Bostrom, C. O. (APL), "Cosmic Ray Intensity Variations during 0200-0700 UT, August 5, 1972," *J. Geophys. Res.*, 80, No. 13, 1 May 1975, pp. 1715-1724.
- Verschell, H. J., Mendell, R. B. and Korff, S. A. (New York University) and Roelof, E. C. (APL), "Two Classes of Cosmic Ray Decrease," *J. Geophys. Res.*, 80, No. 10, 1 April 1975, pp. 1189-1201.
- Waddell, M. C., "Dual Mode PRT System Costs," *Personal Rapid Transit II. Progress Problems Potential*, University of Minnesota, February 1974, pp. 571-575.
- Walker, R. E. and Compton, G. E. (APL) and Langham, M. E. (Johns Hopkins School of Medicine), "Pneumatic Applanation Tonometer Studies. IV. Analysis and Pulsatile Response," *Exptl. Eye Res.*, 20, No. 3, March 1975, pp. 245-253.
- and Langham, M. E. (Johns Hopkins School of Medicine), "Pneumatic Applanation Tonometer Studies. III. Analysis of the Floating Tip Sensor," *Exptl. Eye Res.*, 20, No. 2, February 1975, pp. 167-172.
- Westenberg, A. A. and deHaas, N., "Rate of the O + SO₂ Reaction," *J. Chem. Phys.*, 62, No. 2, 15 January 1975, pp. 725-730.
- and —, "Rates of H + CH₃X Reactions," *J. Chem. Phys.*, 62, No. 8, 15 April 1975, pp. 3321-3325.
- and —, "Reaction Rates of O + CH₃Br and OH + CH₃Cl," *J. Chem. Phys.*, 62, No. 11, 1 June 1975, pp. 4477-4479.
- Whisnant, J. M. and Anand, D. K., "Invariant Surfaces for Rotor Controlled Satellites in Highly Elliptical Orbits," *Z. Angew. Math. u. Mech.*, 54, No. 9, September 1974, pp. 563-565.
- Wiley, R. E. (Bendix) and Pisacane, V. L. (APL), "The Motion of an Artificial Satellite in a Nonspherical Gravitational Field and an Atmosphere with a Quadratic Scale Height," *J. Astronaut. Sci.*, XXI, Nos. 5 and 6, March-June 1974, pp. 230-243.
- Yionoulis, S. M. and Black, H. D., "A Two Satellite Technique for Measuring the Deflection of the Vertical (The DOVIMETER)," *Proceedings International Symposium Applied Marine Geodesy*, June 1974, pp. 331-342.
- Zmuda, A. J., "The Geomagnetic Field and Its Harmonic Description," *Geomagnetism and Aeronomy*, 13, No. 6, 1973, pp. 929-939.
- and Armstrong, J. C., "The Diurnal Flow Pattern of Field-Aligned Currents," *J. Geophys. Res.*, 79, No. 31, 1 November 1974, pp. 4611-4619.
- , Potemra, T. A. and Armstrong, J. C., "Transient Parallel Electric Fields from Electromagnetic Induction Associated with Motion of Field-Aligned Currents," *J. Geophys. Res.*, 79, No. 28, 1 October 1974, pp. 4222-4226.
- et al., "The Geomagnetic Field of External Origin as Observed at the Earth's Surface," *Trans. Am. Geophys. Union*, 55, No. 6, June 1974, pp. 588-599.

AUTHOR INDEX

AUTHOR INDEX

A

- Adrian, F. J.—"Photoexcited Triplet Mechanism of Chemically Induced Electron Spin Polarization," p. 86

B

- Barger, C. B., O. J. Deters, L. W. Ehrlich, F. F. Mark, V. O'Brien, and M. H. Friedman—"Calculations and Measurements of Simulated Arterial Flows," p. 50
- Becraft, W. A.—See Luke, P. J.
- Bird, J. F., R. W. Flower, and G. H. Mowbray—"Elemental Phenomenon of Vision," p. 46
- Blum, B. I.—"JHH Mini Record System," p. 42
- Bostrom, C. O.—See Potemra, T. A.
- Brickner, E. L.—"DAT—A Mobile Data Acquisition System," p. 62
- Brown, N. K.—"A 'Store and Forward' Telemetry Computer Program Designed Using Computer Simulation," p. 31

C

- Chubbuck, J. G.—See Viernstein, L. J.

D

- deHaas, N.—See Westenberg, A. A.
- Deters, O. J.—See Barger, C. B.
- Dwarkin, M. L., J. W. Follin, Jr., R. E. Miller, and D. W. Stowe—"Electronic Beamsteering for a Parametric Sonar," p. 74

E

- Eckard, L. D., Jr.—"GEOS-C Spacecraft Launch and Early Orbit Operations," p. 27
- Ehrlich, L. W.—See Barger, C. B.

F

- Finkel, A.—See Schenkel, F. W.
- Flower, R. W.—See Bird, J. F.
- Follin, J. W., Jr.—See Dwarkin, M. L.
- Foner, S. N. and B. H. Nall—"Attenuation of Sound by Rigid Spheres," p. 90
- Friedman, M. H.—See Barger, C. B.
- Fristrom, R. M., C. Grunfelder, and L. W. Hunter—"Moving Wire Technique Studies of Ablation, Ignition, and Extinction of Polymer Flames," p. 56

G

- George, J. F.—See Perini, L. L.
- Goldhirsh, J.—"Prediction of Rain Attenuation Statistics," p. 35
- Grunfelder, C.—See Fristrom, R. M.

H

- Hanes, R. M.—See Perini, L. L.
- Hunter, L. W.—See Fristrom, R. M.

L

- Leffel, C. S., Jr.—"The Earth's Electrostatic Field as an Obstacle Sensor," p. 77
- Levy, A.—See Perini, L. L.
- Luke, P. J., J. L. Machamer, and W. A. Becraft—"Error Correction Encoder/Error Correction Decoder," p. 79
- Lyall, K.—See Perini, L. L.

M

- Machamer, J. L.—See Luke, P. J.
- Makofski, R. A.—See Perini, L. L.
- Mark, F. F.—See Barger, C. B.
- See Perini, L. L.
- Miller, R. E.—See Dwarkin, M. L.
- Mowbray, G. H.—See Bird, J. F.

N

- Nall, B. H.—See Foner, S. N.

O

- O'Brien, V.—See Barger, C. B.

P

- Perini, L. L., R. A. Makofski, J. F. George, R. M. Hanes, and F. F. Mark (APL); A. Levy and K. Lyall (CMPR)—"Small-Car Study," p. 64
- Poehler, T. O.—"Organic Conductors," p. 84
- Potemra, T. A.—"Field-Aligned Currents in the Southern Auroral Zone Measured by Triad," p. 22
- and C. O. Bostrom—"Characteristic Energy Spectra of 1 to 500 eV Electrons Observed in the Auroral Zones from Atmosphere Explorer-C," p. 20

R

Rible, H. B.—"Completion and Launching of Small Astronomy Satellite-C," p. 24

Rueger, L. J.—"Hydrogen Maser Frequency Standard in Operation at APL Time and Frequency Standards Laboratory," p. 30

S

Sadilek, A. C.—"DISCOS System for the TIP-II Satellite," p. 14

Schenkel, F. W. and A. Finkel—"Nap-of-the-Earth Radar (NOTER)," p. 72

Schmeisser, G., Jr.—See Seamone, W.

Seamone, W. (APL) and G. Schmeisser, Jr. (JHMI)—"Evaluation of Powered Medical Manipulator," p. 44

Silver, D. M.—"Molecular Energies and Structure," p. 92

Stowe, D. W.—See Dwarkin, M. L.

V

Viernstein, L. J. and J. G. Chubbuck—"A Monitor for Intracranial Pressure," p. 48

Voss, P. J.—"Evaluation of Radar Processing Subsystem," p. 58

W

Wagner, G. D.—"Hybrid Microcircuits for TIP-II and TIP-III Satellites," p. 16

Westenberg, A. A. and N. deHaas—"Reaction Rates of H and O with Methyl Halides," p. 87

END 11-77
DDC